AN ELECTRIFICATION SOLUTION FOR ISTANBUL METROBUS LINE

İSTANBUL METROBÜS HATTI İÇİN BİR ELEKTRİKLİ ARAÇ ÇÖZÜMÜ

MUSTAFA NİCEM TANYERİ

ASSOC. PROF. DR. SELAHATTİN ÇAĞLAR BAŞLAMIŞLI
Supervisor

Submitted to

Graduate School of Science and Engineering of Hacettepe University

as a Partial Fulfillment to the Requirements

for the Award of the Degree of Master

in Mechanical Engineering

2019

This work titled **"An Electrification Solution for Istanbul Metrobus Line"** by **MUSTAFA NİCEM TANYERİ** has been approved as a thesis for the Degree of **Master of Science in Mechanical Engineering** by the Examining Committee Members mentioned below.
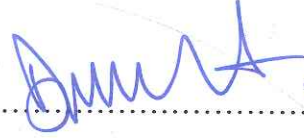
Assoc. Prof. Dr. Selis ÖNEL
Head ....

Assoc. Prof. Dr. Selahattin Çağlar BAŞLAMIŞLI
Supervisor ....

Assoc. Prof. Dr. Mesut DÜZGÜN
Member ....

Asst. Prof. Dr. Bilsay SÜMER
Member ....

Asst. Prof. Dr. Selçuk HİMMETOĞLU
Member ....

This thesis has been approved as a thesis for the Degree of **Master of Science in Mechanical Engineering** by Board of Directors of the Institute of Graduate School of Science and Engineering on ...../...../......

Prof. Dr. Menemşe GÜMÜŞDERELİOĞLU
Director of the Institute of
Graduate School of Science and Engineering

To my family and all friends…

ETHICS

In this thesis study, prepared in accordance with the spelling rules of Institute of Graduate School of Science and Engineering of Hacettepe University,

I declare that

- all the information and documents have been obtained in the base of the academic rules
- all audio-visual and written information and results have been presented according to the rules of science ethics
- in case of using other works, related studies have been cited in accordance with the scientific standards
- all cited studies have been fully referenced
- I did not do any distribution in the data set
- and any part of this thesis has not been presented as another thesis study at this or any other university

20/06/2019

MUSTAFA NİCEM TANYERİ

YAYINLANMA FİKRİ MÜLKİYET HAKLARI BEYANI

Enstitü tarafından onaylanan lisansüstü tezimin/raporumun tamamını veya herhangi bir kısmını, basılı (kağıt) ve elektronik formatta arşivleme ve aşağıda verilen koşullarla kullanıma açma iznini Hacettepe üniversitesine verdiğimi bildiririm. Bu izinle Üniversiteye verilen kullanım hakları dışındaki tüm fikri mülkiyet haklarım bende kalacak, tezimin tamamının ya da bir bölümünün gelecekteki çalışmalarda (makale, kitap, lisans ve patent vb.) kullanım hakları bana ait olacaktır.

Tezin kendi orijinal çalışmam olduğunu, başkalarının haklarını ihlal etmediğimi ve tezimin tek yetkili sahibi olduğumu beyan ve taahhüt ederim. Tezimde yer alan telif hakkı bulunan ve sahiplerinden yazılı izin alınarak kullanması zorunlu metinlerin yazılı izin alarak kullandığımı ve istenildiğinde suretlerini Üniversiteye teslim etmeyi taahhüt ederim.

Yükseköğretim Kurulu tarafından yayınlanan *"Lisansüstü Tezlerin Elektronik Ortamda Toplanması, Düzenlenmesi ve Erişime Açılmasına İlişkin Yönerge"* kapsamında tezim aşağıda belirtilen koşullar haricince YÖK Ulusal Tez Merkezi / H. Ü. Kütüphaneleri Açık Erişim Sisteminde erişime açılır.

- ☐ Enstitü / Fakülte yönetim kurulu kararı ile tezimin erişime açılması mezuniyet tarihimden itibaren 2 yıl ertelenmiştir.

- ☐ Enstitü / Fakülte yönetim kurulu gerekçeli kararı ile tezimin erişime açılması mezuniyet tarihimden itibaren .... ay ertelenmiştir.

- ☐ Tezim ile ilgili gizlilik kararı verilmiştir.

20 / 06 / 2019

MUSTAFA NİCEM TANYERİ

ABSTRACT

AN ELECTRIFICATION SOLUTION FOR ISTANBUL METROBUS LINE

Mustafa Nicem TANYERI

Master of Science, Department of Mechanical Engineering
Supervisor: Assoc. Prof. Dr. Selahattin Çağlar BAŞLAMIŞLI
June 2019, 186 pages

In the present case, Istanbul Metrobus Line is operated by Metrobus vehicle with internal combustion engines. This situation is not suitable and sustainable in terms of operating cost and environment pollution. If this line was operated with electric vehicles, it would have lower operation costs and would reduce harmful effects to the environment. As an alternative solution, in this thesis, economically and technically the most suitable electric vehicle solution is determined according to the requirement obtained by driving cycle, environmental conditions, passenger occupancy rates and characteristic of the vehicle.

In July 2018, in order to determine the characteristic of the vehicle, a coast down test was performed with an 18 meter articulated Metrobus. Additionally, to create the driving cycle; position, velocity, acceleration and time data were acquired from a Metrobus in service with IMU and GPS. Passenger flow data were generated from data that were obtained from the bus operator company. So as to find out HVAC system requirement of the Metrobus, weather data of Istanbul is obtained from Turkish State Meteorological Service and with the solar position data calculated heat loads of the vehicle were determined according to ASHRAE Standard. According these data, all system requirements are obtained.

First of all, according to power requirements of the 18-m articulated bus, the traction system is selected and a suitable gearbox ratio for that traction system is determined to fulfill the system requirements. Secondly, the most important sub-system for passenger comfort, HVAC, is selected in compliance with the weather data. Thirdly, charger and batteries of different chemistry are selected for different lines. Finally, two types of fleets with different charging strategies are designed.

At the end of the study, fleets that have different batteries and different charging strategies are compared with each other and with current diesel Metrobus fleet. For the comparison cost of all components are obtained and total cost of ownership of these three fleets are calculated. The most suitable electrification solution is obtained according to these calculations.

Keywords: Electric bus systems, Electric vehicles technologies, Battery and charging technologies, Economic analysis, Total cost of ownership, System design

ÖZET

İSTANBUL METROBÜS HATTI İÇİN BİR ELEKTRİKLİ ARAÇ ÇÖZÜMÜ

Mustafa Nicem TANYERİ

Yüksek Lisans, Makine Mühendisliği Bölümü

Tez danışmanı: Doç. Dr. Selahattin Çağlar BAŞLAMIŞLI

Haziran 2019, 186 sayfa

Mevcut durumda, İstanbul Metrobüs Hattı, içten yanmalı motorlara sahip Metrobüs araçları ile işletilmektedir. Bu durum işletme maliyeti ve çevre kirliliği açısından uygun ve sürdürülebilir değildir. Bu hat elektrikli taşıtlarla çalıştırılsaydı, işletme maliyetlerini düşürür ve çevreye zararlı etkileri azaltır. Alternatif bir çözüm olarak, bu tezde ekonomik ve teknik olarak en uygun elektrikli araç çözümü; sürüş döngüsü, çevresel koşullar, yolcu doluluk oranları ve aracın karakteristiği ile elde edilen gereksinime göre belirlenmiştir.

Temmuz 2018'de, aracın karakteristiğini belirlemek için 18 metre mafsallı Metrobüs ile serbest durma testi yapıldı. Ek olarak, sürüş döngüsünü oluşturmak için; IMU ve GPS ile hizmet halindeki bir Metrobüs'ten konum, hız, ivme ve zaman verileri alındı. Yolcu akış verileri, otobüs operatöründen elde edilen veriler ile hesaplandı. Metrobüs'ün iklimlendirme sistemi güç ihtiyacını bulmak için, hava durumu verilerine ve güneş yüklerine göre ASHRAE standartlarına uygun olarak hesaplanmalar yapılmıştır. Tüm bu veriler ile sistem gereksinimleri elde edilmiştir.

Öncelikle, 18 metre mafsallı araç gövdesi seçilmiştir. Daha sonra, güç gereksinimlerine göre, çekiş sistemi ve sistem gereksinimlerini karşılamak için çekiş sistemi ile uyumlu çalışan uygun bir dişli kutusu seçilmiştir. Yolcu konforu için en önemli alt sistem olan

iklimlendirme sistemi, hesaplanan hava durumu verilerine göre seçilmiştir. Şarj cihazları ve farklı kimyalara sahip piller, farklı hatlar için seçilmiştir. En sonunda, farklı şarj stratejileri olan iki tür elektrikli filo tasarlanmıştır.

Çalışma sonunda, farklı bataryalara ve farklı şarj stratejilerine sahip filolar birbirleriyle ve mevcut dizel Metrobüs filosuyla karşılaştırıldı. Karşılaştırma için tüm bileşenlerin maliyeti paylaşılmıştır ve bu üç filonun toplam maliyeti hesaplanmıştır. Bu hesaplamalara göre İstanbul Metrobüs Hattı için en uygun elektrikli Metrobüs seçilmiştir.

Anahtar Kelimeler: Elektrikli otobüs sistemleri, Elektrikli araç teknolojileri, Batarya ve şarj teknolojileri, Ekonomik analiz, Toplam sahip olma maliyeti, Sistem tasarımı

ACKNOWLEDGMENTS

TABLE OF CONTENT

LIST OF TABLES

LIST OF FIGURES

SYMBOLS AND ABBREVIATIONS

Symbols

ρ	density of the air
g	gravitational acceleration
m	mass
v	velocity
a	acceleration
$R_{air}, R_{roll}, R_{grad}, R_{inertia}$	resistance forces
$P_{air}, P_{roll}, P_{grad}, P_{inertia}$	resistance powers
$V_{i1}, V_{i2}, V_{f1}, V_{f2}$	coast-down test velocities
t_1, t_2	coast-down test times
a_1, a_2	coast-down test accelerations
n_{bus}	number of bus
d_{bus}	passenger occupancy rate of the bus
$n_{bus\ capacity}$	passenger capacity of the bus
$n_{passenger}$	number of passenger in the bus
$\dot{Q}$	heat flows
M	metabolic heat production rate
A_{DU}	DuBois area
W_{avg}	average weight of a person
H_{avg}	average height of a person
θ_i	incident angle
γ	azimuth angle
β	altitude angle

Σ	surface tilt angle
δ	solar declination angle
L	latitude
H	hour angle
n_{day}	day of the year
S	surface are of the vehicle
U	overall heat transfer coefficient
$I_{Dir}, I_{Dir}, I_{Ref}$	irradiances
T_s, T_i	temperatures
λ	thickness of the material
k	conduction coefficient
h_o, h_i	convection coefficients
$\dot{V}_{ven}$	air flow rate for ventialation
i	electric current
$\emptyset_a, \emptyset_b, \emptyset_c$	phases
$r_{wheel\,eff}$	effective tire radius
$\varphi_{gearbox}$	gearbox ratio
η	efficiency
T	torques
F	forces
P	powers
μ	adhesion coefficients
$€$	Euro currency

Abbreviations

BRT	Bus Rapid Transit
EV	Electric Vehicle
HVAC	Heating, Ventilation and Air Conditioning
GPS	Global Positioning System
IMU	Inertial Measurement Unit
DC	Direct Current
AC	Alternating Current
CAD	Computer Aided Design
LTO	Lithium Titanate Battery
NMC	Lithium Nickel Manganese Cobalt Oxide Battery
LFP	Lithium Iron Phosphate Battery
TCO	Total Cost of Ownership

1 INTRODUCTION

1.1 Istanbul Metrobus Network

Istanbul Metrobus Network is a bus rapid transit (BRT) line. BRT has been defined by Federal Transit Administration as a rapid mode of transportation that can provide the quality of rail transit and the flexibility of buses. BRT is a flexible, rapid transit system that combines stations, buses, services, roads into an integrated system. Articulated diesel buses are widely used in BRT systems. [1]

In order to reduce the traffic density in Istanbul's main arteries and to provide fast and comfortable transportation, the Metrobus Network was first put into service in 2007. Today, with a total length of 50 km, from Beylidüzü to Söğütlüçeşme, Metrobus Network transports about 950 thousand passengers per day by passing through 44 stations from a dedicated bus route. The network uses only the vehicle road on the Fatih Sultan Mehmet Bridge, which connects Europe and Asia; other parts of the network are separated. Map of the Network is given in Figure 1-1 Map of the Istanbul Metrobus NetworkFigure 1-1.

Figure 1-1 Map of the Istanbul Metrobus Network [2]

Stations of the network are given in Table 1-1.

Table 1-1 Station of the Metrobus Network

No	Station	No	Station
1	Beylikdüzü	23	İncirli
2	Hadımköy	24	Zeytinburnu
3	Cumhuriyet Mah.	25	Merter
4	Beylikdüzü Belediye	26	Cevizlibağ
5	Beylikdüzü	27	Topkapı
6	Güzelyurt	28	Maltepe
7	Haramidere	29	Edirnekapı
8	Haramidere Sanayi	30	Ayvansaray
9	Saadetdere Mah.	31	Halıcıoğlu
10	Mustafa Kemal Paşa	32	Okmeydanı
11	Cihangir Üniversite Mah.	33	Darülazece
12	Avcılar Üni.Kampüsü	34	Okmeydanı Hastane
13	Şükrübey	35	Çağlayan
14	Büyükşehir Bld. Sos. Tesisleri	36	Mecidiyeköy
15	Küçük Çekmece	37	Zincirlikuyu
16	Cennet Mah.	38	Boğaziçi Köprüsü
17	Florya	39	Burhaniye
18	Beşyol	40	Altunizade
19	Sefaköy	41	Acıbadem
20	Yenibosna	42	Uzunçayır
21	Şirinevler	43	Fikirtepe
22	Bahçelievler	44	Söğütlüçeşme

Metrobus Network is a hybrid system. Some features of the line are similar to public buses; others are similar to the metro. For example, the vehicle is an articulated bus with rubber tires, but it has a dedicated route similar to metro and passengers are validating their ticket at the entrance of the stations, not on the bus. A photo of a station is shown in Figure 1-2.

Figure 1-2 A Metrobus Station [3]

Istanbul Metrobus Network has one track, in this track there are 8 different lines. These lines are given in Table 1-2.

Table 1-2 Istanbul Metrobus Lines

Line Code	First Station	Last Station	Working hours
34	Avcılar	Zincirlikuyu	Daytime (Partially)
34A	Söğütlüçeşme	Cevizlibağ	Daytime (Partially)
34AS	Avcılar	Söğütlüçeşme	Daytime
34BZ	Beylikdüzü	Zincirlikuyu	Daytime
34C	Beylikdüzü	Cevizlibağ	Daytime (Partially)
34G	Beylikdüzü	Söğütlüçeşme	Night
34U	Uzunçayır	Zincirlikuyu	Daytime (Partially)
34Z	Zincirlikuyu	Söğütlüçeşme	Daytime (Partially)

In this work, five main lines (34, 34Z, 34AS, 34BZ, 34C) are considered because 34U and 34A don't have many buses and their working hours are limited. On the other hand 34G is a special line that works only from 24:00 to 06:00 and it doesn't have many buses too. Working hours of five main lines are from 06:00 to 24:00.

There are 3 different vehicles in Metrobus fleet with different exhaust emission standard but the fuel of these vehicles is diesel. Composition of the Metrobus fleet is presented in Table 1-3.

Table 1-3 Fleet of the Metrobus Network

Brand and model	Exhaust emission standard	Fuel	Number
Company A – Model 1	EURO 4/5	Diesel	249
Company B – Model 1	EURO 5	Diesel	49
Company A – Model 2	EURO 5	Diesel	295
		Total number	593

1.2 Motivation and Objective

Global warming probably is the one the biggest environmental problems of today's world. Over the last fifteen years, environmental foundations and organizations have invested hundreds of millions of dollars into combating global warming [4]. Global warming is partly due to transportation activities which produce substantial amounts of carbon dioxide emissions. In addition, these have side effects like noise pollution and traffic congestion. It is believed that the transportation sector, which consumes the quarter of the world's energy production, should be made more environmentally sensitive for a sustainable growth [5]. Use of electric buses for public transportation may be an alternative solution in order to decrease noise and air pollutions [6]. As a matter of fact, due to ecological and economic concerns, there is an increasing interest in electric buses. Bus producers are observed to invest increasingly in the production of electric and hybrid buses [7].

As far as fuel and electrical energy consumptions calculated for the SORT 2 driving cycle for 12-meter buses are concerned, it is shown that electrical buses perform better than buses with internal combustion engines powered with CNG or diesel fuel. Energy consumptions per km of CNG, diesel fuel and electric buses are 4.98 kWh, 3.90 kWh and 0.95kWh, respectively [8].

For bus operators, it may sometimes make sense to pick up a ready-made electric bus; however, for large bus lines that have thousands of passengers daily by a populous bus fleet, it may be more efficient to use a bus that is designed especially for the specific line. In order to design an efficient electric bus for a specific line, design requirements should be carefully determined.

The objective of this study is designing a holistic electric vehicle system solution for Istanbul Metrobus Network and comparing the solution with the current fossil fuel based transportation. For the design, route specific requirements, passenger movements, environmental conditions, costs are considered. Additionally, the labor force, infrastructure, abilities and demands of the bus operator are also considered in the design phase for the implementation.

1.3 Electric Vehicle System of ASELSAN

Avenue EV is an electric bus that is developed by ASELSAN's. During the design phase a bus manufacturer was responsible for the chassis and mechanical parts, the responsibilities of ASELSAN was the electric motor, inverter, electric vehicle control unit, power distribution unit and driver interface panel.

Thanks to its experience and knowledge from Avenue EV, ASELSAN is planning to be responsible for the different electrification projects. In this study to minimize the design costs, it is desired to use electric vehicle system of ASELSAN. Electric vehicle system of ASELSAN is shown in Figure 1-3.

Figure 1-3 Electric Vehicle System of ASELSAN [9]

In the scope of these study units for the traction are evaluated. These units are;

- Traction motor and inverter,
- Motor drive and control unit,
- Auxiliary power supply

1.4 Organization and Content Thesis

This study consists of 4 main stages, tests&analysis, determination of system requirement from tests&analysis data, system design and comparison.

In the first stage, by a coast down test, characteristic of the vehicle is obtained and by a driving cycle test, velocity, acceleration, slope profile of the vehicle and the network is obtained. Furthermore, passenger density data and vehicle schedule, which are obtained from operator company, are processed in order to obtain the number of passenger in Metrobus between each station for each hour. Additionally, weather data which contain temperature and relative humidity of Istanbul are presented.

From the test results and data analysis, power consumption of traction system is obtained. Similarly, auxiliary power consumptions and consumptions due to inefficiencies of the vehicle are predicted.

In the third stage, according to requirements, a suitable electric vehicle system is designed. Each component such as, engine, HVAC system, gearbox, battery are selected carefully according to system requirements obtained in previous part. After the composition of the each suitable electric vehicle solution, energy consumption of the vehicle is recalculated. The reason of this recalculation is that, each electric vehicle solution has different energy consumption due their different weight, inefficiencies etc. Furthermore, potential of the regenerative braking of the vehicle is calculated to determine the energy that can be recuperated by the braking system.

Finally in the last stage, current fossil fuel based Metrobus Network is compared with proposed electric bus solution in this study.

To summarize the organization of the study, a flow chart of the selection process of the solution is shown in Figure 1-4.
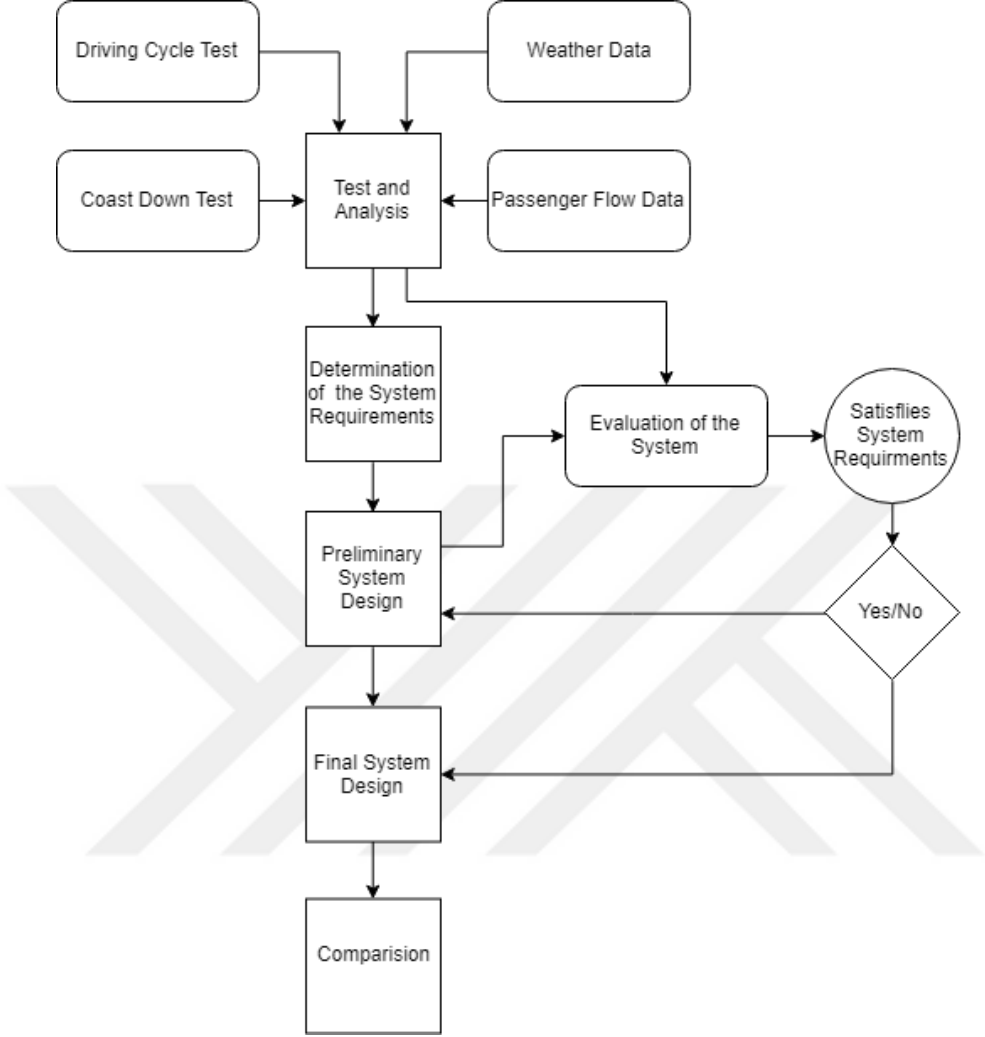
Figure 1-4 Flow chart of the system design

2 LITERATURE REVIEW

2.1 Electrification

P. Sinhuber presented a method to determine the route specific energy consumption of local public transport buses and the method is applied to different bus lines. In the study internet mapping services are being used to build and adjust a set of route data that is being used as simulation input. Results of the study showed that buses require very heavy batteries with today's common battery energy densities for the overnight charging strategy [10]. M.Rogge developed a model of a fast charging battery buses in order to determine the energy consumption and battery requirement of a specific route. The charging strategy based on charging the battery during dwell time has a strong linkage between vehicle scheduling and the infrastructure of the line [11]. In the work of A. Kunith energy consumption of each route segment of a bus line was determined according to several data such as, bus type, traffic and route. Then, a mixed-integer linear optimization model was developed so as to minimize the number of location of charging stations and the battery capacity of a fast charging electric bus [12]. An economic analysis is conducted by means of total cost of owner ship the study of D.Göhlich. The study started with the development of a simulation model to simulate the daily energy need. Then according to model, potential electric bus solution determined and evaluated [13]. Additionally, in another study, D.Göhlich suggested a holistic design methodology determine the most suitable electric bus solution for a given strategic and operational requirement. The relevant energy sources, charging strategies and interfaces, on-board energy sources, drive motors, drive topologies, body types and HVAC systems are structured by a morphological matrix and analyzed. In the study researcher concluded that HVAC system is the most energy consuming auxiliary system therefore must be given special attention in electric bus system design. Additionally, the heating case is considered as the most critical condition if zero-emission operation is required [14].

2.2 Batteries and total cost of ownership

In the study of O.Vilppo and J.Markkula, an economic feasibility analysis is performed for electric buses that are the only medium of transport of a mid-sized city. Total cost of ownership of electric buses and diesel buses are compared and two types of li-ion batteries are compared which are LFP and LTO. Additionally, two types of charging strategies are compared. These charging strategies are depot charging and end stop charging. Thanks to the longer life cycle of LTO batteries, they are better solution than LFP. Furthermore,

positive effects such as longer cycle life, less heating, flexibility and negative effects such as higher cost initial cost, higher weight of oversizing the battery compared [15].In the study of M. Patkany et al. lifecycle costs of electric bus and diesel bus are compared. In the study time value of money is considered. At the beginning of the study theoretical background of life cycle cost is given and the life cycle of diesel and electric bus are calculated accordingly. Additionally, prices of different component from different source are shared [16].A.Lajunen and T.Lipman evaluated the carbon dioxide emissions and life cycle costs of different types of city buses. In the Autonomie vehicle simulation software, a model is developed for different powertrains. The carbon oxide emissions of different type of buses are calculated. For the calculations, two different operating environment case are considered which are California and Finland. Carbon emission, maintenance, operating and purchasing are considered for the life cycle cost calculation [17]. E. C. McKenzie presented a life cycle cost assessment and green emissions of different transit buses. It is found out that alternative fuel buses are able to reduce the operating costs of public buses [18]. A.Milner proposed a new aging model for li-ion batteries based on crack propagation models. An exponential dependence of aging on stress such as discharge depth is provided. Measure of stress is derived from arbitrary charge and discharge. Also, the model is combined with an empirical circuit model [19].

2.3   Thermal loads

Exergy analysis was implemented to improve the inter-city bus air-conditioning system design in Tosun et al. [20]. In this study hourly cooling capacity was determined with analysis program (HAP). D. Ružić investigated thermal interaction between a human body and a tractor cab. In this study a heat exchange model for tractor cab was presented. From the model, total heat loads of the cabin and sources of the heat such as sun light and powertrain were calculated. Additionally, efficiency of the air distribution system and thermal sensation were evaluated [21]. In the study of F. Stancato et al. (1992) a mathematical model was developed to simulate cooling loads in a cab and the results of the simulation were compared with experimental results [22]. M.A. Fayazbakhsh et al. developed a model to calculate the heat load of an internal combustion engine car. This comprehensive model consists of each heat source of a vehicle such as, metabolic loads, solar loads, powertrain loads. In the study from each load overall heat load of a vehicle was determined. [23]

2.4 Regenerative braking

In the study of F. Sangtarash, effects of different regenerative braking strategies are investigated. For this investigation a traction system model of a hybrid bus is developed in AVL/CRUISE software. Finally, the braking performance and energy recovery from the braking system is compared for these different approaches [24]. In the study of, J. Zhang et al., an efficient method to assist hybrid electric buses for better fuel is provided. In this study, three different regenerative braking systems are described and tested. Results of the study indicate that, all systems provide energy recovery while operating safe and predictable manner [25].

2.5 Contribution of the thesis

In the literature, there are studies on regenerative braking, thermal loads, electric vehicle design, battery sizing. In these studies, only the relevant subjects are discussed independently of the other subjects. However, all these issues affect each other. For example, capacity of the battery changes the energy consumption of the vehicle due to its weight, energy consumption of the vehicle changes the energy requirement of the battery or similarly regenerative braking system changes reduces the energy consumption of the vehicle. In this thesis, these mutual effects are considered and system is designed according to this effects.

Additionally, in the literature there are electrification studies. In these studies, several details such as passenger occupancy rates, thermal loads, inefficiencies are omitted or assumed to be constant value. In this thesis, electric Metrobus lines are designed according to hourly passenger occupancy rates and hourly thermal loads. This leads to calculate accurate energy consumption values, in other words accurate battery size.

Furthermore, several vehicle dynamics calculations and HVAC calculations are done for the selection of the regenerative braking strategy and HVAC system, respectively. This is another feature that distinguishes this inclusive work from others.

3 TEST AND ANALYSIS OF THE VEHICLE AND METROBUS NETWORK

3.1 Bus Characteristic

As the operator company has no intention to change the current infrastructure, stations and roads that was designed for current articulated bus, body of the electric vehicle assumed to be the same as the bus Company A – Model 1. Body properties of the vehicle are listed in Table 3-1.

Table 3-1 Body properties of Company A – Model 1[19]

Empty weight	18500 kg
Maximum weight	32000 kg
Tires	275/70/T22.5
Number of seats	43+1
Maximum number of passenger	181
Length	19725 mm
Width	2550 mm
Maximum height	3120 mm
Distance between 1.and 2.axle	5900 mm
Distance between 2. And 3. Axle	5990 mm
Distance between 3. And 4. Axle	1600 mm

3.1.1 Background

Figure 3-1 shows the main resistive and tractive forces acting on the vehicle.
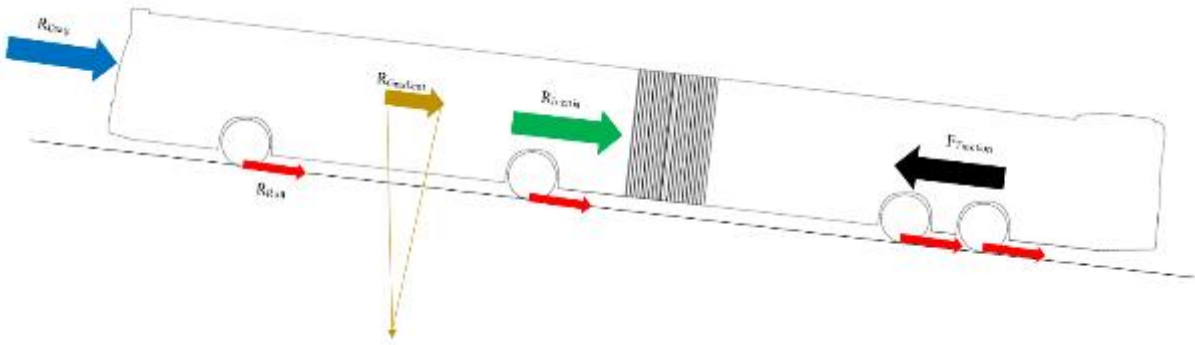
Figure 3-1 Forces acting on the vehicle

The drag resistance force acting on the vehicle [20];

$$R_{Drag} = \frac{1}{2} C_d \rho A v^2 \tag{3.1}$$

Where C_d refers to drag coefficient of the vehicle, ρ refers to density of the air, A refers to front area of the vehicle and v refers to velocity of the vehicle.

The rolling resistance force acting on the vehicle [27];

$$R_{Roll} = C_r m g \tag{3.2}$$

Where C_r refers to rolling coefficient of the vehicle, m refers to mass of the vehicle and g refers to gravitational acceleration.

The gradient resistance force acting on the vehicle [27];

$$R_{grad} = m g sin(\theta) \tag{3.3}$$

Where m refers to mass of the vehicle, g refers to gravitational acceleration and θ refers to slope of the road.

The inertial resistance force acting on the vehicle [27];

$$R_{inertia} = m_{eq} a \tag{3.4}$$

Where m_{eq} refers to equivalent mass of the vehicle and a refers to the acceleration of the vehicle. From the calculation based on 3D CAD models of the rotating part it is found out rotational inertias of rotating parts are very small compared to the total mass of the vehicle. Thus it is assumed that m_{eq} is equal to m.

3.1.2 Coast-Down test

Coast down is one of the most frequent tests for motor vehicles and consists in vehicle launch from a certain speed with the engine ungeared, simultaneously recording the speed and travelled distance until vehicle stops. Aim of this test is to evaluate the values of the resistant forces acting on the vehicle at certain speed and road conditions [28].

3.1.2.1 Test Conditions

3.1.2.1.1 Test Track

The coast down test was performed at Istanbul-Turkey. The test track is not a dedicated track for vehicle tests, but it is convenient track for coast down tests because the elevation difference is negligible and it is straight. The change in elevation of the track versus time is given in Figure 3-2. Elevation data was acquired during the cost down test and the

elevation of the start point assumed to be zero reference point. As it can be seen from the figure the maximum elevation change is less than 1.6 m so, the test track can be considered straight.
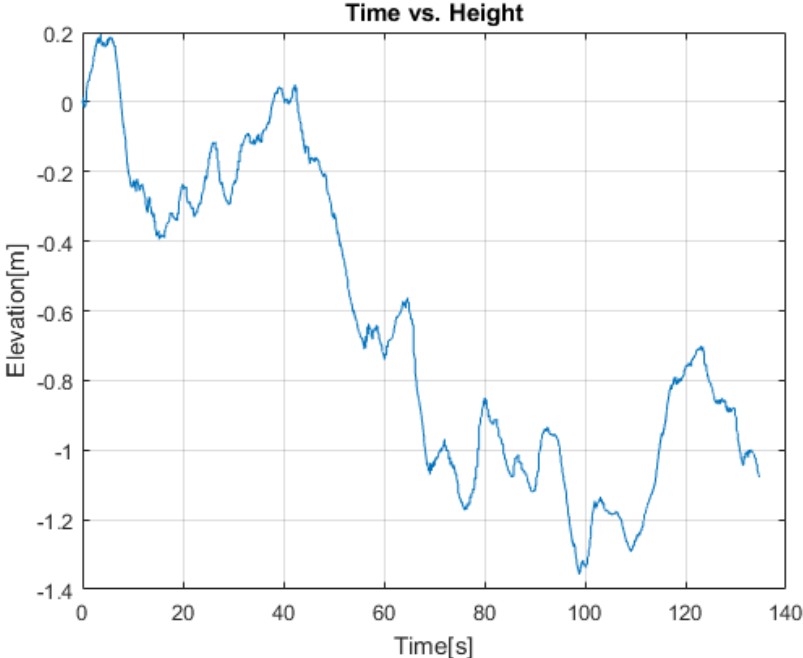
Figure 3-2 Change in elevation versus time

The test track shown on the map with red line in the Figure 3-3.
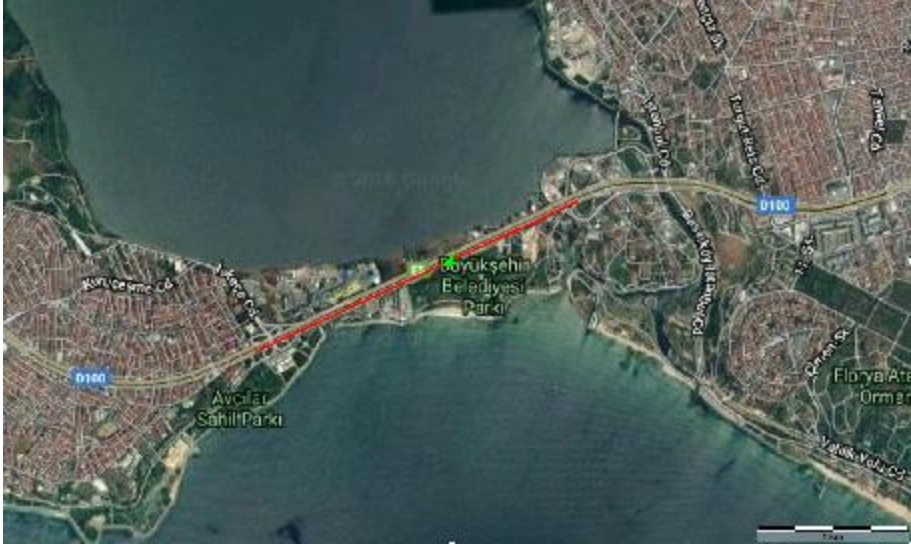
Figure 3-3 Test track

During the test there was not any other vehicle in both direction of the test road. Photos from the test track show in Figure 3-4 and Figure 3-5 .

Figure 3-4 Photo from the test track

Figure 3-5 Photo from the test track

3.1.2.1.2 Wind, temperature and humidity

Wind speed was measured during the test with an anemometer. Photos of some measurement during the test are shown in Figure 3-6 and Figure 3-7. The speed of the wind was very low; it fluctuated between 0-1 m/s. Since the wind speed was low it is neglected.

Figure 3-6 Wind speed measurement

Figure 3-7 Wind speed measurement

Weather conditions at test day according to Turkish State Meteorological Service are given in Table 3-2.

Table 3-2 Weather conditions at test day

Parameter	Value
Time	05 July 2018 between 13.00 and 15.00
Location	Turkey-Istanbul-Küçükçekmece
Temperature	33 °C
Humidity	60 %
Wind speed	0-1 m/s (negligible)

3.1.2.1.3 Vehicle

The test vehicle is Company A – Model 1. Technical data of the vehicle are given in Table 3-3 [26] [29].

Table 3-3 Technical data of Company A – Model 1

Torque	1600 Nm @1100rpm
Maximum power	260kW
Transmission	Automatic
Empty weight	18500 kg
Maximum weight	32000 kg
Tires	275/70/T22,5
Number of seats	43+1
Maximum number of passenger	181
Length	19725 mm
Width	2550 mm
Maximum height	3120 mm
Distance between 1.and 2.axle	5900 mm
Distance between 2. And 3. Axle	5990 mm
Distance between 3. And 4. Axle	1600 mm

3.1.2.1.4 Test Equipment

Test was performed with an inertial measurement unit (IMU) with global positioning system (GPS). Data acquisition frequency during the test was 10 Hz.

Navigation specifications of the device are given in Table 3-4 [30].

Table 3-4 Navigation specification of the IMU

Parameter	Value
Horizontal position accuracy	2.0 m
Vertical position accuracy	3.0 m
Velocity accuracy	0.05 m/s
Roll & Pitch accuracy (static-dynamic)	$0.1^{o} - 0.2^{o}$
Heading accuracy (static-dynamic)	$0.5^{o} - 0.8^{o}$
Output data rate	Up to 100Hz

Sensor specifications of the device are given in Table 3-5 [30].

Table 3-5 Sensor specifications of IMU

Parameter	Accelerometers	Gyroscope	Magnetometers	Pressure
Range	2 g 4 g 16 g	$250^{o}/s$ $500^{o}/s$ $2000^{o}/s$	2 G 4 G 8 G	10 to 120 kPa
Noise density	150 μg/Hz	$0.008^{o}/s/\sqrt{Hz}$	210 μg /√Hz	0.56Pa√Hz
Bandwidth	400 Hz	400 Hz	110 Hz	50 Hz

GNSS specifications of the IMU are given Table 3-6 [30].

Table 3-6 GNSS specifications of IMU

Parameter	Value
Update rate	10Hz
Horizontal position accuracy	2.5 m
Velocity accuracy	0.05 m/s
Timing accuracy	30 ns
Acceleration limit	4 g

Principle axes of the vehicle are illustrated in Figure 3-8.
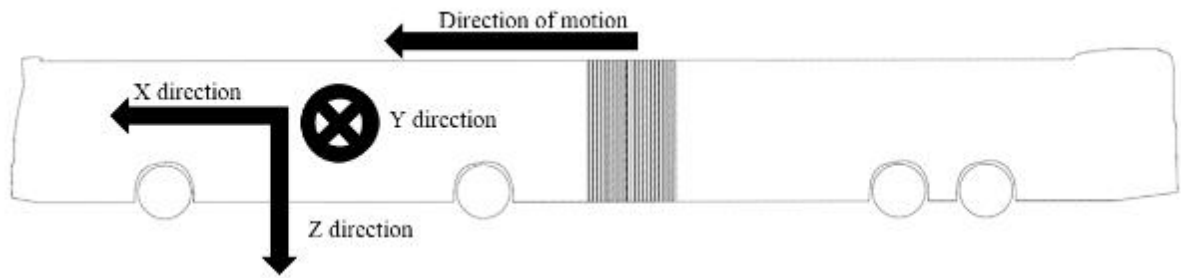
Figure 3-8 Principle axes of the vehicle

The longitudinal position of the IMU is determined randomly since the lateral motions of the vehicle were not important for the test. However, since the lateral position of the IMU is important for the measurement of the longitudinal motions of the vehicle, IMU was placed at the middle of the vehicle in y direction. Photo of the computer connected to IMU and IMU device (inside red circle) is given in Figure 3-9 .
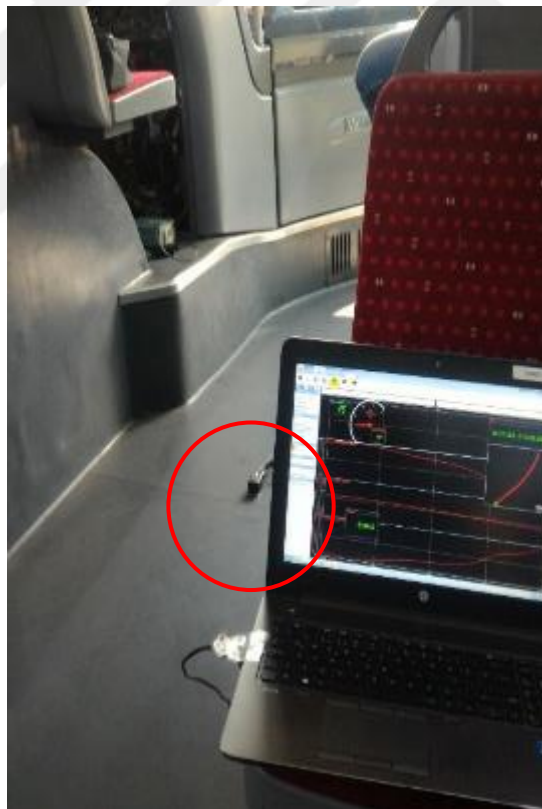
Figure 3-9 Photo of the test computer and IMU

In order to get the best connection between satellites and GPS, GPS antenna was placed outside of the vehicle. Relative position of the GPS antenna with respect to IMU device was described in the IMU software so as to obtain best accuracy. Photo of the GPS antenna can be seen in Figure 3-10 .

Figure 3-10 Position of the GPS antenna

3.1.2.2   Test Results

The change in velocity versus time is shown in Figure 3-11.
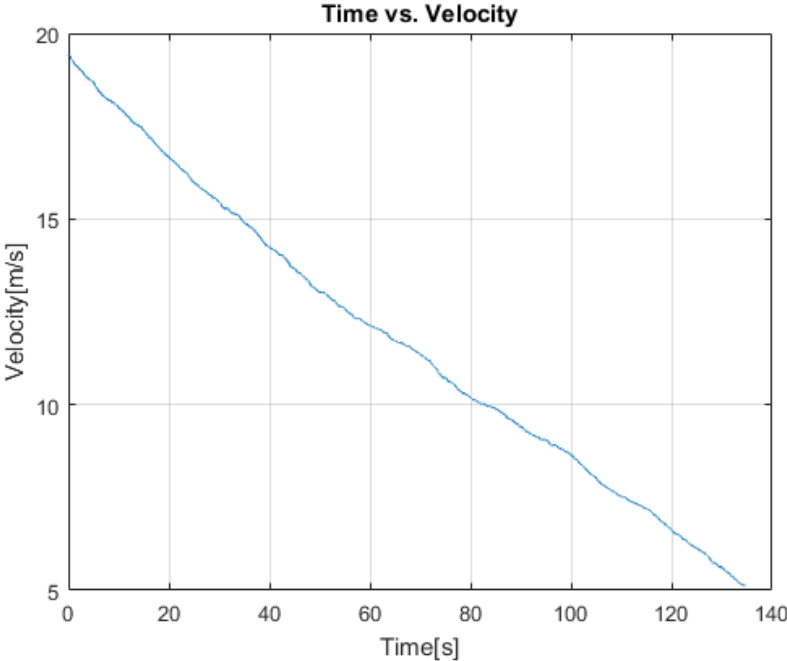
Figure 3-11 Change in velocity versus time.

The distance travelled of vehicle with respect to time is given in Figure 3-12.
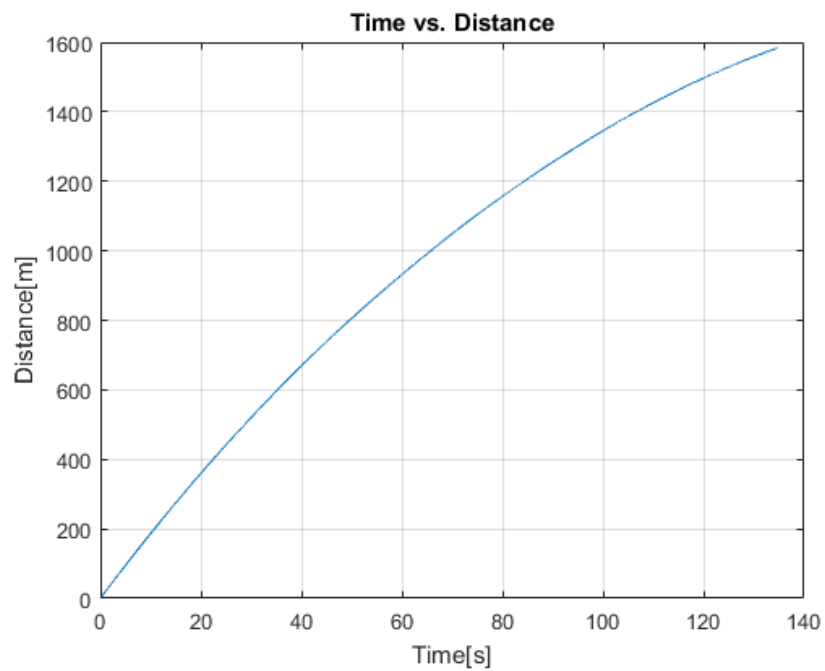
Figure 3-12 Distance travelled of vehicle against time

The change in slope versus time is shown in Figure 3-13.
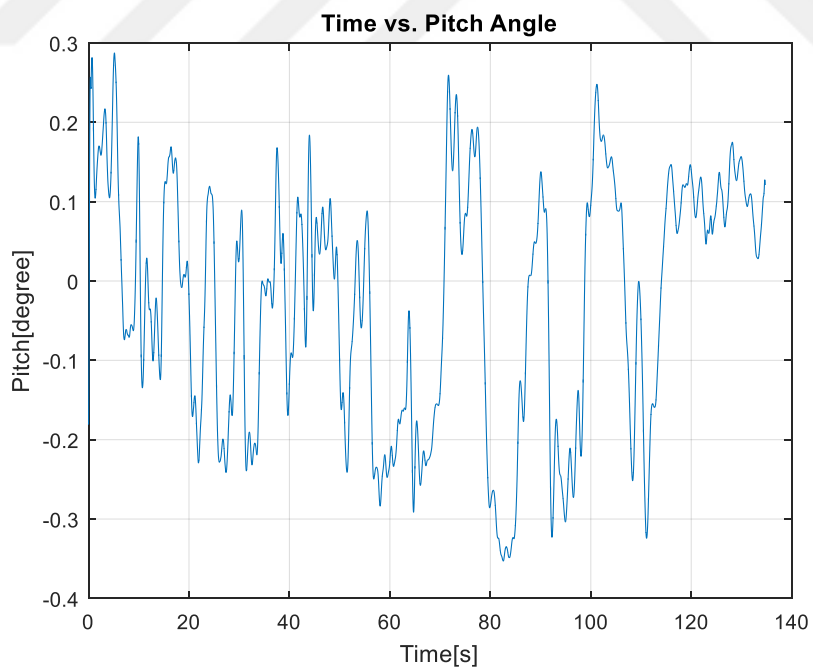
Figure 3-13 The change in slope versus time

It can be seen in Figure 3-13 slope changes between -0.4 and 0.3. The force due to slope is obtained from equation (3.5).

$$R_{grad} = mg sin(\theta) \qquad (3.5)$$

where

$$g = 9.81 \ \frac{m}{s^2} \qquad (3.6)$$

and m refers to mass of the vehicle, θ refers to slope of the road in degree.

The force obtained from equation (3.5) versus time is given in Figure 3-14.
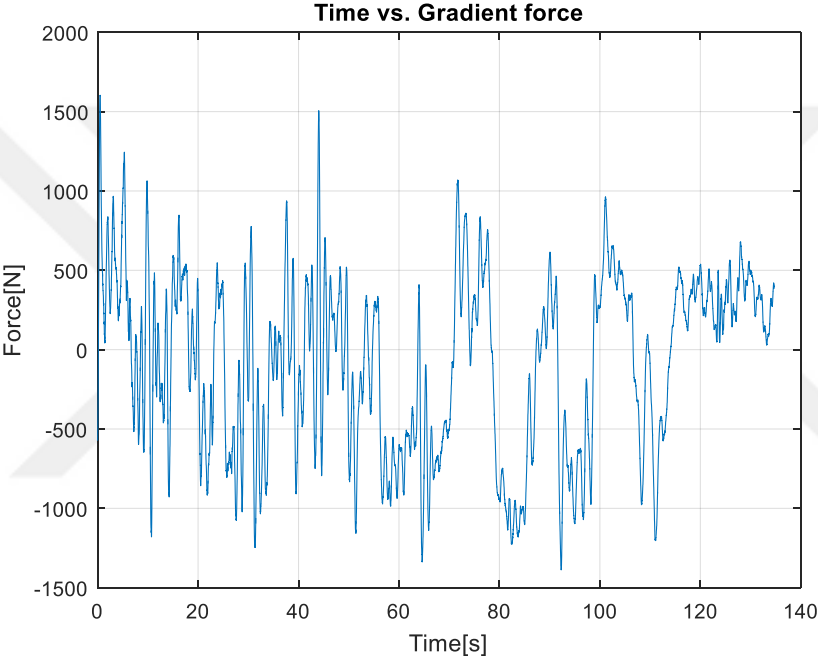
Figure 3-14 Gradient force versus time

The acceleration of the vehicle due to gradient force is obtained from equation (3.7).

$$a_{grad} = \frac{R_{grad}}{m} \tag{3.7}$$

The acceleration of the vehicle obtain from equation (3.7) versus time is given in Figure 3-15.
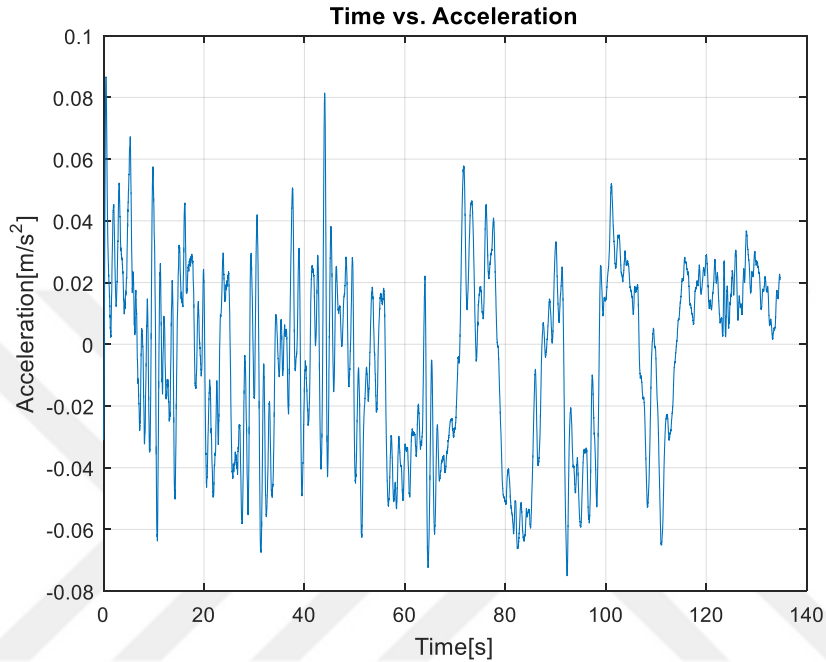
Figure 3-15 Acceleration due to gradient force versus time

The effect of the acceleration due to gradient force on the velocity of the vehicle is obtained from equation (3.8).

$$v_{vehicle\ without\ slope} = v_{vehicle} - a_{grad} x \Delta t \tag{3.8}$$

Where $v_{vehicle}$ refers to the velocity of the vehicle measured during the test, $v_{vehicle\ without\ slope}$ refers to the velocity of the vehicle without the effect of gradient force.

$v_{vehicle\,without\,slope}$ is obtained from equation (3.8) and $v_{vehicle}$ versus time is given in Figure 3-16.
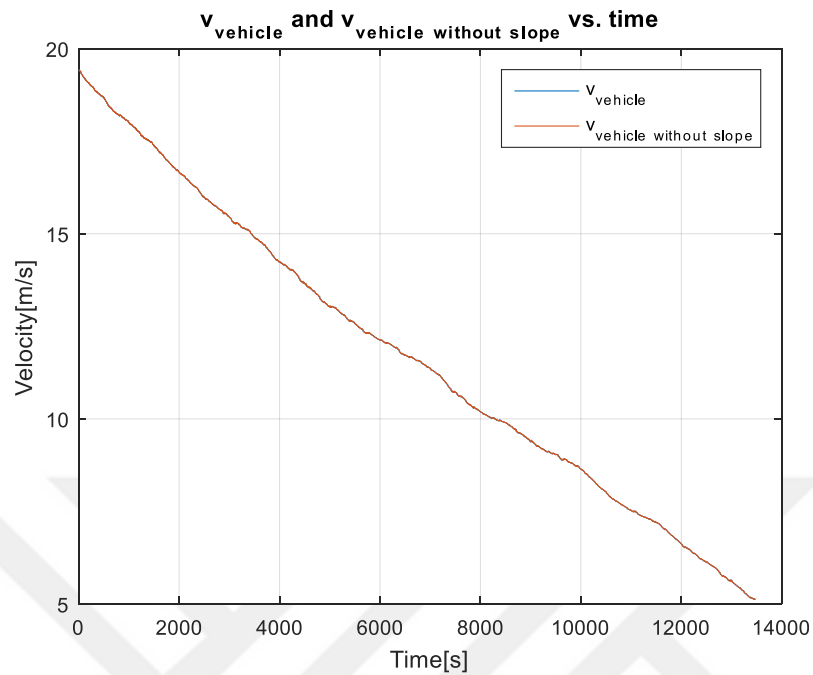
Figure 3-16 Velocity of the vehicle measured during the test and vehicle speed without effect of the gradient force

As it can be clearly seen in Figure 3-16, the effect of the gradient force on vehicle velocity due to the slope change is negligible. So, for the coast down calculation, measured velocity of the vehicle is considered.

In order to calculate C_d and C_r which refer drag resistance coefficient and rolling resistance coefficient, respectively, a second degree polynomial curve is fitted to the set of velocity data point. Velocity of the vehicle and the polynomial fitted to the velocity data versus time are shown in Figure 3-17.
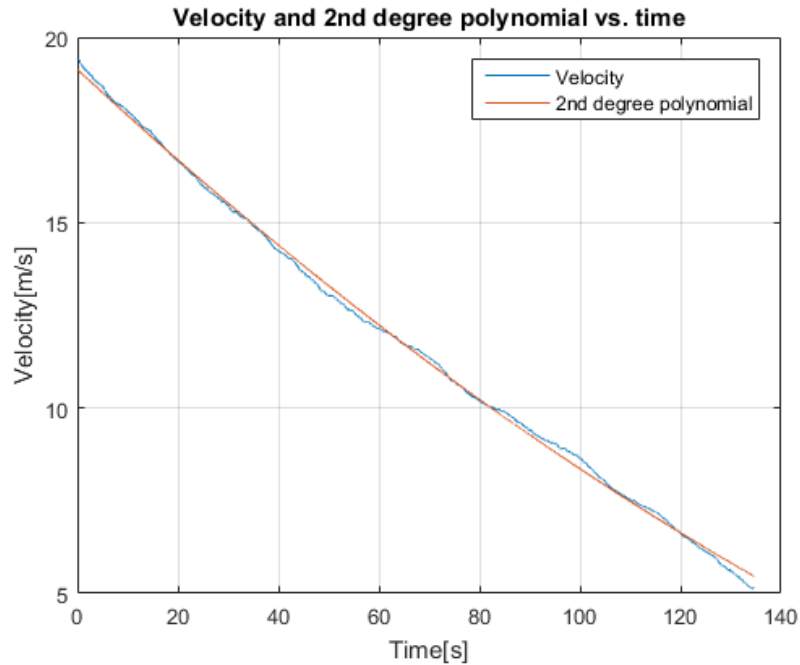
Figure 3-17 Velocity and 2nd degree polynomial

C_d and C_r can be determined from two coast-down tests: one at a high speed and the other at a lower speed, however, since the test track was long enough to perform high speed test and low speed test in one go, one test was performed.

Table 3-7 Measurement of coast down test

	High-speed test	Low-speed test
Initial speed	V_{i1}	V_{i2}
Final speed	V_{f1}	V_{f2}
Time duration	t_1	t_2
Average speed	$V_1 = \dfrac{V_{i1} + V_{f1}}{2}$	$V_2 = \dfrac{V_{i2} + V_{f2}}{2}$
Average deceleration	$a_1 = \dfrac{V_{i1} - V_{f1}}{t_1}$	$a_2 = \dfrac{V_{i2} - V_{f2}}{t_2}$

$$R_{air1} + R_{roll1} = 0.5\rho C_d A V_1^2 + C_r mg = ma_1 \tag{3.9}$$

$$R_{air2} + R_{roll2} = 0.5\rho C_d A V_2^2 + C_r mg = ma_2 \tag{3.10}$$

$$C_d = \frac{m(a_1 - a_2)}{0.5\rho A(V_1^2 - V_2^2)} \tag{3.11}$$

$$C_r = \frac{a_1 V_2^2 - a_2 V_1^2}{g(V_2^2 - V_1^2)} \tag{3.12}$$

The frontal area of the vehicle is 8.04 m^3 and from equations (3.9), (3.10), (3.11) and (3.12) C_d and C_r are obtained.

$$C_d = 0.5833 \tag{3.13}$$

$$C_r = 0.0079 \tag{3.14}$$

3.2 Driving Cycle Test

3.2.1 Driving cycle

In order to obtain the driving cycle of all lines a test was performed. An IMU is placed on the bus so as to acquire velocity and acceleration of the vehicle. During the test, there were only the driver and two staffs from the test team. The driver drove the vehicle in standard operation conditions which includes obeying speed regulation and passenger drop-off and pick-up times. Thus a general driving cycle is obtained. Change of the velocity of the bus versus time and change of the acceleration of the bus versus time are given in Figure 3-18 and Figure 3-19, respectively.
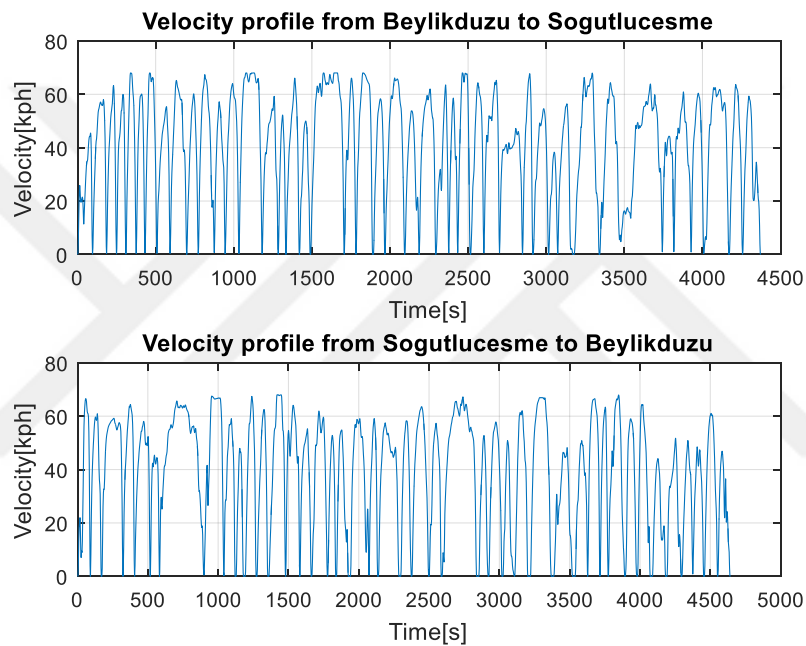
Figure 3-18 Velocity of the bus versus time
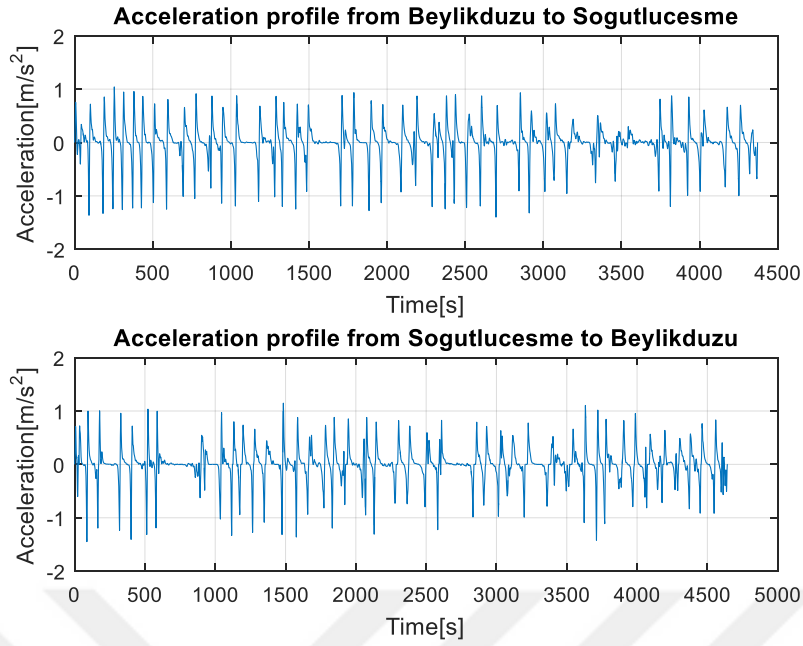
Figure 3-19 Acceleration of the bus versus time

In addition to velocity and acceleration data, other auxiliary data such as altitude above sea level, position of the bus and distance travelled are acquired. Change of the distance travelled versus time is given in Figure 3-20.
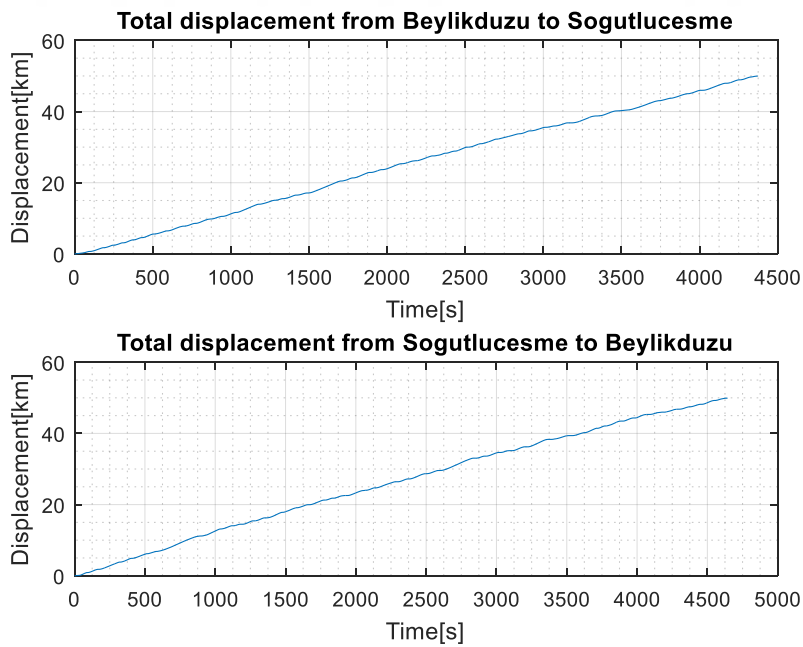
Figure 3-20 Distance travelled versus time

Change of the altitude above sea level versus time is given in Figure 3-21.
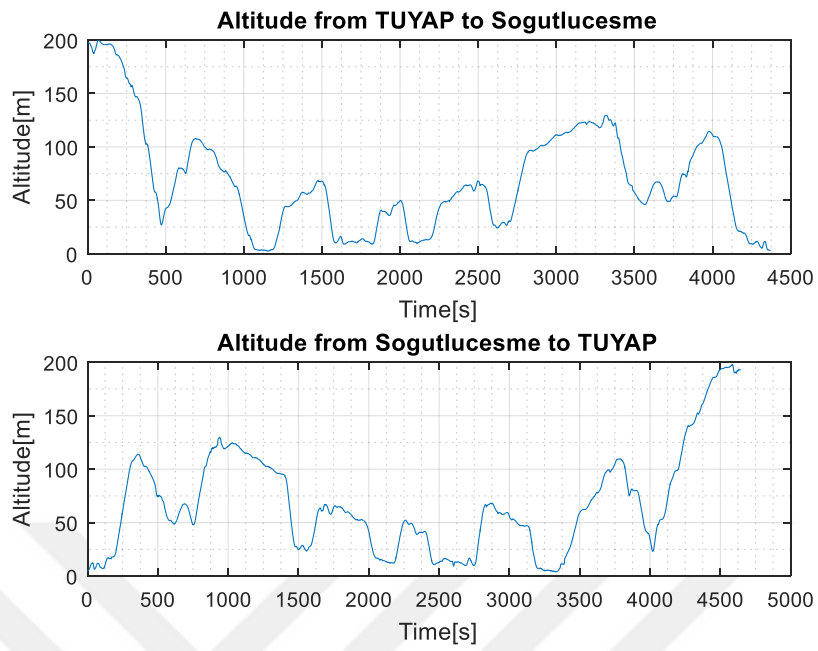
Figure 3-21 Altitude versus time

3.3 Passenger Flow and Bus schedule

Number of passengers in the Metrobus is an important parameter to estimate the power requirement because the mass of the fully loaded Metrobus which is about 2 times of an empty Metrobus.

In order to calculate number of passengers transported between two stations, hourly passenger occupancy rates and number of buses assigned are obtained from bus operator company.

Buses start to transport passenger from first station of each line. In order to determine the number of buses running between two stations within a certain time interval, travel time between each station were measured. Time intervals and stations are represented in Figure 3-22.
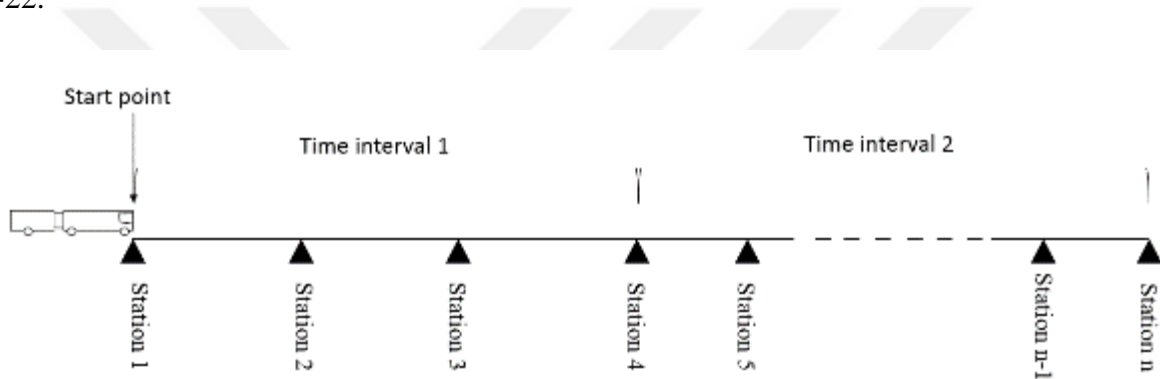
Figure 3-22 Representation of time intervals and stations

From these data, firstly number of buses running between two stations by hour is obtained. Secondly, from equation (3.15) number of passenger transported from one station to another station is obtained for each station.

$$n_{bus} x \ d_{bus} x \ n_{bus \ capacity} = n_{passenger} \qquad (3.15)$$

Where n_{bus} refers to the number of bus that passes between each station by hour, d_{bus} refers to hourly passenger density in the bus, $n_{bus \ capacity}$ refers to the passenger capacity of the bus ,which is 181, and $n_{passenger}$ refers to the number of passenger transported between two stations.

3.3.1 Passenger occupancy rates

The change of passenger occupancy rate by hour and station in Söğütlüçeşme direction is illustrated in Figure 3-23 as a heat map. As it can be seen from the heat map around 8 o'clock buses are crowded because business hours start at 9 o'clock. Another important point in the heat map is, there are sharp changes at 11th, 26th and 37th stations since they are transfer stations for subways and they also the last or first station of lines.
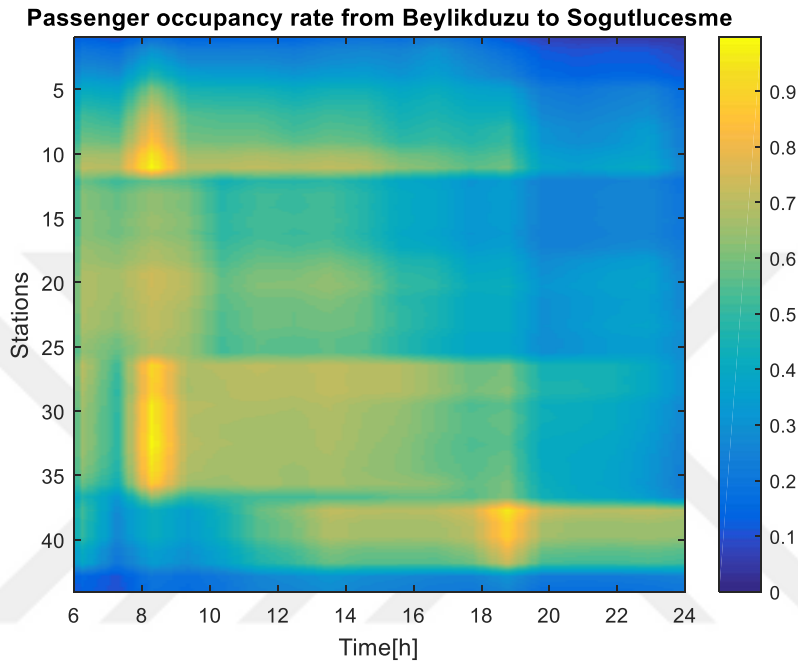
Figure 3-23 Passenger occupancy rate from Beylikdüzü to Söğütlüçeşme

The change of passenger occupancy rate by hour and station in Beylikdüzü direction is illustrated in Figure 3-24 as a heat map. As it can be seen from the heat map around 18 o'clock buses are crowded because business hours finish at 18 o'clock. Another important point in the heat map is there are sharp changes at 11th, 26th and 37th stations since they are transfer stations for subways and they also the last or first station of lines.
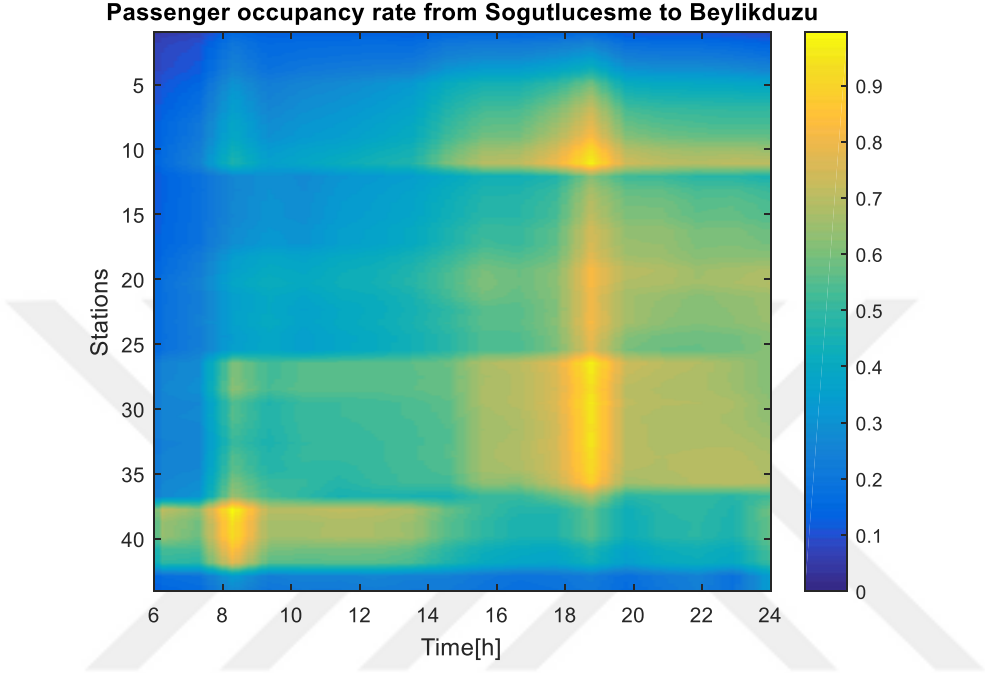
Figure 3-24 Passenger occupancy rate from Sogutlucesme to Beylikduzu

3.3.2 Number of bus in service

The number of bus in service by hour and by station is illustrated in Söğütlüçeşme and Beylikdüzü direction in Figure 3-25 and Figure 3-26, respectively. As it can be seen from maps there are increases from 7h to 9h and from 18h to 21h. The reason of this increase is the bus operator company assigns more Metrobus in order to overcome the growing crowd of passengers who is going to work or home. Additionally, sharp changes at end point or star point of lines at 11th, 26th and 37th stations can be observed easily.
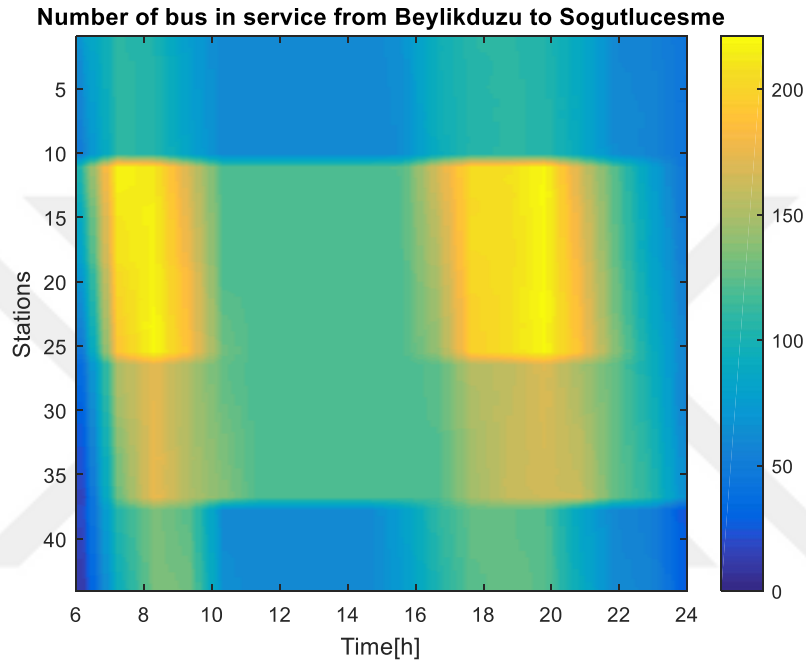
Figure 3-25 Number of bus in service from Beylikdüzü to Söğütlüçeşme

The average number of the passenger is 84.41.
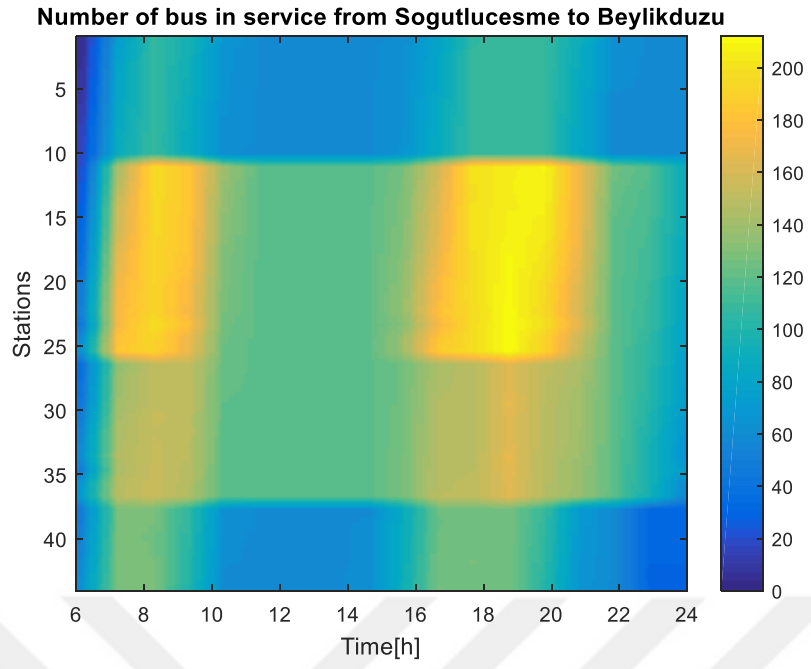
Figure 3-26 Number of bus in service from Söğütlüçeşme to Beylikdüzü

3.3.3 Number of passenger

From equation (3.15) total number of passenger is obtained.

The number of passenger by hour and station is illustrated in Figure 3-27 as a heat map. As it can be seen from the heat map around 8 o'clock there is an increase in number of passenger in Söğütlüçeşme direction. The reason of this increase is the working hours and location of workplaces and settlements. Workplaces are generally located in the city center and settlements are located at areas around the city center.
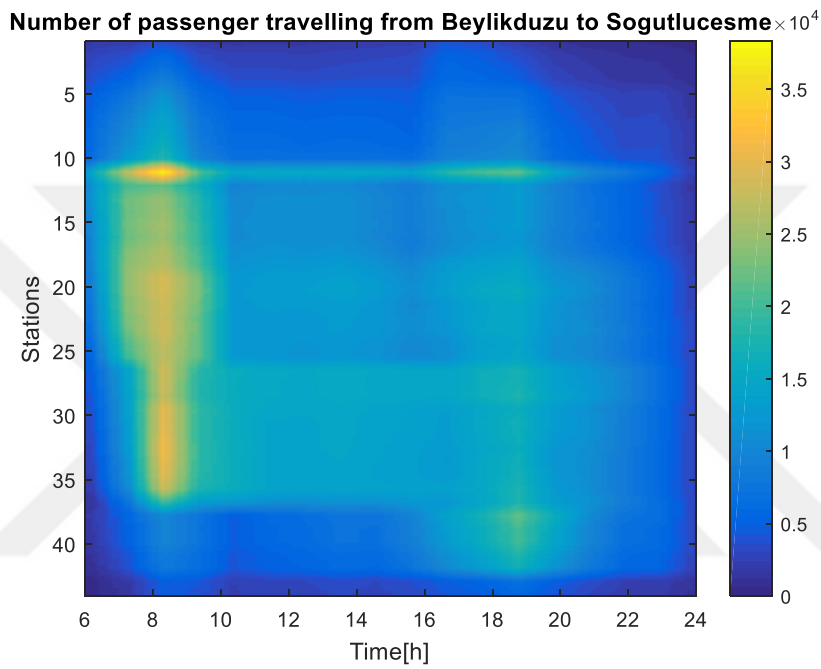
Figure 3-27 Number of passenger travelling from Söğütlüçeşme to Beylikdüzü

On the contrary round 19 o'clock there is an increase in number of passenger in Beylikdüzü direction as it can be observed from Figure 3-28 because people are trying to go home from their workplaces.
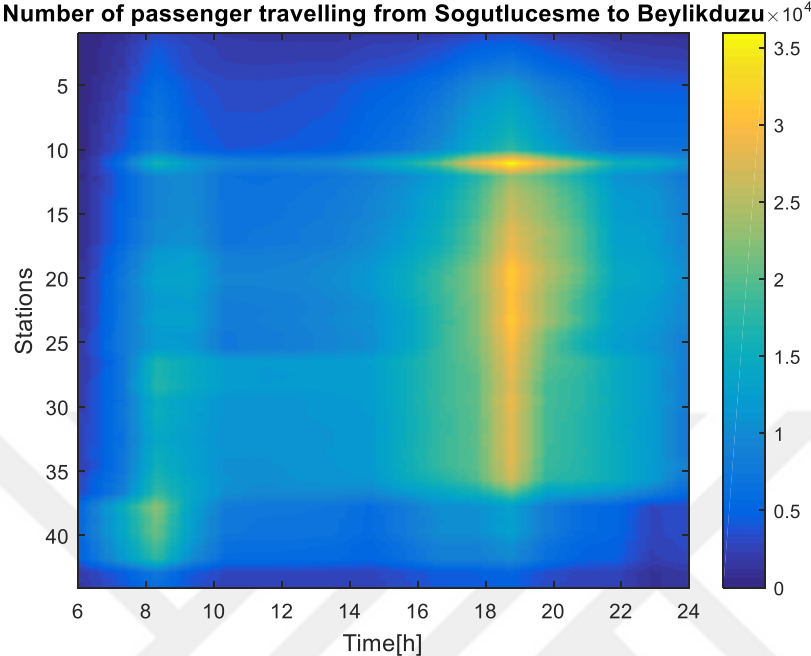
Figure 3-28 Number of passenger travelling from Beylikdüzü to Söğütlüçeşme

3.4 Weather Data and HVAC Model

In order to design an efficient electric bus for a specific line, design requirements should be carefully determined. Special care should be given to requirements imposed by energy consuming sub-systems, such as the HVAC (Heating, ventilation and air conditioning) system. To design and select elements of a bus HVAC system, it is crucial to accurately determine the heating and cooling loads [31]. Energy consumption of the HVAC system accounts for about 20% of the total energy consumption of a bus [32]. Underestimated HVAC energy consumption may lead to thermal comfort problems, while an overdesigned HVAC system may increase manufacturing and operating costs.

In this section, the weather data such as temperature and relative humidity of Istanbul is examined. Moreover, a calculation model for the determination of the energy requirements of a HVAC system is presented.

3.4.1 Weather Data

Temperature, relative humidity data are obtained from Turkish State Meteorological Service. The station of measurement is Istanbul Regional Meteorological Measurement Center and it is located at Istanbul. Period of temperature and relative humidity data is one hour and the duration is one year. Temperature data of outside temperature data of Istanbul is shown in Figure 3-29.
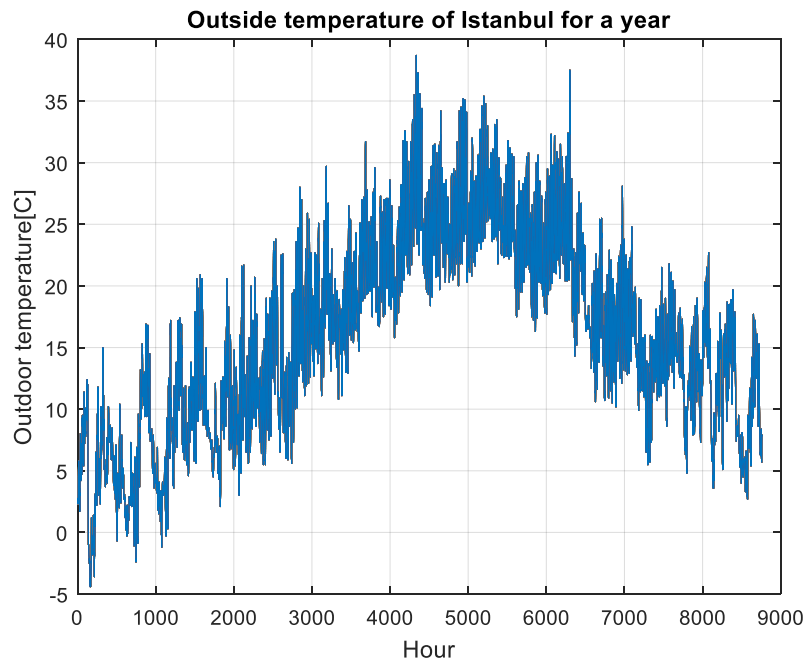
Figure 3-29 Outside temperature data of Istanbul

Relative humidity is the ratio of the water vapor in a given moist air sample to the air sample saturated at the same temperature and pressure [33]. Relative humidity data of Istanbul is shown in Figure 3-30.
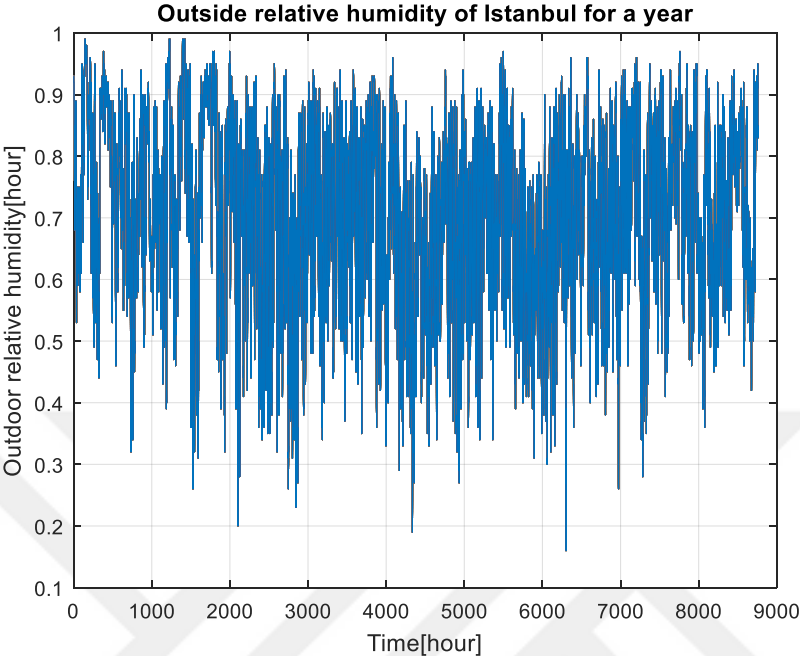
Figure 3-30 Outside relative humidty data of Istanbul

To calculate the solar heat load to which the BRT is exposed, sunrise and sunset data must be considered. Sunset and sunrise times of Istanbul are given in Figure 3-31.
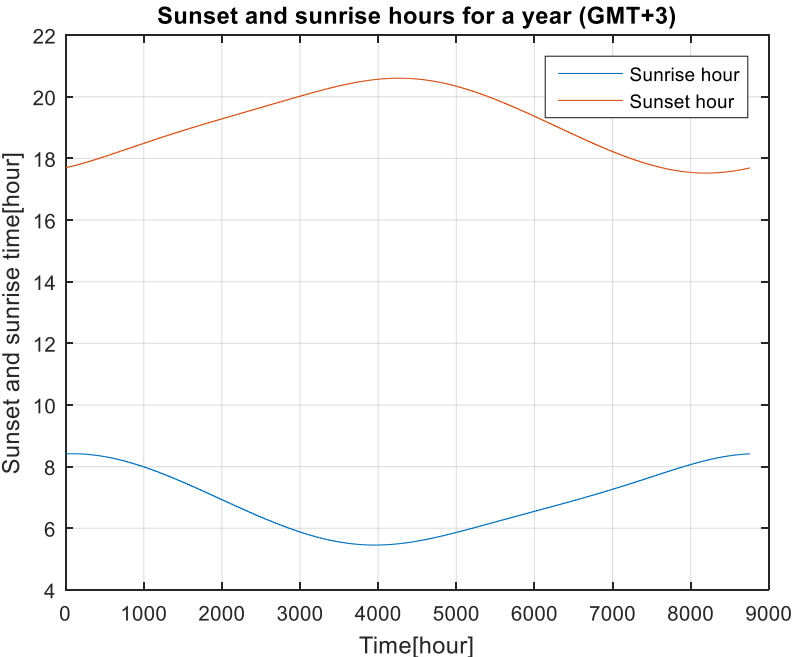
Figure 3-31 Sunset and sunrise time of Istanbul

3.4.2 Heat Model

Heat gain refers to the transfer of heat into or out of the bus cabin through a variety of component. There are nine main components of heat gain of an internal combustion bus. These component may support the HVAC system (for example, radiation that heats up the bus in a cold winter day) or may work against the HVAC system (for example, metabolic heat of passenger that heats up the bus in a hot summer day). In order to determine the HVAC requirements of a bus, the heat load is calculated by an inductive method. Here, the model developed by Fayazbokhsh et al. [22] for a typical car cabin is adapted for the electric bus. The heat load model developed for a typical car cabin is given in equation (3.16).

$$\dot{Q}_{Total} = \dot{Q}_{Met} + \dot{Q}_{Dir} + \dot{Q}_{Dif} + \dot{Q}_{Ref} + \dot{Q}_{Amb} + \dot{Q}_{Exh} + \dot{Q}_{Eng} + \dot{Q}_{Ven} + \dot{Q}_{AC} \quad (3.16)$$

$\dot{Q}_{Total}$ refers to the net total heat flow into bus cabin, $\dot{Q}_{Met}$ is the metabolic heat power generated by passengers, $\dot{Q}_{Dir}$ is the heat power of direct radiation, $\dot{Q}_{Dif}$ is the heat power caused by diffused radiation, $\dot{Q}_{Ref}$ is the heat power of reflected radiation, $\dot{Q}_{Amb}$ is the heat exchange between ambient and bus cabin, $\dot{Q}_{Exh}$ is the heat power due to exhaust system, $\dot{Q}_{Eng}$ is the heat power of the engine, $\dot{Q}_{Ven}$ is the heat power generated by the air that is blown by HVAC system into bus cabin so as to supply fresh air for passengers and $\dot{Q}_{AC}$ is the thermal load created by the air conditioning system to reach the comfort temperature.

Since, there is no exhaust system, $\dot{Q}_{Exh}$ is omitted and since the heat generation of the electric motor is negligible compared to the internal combustion engine $\dot{Q}_{Eng}$ is also assumed to be zero. Loads are calculated for continuous working conditions, so $\dot{Q}_{AC}$ is assumed to be equal to total heat load. Thus, equation (3.16) becomes;

$$\dot{Q}_{Total} = \dot{Q}_{Met} + \dot{Q}_{Dir} + \dot{Q}_{Dif} + \dot{Q}_{Ref} + \dot{Q}_{Amb} + \dot{Q}_{Ven} \quad (3.17)$$

Hence, in order to calculate net heat flow into an electric bus cabin equation (3.17) can be used.

In Figure 3-32 thermal loads acting on an articulated bus are illustrated. In the following sections each components are explained.
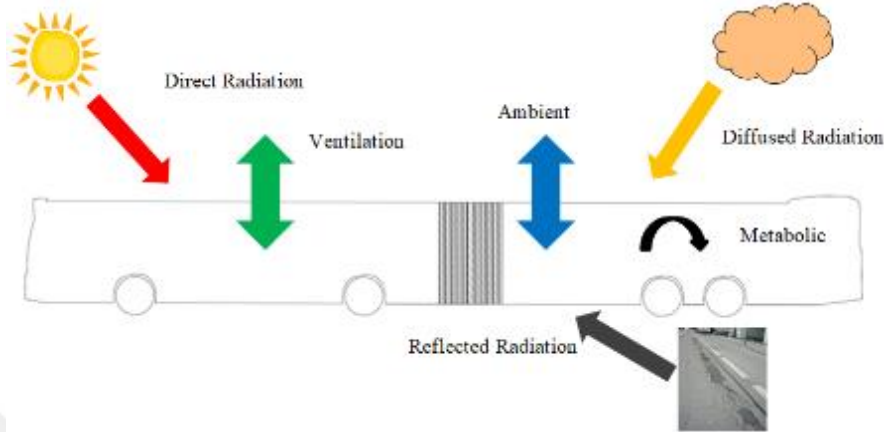
Figure 3-32 Representation of thermal loads

3.4.2.1 Thermal properties of passenger compartment

Passenger capacity of the 18-m articulated Metrobus is 181. Number of seats is 43+1 (one for driver). Surface areas, S, that are obtained from the technical drawings of the Metrobus and transmissivity,τ, of the surfaces for are shown in Table 3-8. According to the safety regulation, the transmittance of visible light through the window should be at least 70% in the US and 75% in Europe. Transmissivity of the windows of the Metrobus is assumed to be 0.75 according to J.W.Lee et al. [34].

Table 3-8 Transmissivity and surface area of each bus surface

Surface	Part	Material	Area (m^2)	Transmissivity
Front	Windshield	Glass	3.25	0.75
	Body	Aluminum	4.21	0
Rear	Windows and doors	Glass	1.95	0.75
	Body	Aluminum	5.20	0
Left	Windows	Glass	17.15	0.75
	Body	Aluminum	39.60	0
Right	Windows	Glass	17.69	0.75
	Body	Aluminum	39.06	0
Top	Body	Aluminum	45.90	0
Bottom	Body	Aluminum	45.90	0

3.4.2.2 Metabolic Heat Load

Passengers in the cabin of the Metrobus create heat load because of their metabolic activities. For the calculation of metabolic load of passengers, they are separated into three different groups; driver, sitting passenger and standing passengers. Therefore, the metabolic load can be calculated from equation (3.18);

$$\dot{Q}_{Met} = \dot{Q}_{Driver} + n_{sitting}\dot{Q}_{sitting} + n_{Standing}\dot{Q}_{Standing} \qquad (3.18)$$

where $\dot{Q}_{Driver}$ refers to the metabolic load of driver and $\dot{Q}_{sitting}$ and $\dot{Q}_{Standing}$ are the metabolic loads of sitting passengers and standing passengers, respectively. Number of passenger is represented with $n_{sitting}$ and number of standing passenger is represented with $n_{Standing}$.

Metabolic load of a person can be calculated from equation (3.19);

$$\dot{Q}_{Met} = MA_{DU} \qquad (3.19)$$

where metabolic heat production rate, M, of a sitting passenger and standing passenger are defined as 60 W/m^2 and 70 W/m^2, respectively while the metabolic heat production rate of a heavy vehicle driver is 185 W/m^2 [33]

A_{DU} refers to the DuBois area which estimates the surface area of a person from the mass and height of the person. (3.20) [35]

$$A_{DU} = 0.202 \; x \; W_{avg}{}^{0.425} \; x \; H_{avg}{}^{0.725} \qquad (3.20)$$

W_{avg} and H_{avg} refer to mass in kilogram and height in meter of a person, respectively.

3.4.2.3 Solar Heat Loads

Solar heat load is always positive, in other words it always increases the heat of the bus cabin. Solar heat load is divided into three components; direct radiation, diffused radiation and reflected radiation. Total solar heat load is the summation of these three components.

Geometry of a bus is assumed to be a rectangular prism. Solar angle of a surface is given in Figure 3-33.
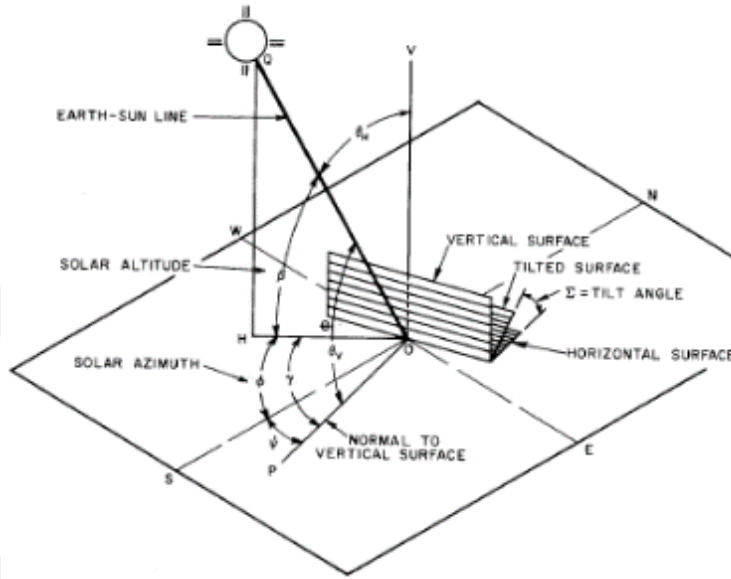
Figure 3-33 Solar angle of a surface [33]

For any surface, the angle between the surface normal and the position of the sun which is the incident angle,θ_i, can be found from equation (3.21). [36]

$$\theta_i = \cos^{-1}(\sin\beta \times \cos\Sigma + \cos\gamma \times \cos\beta \times \sin\Sigma) \qquad (3.21)$$

where, γ is the azimuth angle, β is the altitude angle and Σ is the surface tilt angle.

β can be calculated from equation (3.22)

$$\beta = \sin^{-1}(\sin L \times \sin\delta + \cos L \times \cos\delta \times \cos H) \qquad (3.22)$$

where, δ is the solar declination, L is the latitude and H is the hour angle, where

$$H = 15(Atlantic\ Standard\ Time - 12) \qquad (3.23)$$

Solar declination, δ, can be calculated from equation (3.24).

$$\delta = 23.45 \sin([360(284 + n_{day})]/365) \qquad (3.24)$$

where, n_{day} represents the day of the year.

3.4.2.3.1.1 Direct Radiation

Direct solar radiation (I_{Dir}) is the proportion of the almost rectilinear solar radiation, which reaches the earth's surface from an angle with a distance of 0.25° to the center of the sun and reaches a normal area, which is oriented perpendicularly to the direction of the radiation. [37]

Direct radiation load can be calculated from equation (3.25) [22];

$$\dot{Q}_{Dir} = S\tau I_{Dir}\cos(\theta) \tag{3.25}$$

where, S is the area of the surface, τ is the transmissivity of the surface, I_{Dir} is the direct normal irradiance and $\dot{Q}_{Dir}$ is the heat gain due to direct radiation.

Irradiance of the direct radiation can be calculated from equation (3.26) [33].

$$I_{Dir} = \frac{A}{e^{\left(\frac{B}{\sin(\beta)}\right)}} \tag{3.26}$$

A and *B* are constants that change with months. Values of A and B that are obtained from ASHRAE Handbook of Fundamentals are given in Table 3-9. Data are for 21st day of each month. [33] To increase the resolution of calculation A, B and C values may be interpolated.

Table 3-9 Extraterrestrial Solar Irradiance and Related Data

Month	A $[\frac{W}{m^2}]$	B $[\frac{1}{airmass}]$	C
January	1230	0.142	0.058
February	1215	0.144	0.060
March	1186	0.156	0.071
April	1136	0.180	0.097
May	1104	0.196	0.121
June	1088	0.205	0.134
July	1085	0.207	0.136
August	1107	0.201	0.122
September	1151	0.177	0.092
October	1192	0.160	0.073
November	1221	0.149	0.063
December	1233	0.142	0.057

3.4.2.3.1.2 Diffused Radiation

Diffused radiation is the portion of solar radiation which arrives on the surface of the Earth after single or repeated dispersion in the atmosphere. [37] The diffused radiation heat gain can be calculated from equation (3.27) [22].

$$\dot{Q}_{Dif} = S\tau I_{Dif} \tag{3.27}$$

where, I_{Dif} is given in equations (3.28) and (3.29) [33]. Equation 18a is for surfaces other than vertical and equation 18b is for vertical surfaces.

$$I_{Dif} = CI_{Dir}\frac{1 + \cos(\sum)}{2} \tag{3.28}$$

$$I_{Dif} = CI_{Dir}(0.55 + 0.437\cos(\theta) + 0.313\cos^2(\theta)) \tag{3.29}$$

For vertical surfaces of the bus such as front, back, left and right surfaces equation (3.29) is applied.

3.4.2.3.1.3 Reflected Radiation

Reflected radiation refers to the part of radiation heat gain that is reflected from the ground and strikes the body surfaces of the vehicle [22]. Heat gain due to reflected radiation can be calculated from equation (3.30).

$$\dot{Q}_{Ref} = S\tau I_{Ref} \tag{3.30}$$

where, I_{Ref} is defined in equation (3.31) for all surface orientation [33].

$$I_{Ref} = I_{Dir}(C + \sin(\beta))\rho_g \frac{1 - \cos(\Sigma)}{2} \tag{3.31}$$

where, ρ_g is the reflectivity coefficient of the ground.

3.4.2.4 Ambient Heat Load

There may be difference between outside and inside temperatures. This temperature difference causes heat transfer through surfaces from outside into bus cabin on hot days and heat transfer from bus cabin to outside on cold days. The heat transfer can be calculated from equation (3.32) [22].

$$\dot{Q}_{Amb} = SU(T_s - T_i) \tag{3.32}$$

S is the area of the surface, U is the overall heat transfer coefficient of the surface, T_s and T_i refer to outer surface temperature and cabin temperature of the bus, respectively. U is composed of three parts; conduction of the body, convection of inner and outer surfaces, respectively. U can be calculated from equation (3.33).

$$\frac{1}{U} = \frac{1}{h_o} + \frac{\lambda}{k} + \frac{1}{h_i} \tag{3.33}$$

where λ is the thickness of the material, k is the conduction coefficient of the body, h_o and h_i are the convection coefficients of the outer and inner surfaces, respectively. h_i and h_o are assumed only convective and calculated from equation (3.34) [38].

$$h_o = 9 + 3.5v^{0.66} \tag{3.34}$$

where, v is the relative speed of the air in m/s with respect to corresponding surface. Since the air in the bus cabin assumed to be stationary, from equation (3.34) h_i becomes 9 W/m²K.

3.4.2.5 Ventilation Heat Load

Passengers in the bus consume oxygen for breathing. Since the volume of the bus cabin is limited for the long-term O_2 needs of passengers, fresh air must be supplied into the bus cabin. According to ASHRAE standard 62 it is recommended to supply 8 liter of fresh air per second for one passenger, [39]. The heat load because of air exchange between outside and bus cabin can be calculated from equation (3.35). The first part of the equation is for the calculation of sensible heat load, while the second part is for the calculation of latent heat load.

$$\dot{Q}_{Ven} = \dot{V}_{ven}\rho c_p \Delta T + \dot{V}_{ven}\Delta W(4775 + 1.998\Delta T) \qquad (3.35)$$

where, $\dot{V}_{ven}$ is the air flow rate, ρ is the air density (1.2 kg/m^3), c_p is the specific heat of air (1000 J/(kgK)) and ΔT and ΔW are the temperature difference and humidity ratio difference, respectively.

4 SYSTEM POWER REQUIREMENTS

In this chapter, power of drag, roll, gradient and inertial resistances are calculated. At the end, total resistive power and total energy consumption are obtained. In all calculation, bus is considered empty.

4.1 Power Requirements

4.1.1 Traction consumption

4.1.1.1 Drag resistance

Drag coefficient of the vehicle, C_d is obtained in 3.1.2.2 in equation (3.13).

$$C_d = 0.5833 \tag{3.13}$$

Density of the air assumed to be 1.227 kg/m³.

$$\rho = 1.227\frac{kg}{m^3} \tag{4.1}$$

At each data point drag force is calculated from equation (4.2).

$$R_{Drag} = \frac{1}{2}C_d\rho Av^2 \tag{4.2}$$

Drag resistance force is multiplied with velocity of the vehicle, and then resistive power of drag is obtained in equation (4.3) for every second of Metrobus service in the line.

$$P_{Drag} = vR_{Drag} \tag{4.3}$$

Finally, according to driving cycle the resistive power of air drag is determined in both directions. Changes in resistive power of air drag versus time in both directions are shown in Figure 4-1.
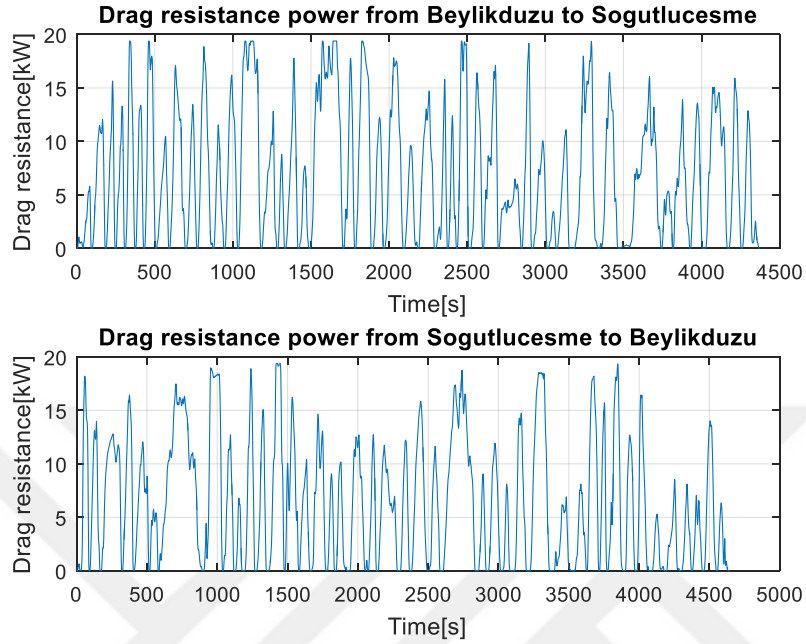
Figure 4-1 Drag resistance of the vehicle

4.1.1.2 Rolling resistance

Rolling resistance coefficient of the vehicle, C_r, is obtained in 3.1.2.2 in equation (3.14).

$$C_r = 0.0079 \tag{3.14}$$

At each data point drag force is calculated from equation (4.4).

$$R_{Roll} = C_r mg \tag{4.4}$$

Rolling resistance force is multiplied with velocity of the vehicle, and then resistive power of rolling is obtained in equation (4.5) for every second of Metrobus service in the line.

$$P_{Roll} = v R_{Roll} \tag{4.5}$$

As it can be observed from equation (3.2) the weight of the vehicle has an impact on the rolling resistance. So, the rolling resistance of the vehicle is investigated for different weight conditions in both directions. These conditions are,

- Empty vehicle
- Fully loaded vehicle (with 181 passengers)
- Loaded vehicle according to passenger occupancy rate of each station at morning peak hour
- Loaded vehicle according to passenger occupancy rate of each station at afternoon peak hour

Changes in rolling resistance power of the empty vehicle versus time in both directions are shown in Figure 4-2.
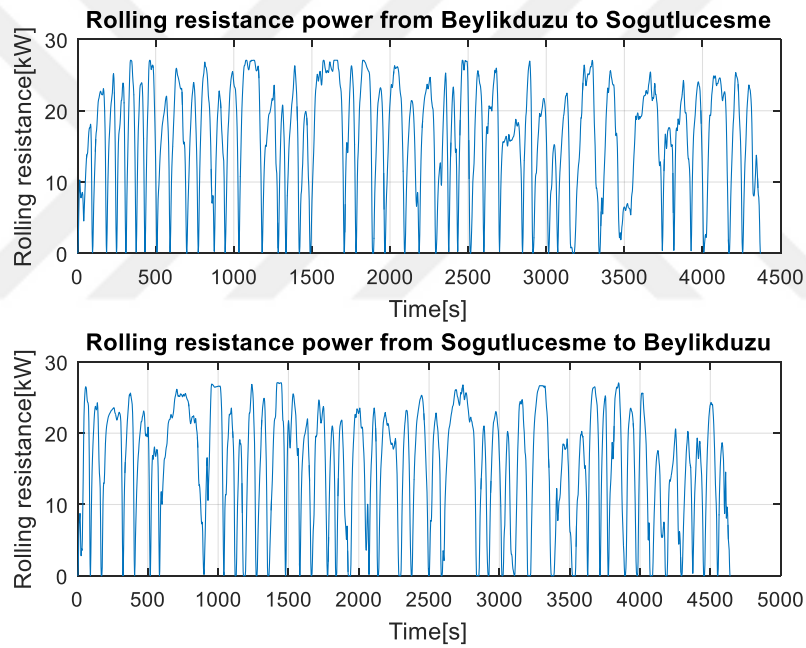
Figure 4-2 Rolling resistance of empty vehicle

Changes in rolling resistance power of the vehicle in service at 9:00(morning peak hour) and 19:00(afternoon peak hour) versus time in both directions are shown in Figure 4-3 and Figure 4-4 .
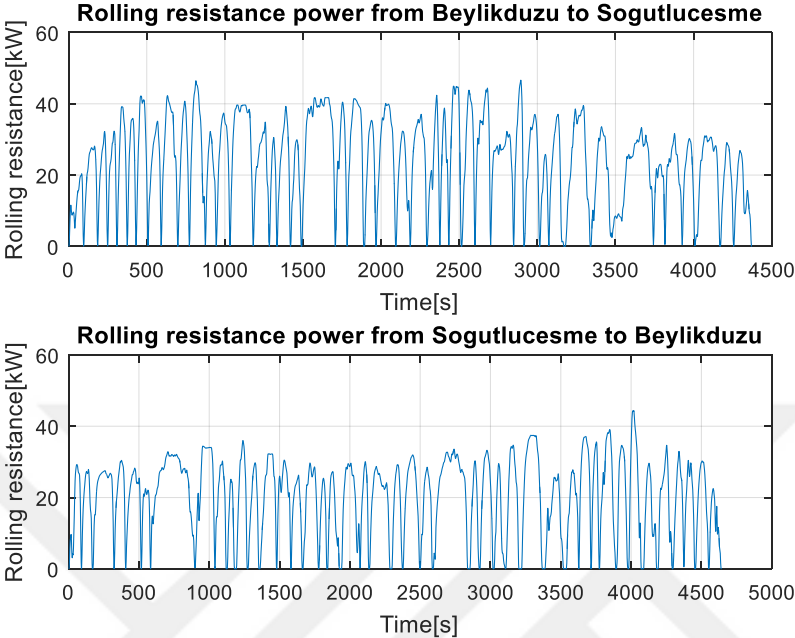
Figure 4-3 Rolling resistance of the vehicle at morning peak hour
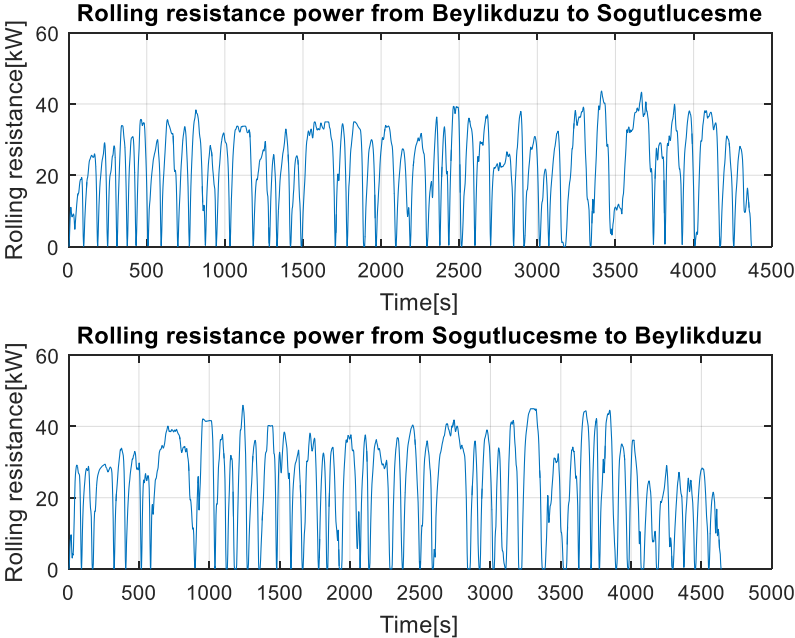
Figure 4-4 Rolling resistance of the vehicle at afternon peak hour

Changes in rolling resistance power of the fully loaded vehicle versus time in both directions are shown in Figure 4-5.
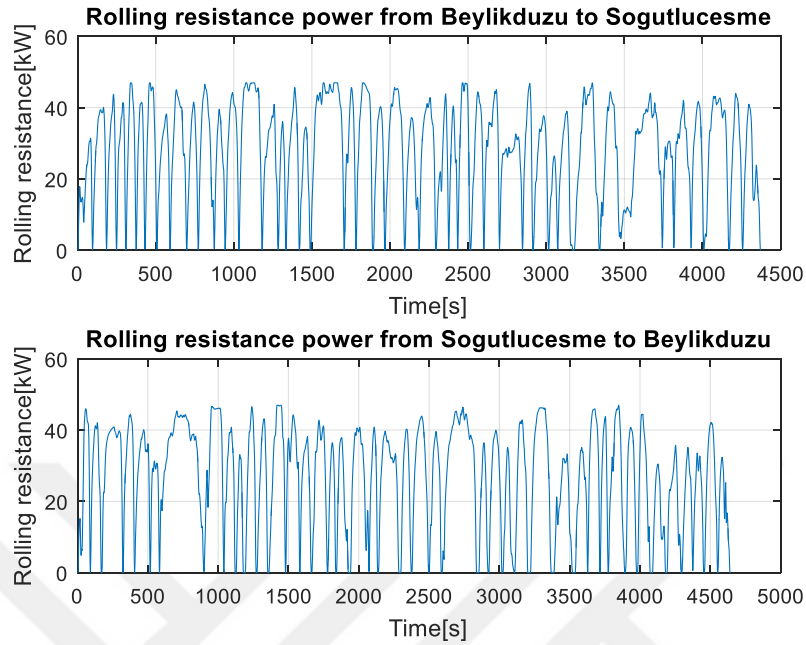
Figure 4-5 Rolling resistance of fully loaded vehicle

4.1.1.3 Gradient resistance

Gradient resistance force acting on the vehicle was given in equation (3.3);

$$R_{grad} = mgsin(\theta) \tag{3.3}$$

Gradient resistance force is multiplied with velocity of the vehicle, and then resistive power of gradient is obtained in equation (4.6) for every second of metrobus service in the line.

$$P_{grad} = vR_{grad} \tag{4.6}$$

As it can be observed from equation (3.3) the weight of the vehicle has an impact on the rolling resistance. So, the gradient resistance of the vehicle is calculated for different weight conditions in both directions. These conditions are,

- Empty vehicle
- Fully loaded vehicle (with 181 passengers)
- Loaded vehicle according to passenger occupancy rate of each station at morning peak hour
- Loaded vehicle according to passenger occupancy rate of each station at afternoon peak hour

51

Changes in gradient resistance power of the empty vehicle versus time in both directions are shown in Figure 4-6
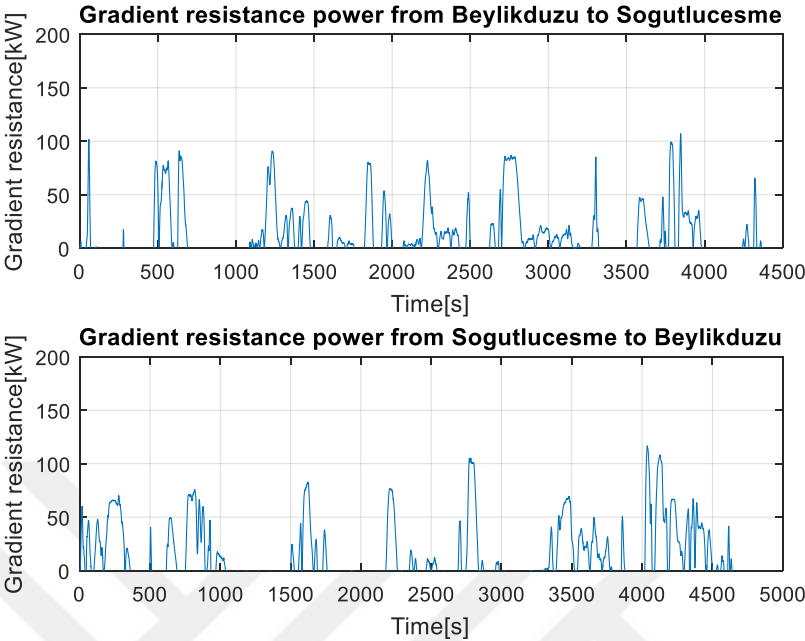
Figure 4-6 Gradient resistance of empty vehicle

Changes in gradient resistance power of the vehicle in service at 9:00(morning peak hour) and 19:00(afternoon peak hour) versus time in both directions are shown in Figure 4-7and Figure 4-8.
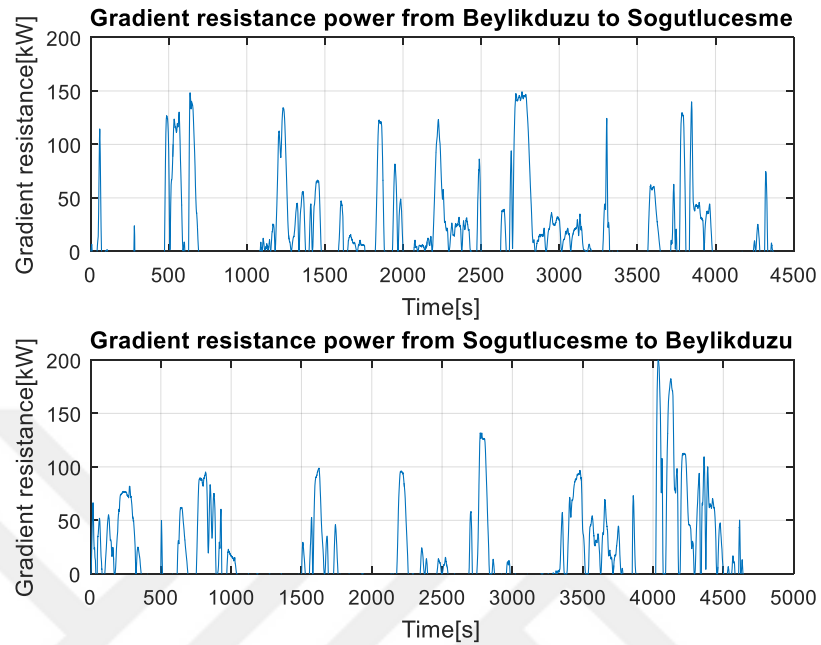
Figure 4-7 Gradient resistance of the vehicle at morning peak hour
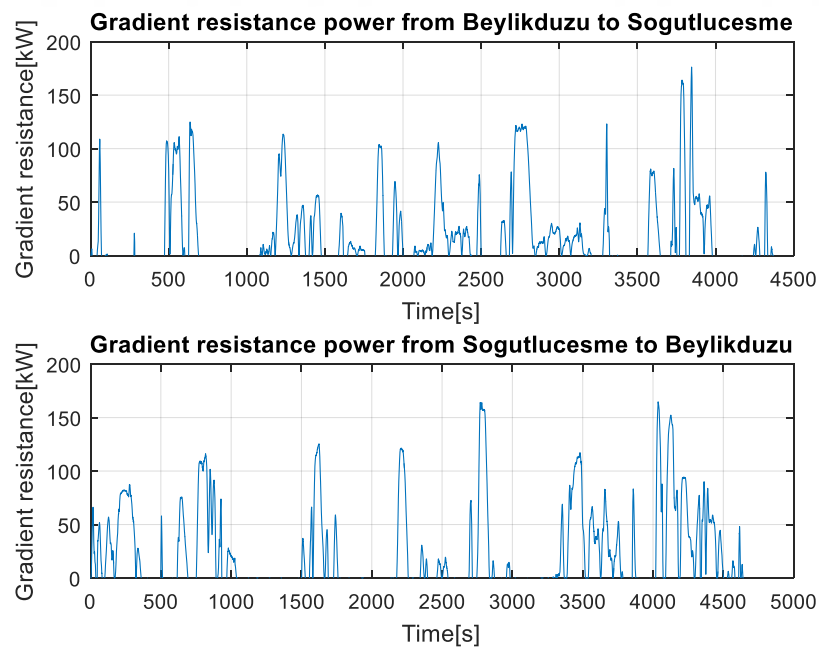
Figure 4-8 Gradient resistance of the vehicle at afternon peak hour

Changes in gradient resistance power of the fully loaded vehicle versus time in both directions are shown in Figure 4-9.
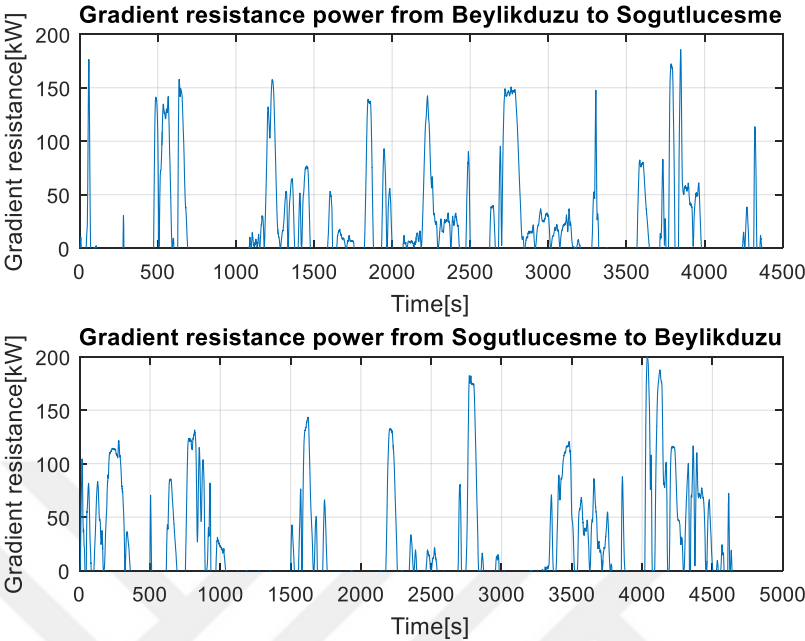
Figure 4-9 Gradient resistance of fully loaded vehicle

4.1.1.4 Inertial resistance

Inertial resistance force acting on the vehicle was given in equation (3.4);

$$R_{inertia} = m_{eq}a \qquad (3.4)$$

Inertial resistance force is multiplied with velocity of the vehicle, and then resistive power of inertia is obtained in equation (4.7) for every second of metrobus service in the line.

$$P_{inertia} = vR_{inertia} \qquad (4.7)$$

As it can be observed from equation (3.4) the weight of the vehicle has an impact on the rolling resistance. So, the gradient resistance of the vehicle is calculated for different weight conditions in both directions. These conditions are,

- Empty vehicle
- Fully loaded vehicle (with 181 passengers)
- Loaded vehicle according to passenger occupancy rate of each station at morning peak hour
- Loaded vehicle according to passenger occupancy rate of each station at afternoon peak hour

Changes in inertial resistance power of the empty vehicle versus time in both directions are shown in Figure 4-10.
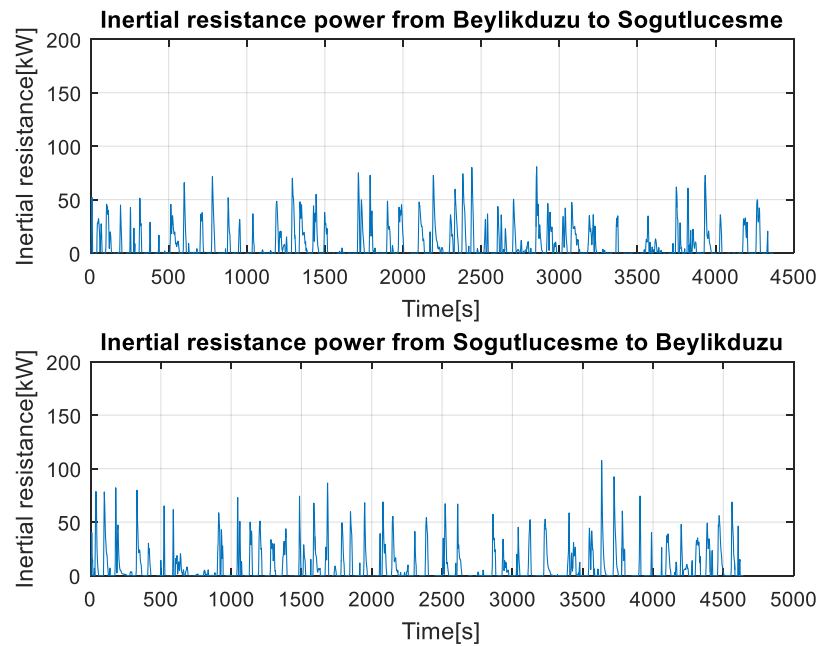
Figure 4-10 Inertial resistance of empty vehicle

55

Changes in inertial resistance power of the vehicle in service at 9:00(morning peak hour) and 19:00(afternoon peak hour) versus time in both directions are shown in Figure 4-11and Figure 4-12.
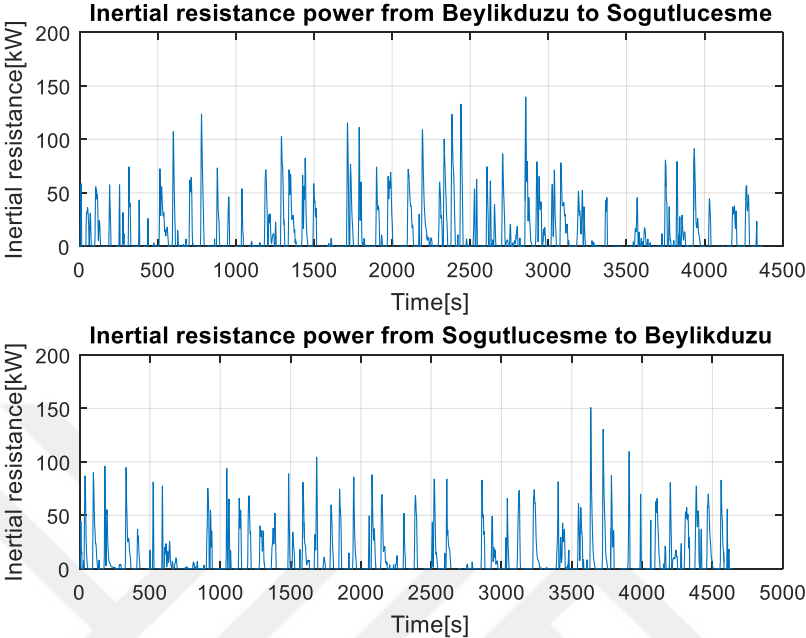
Figure 4-11 Inertial resistance of the vehicle at morning peak hour
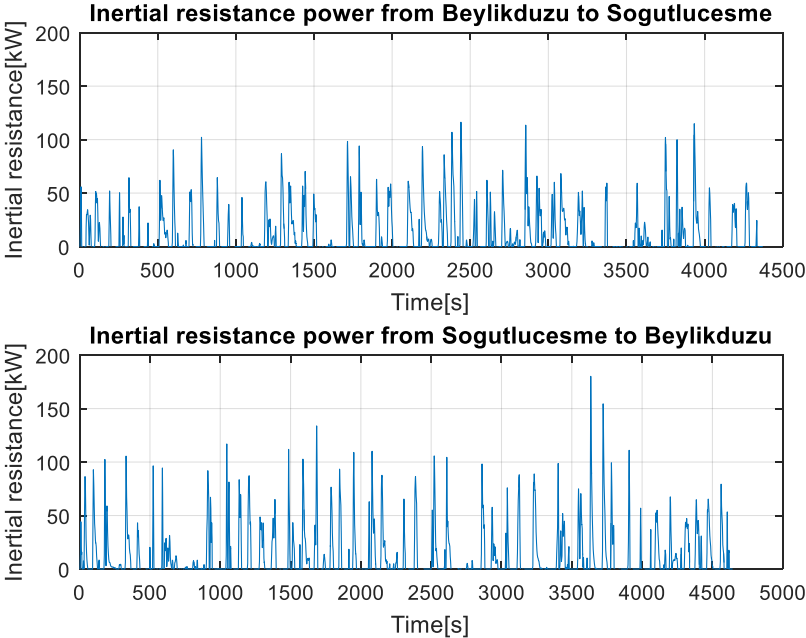
Figure 4-12 Inertial resistance of the vehicle at afternon peak hour

Changes in inertial resistance power of the fully loaded vehicle versus time in both directions are shown in Figure 4-13.
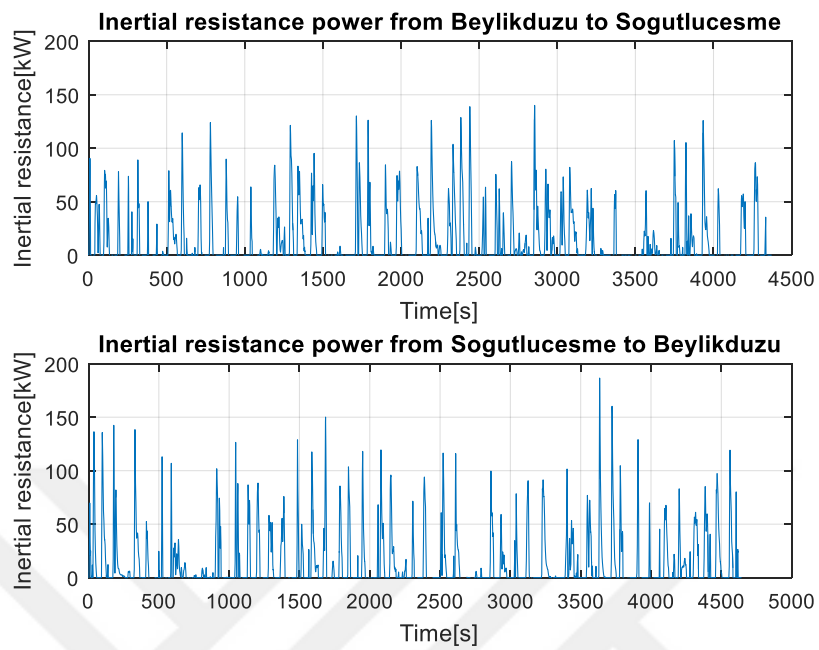
Figure 4-13 Inertial resistance of fully loaded vehicle

4.1.1.5 Total traction resistance

Total resistive power is the summary of all resistive powers, in other word it is the traction energy consumed instantaneously along the bus line and it is obtained from equation (4.8).

$$P_{total\ resistive} = P_{Drag} + P_{Roll} + P_{gradient} + P_{inertia} \qquad (4.8)$$

Total energy consumptions are calculated for different passenger occupancy rates for two peak hours, for empty vehicle and fully loaded vehicle. Change in total resistive power versus time for empty vehicle is shown Figure 4-14.
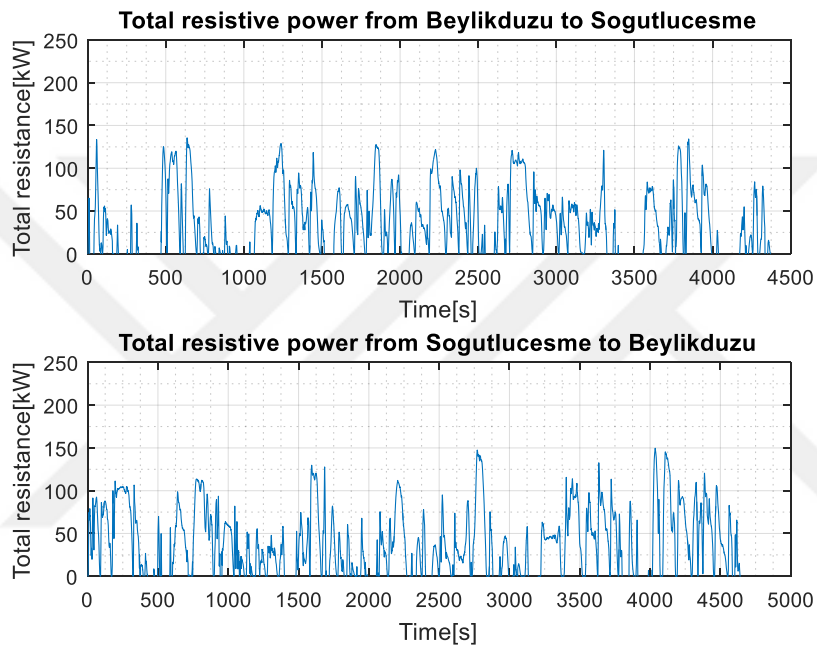
Figure 4-14 Total resistive power of empty vehicle

Changes in total resistance power of the vehicle in service at 9:00(morning peak hour) and 19:00(afternoon peak hour) versus time in both directions are shown in Figure 4-15and Figure 4-16, respectively.
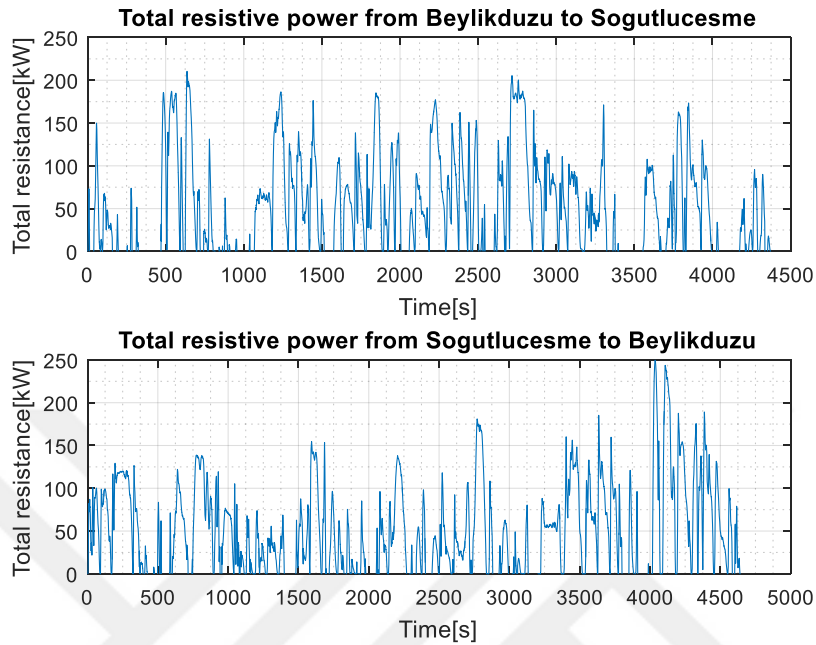
Figure 4-15 Total resistance of the vehicle at morning peak hour
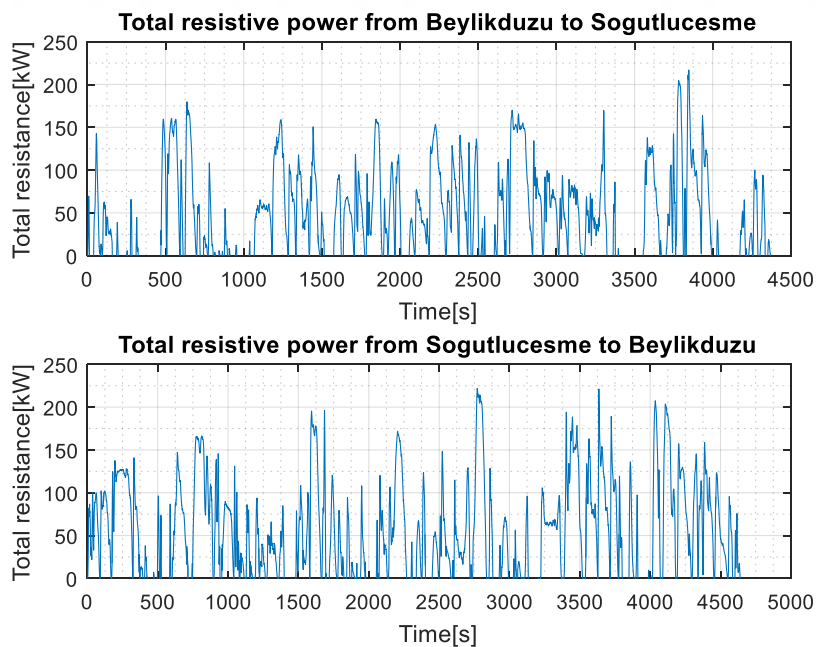
Figure 4-16 Total resistance of the vehicle at afternoon peak hour

59

Change in total resistive power versus time for empty vehicle is shown Figure 4-17.
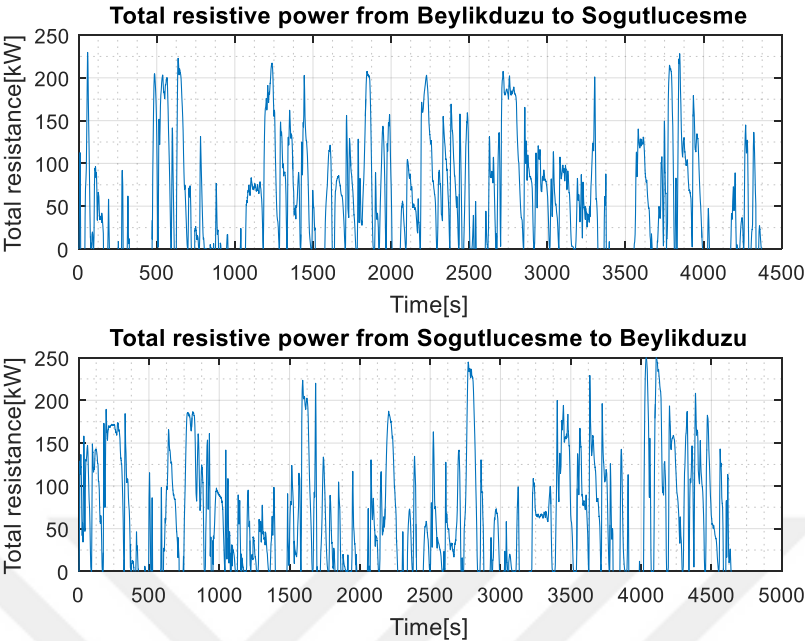
Figure 4-17 Total resistive power of fully loaded vehicle

Total resistive energy for each direction for different load conditions are shown in Figure 4-18, Figure 4-19, Figure 4-20 and Figure 4-21.
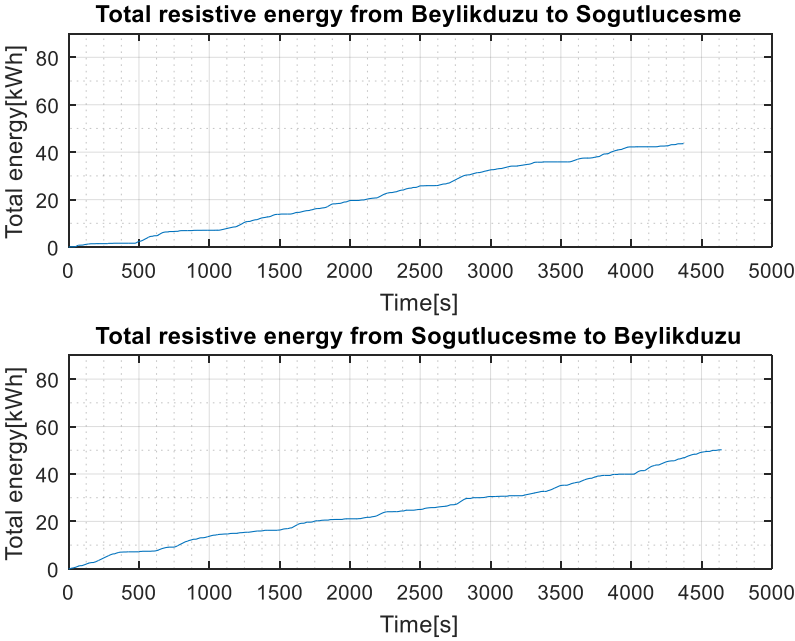
Figure 4-18 Total resistive energy of empty vehicle
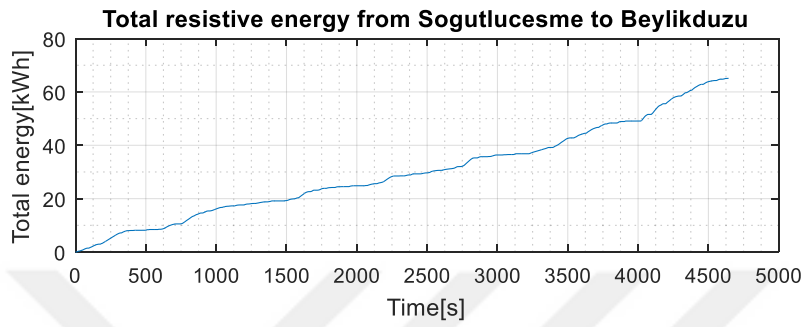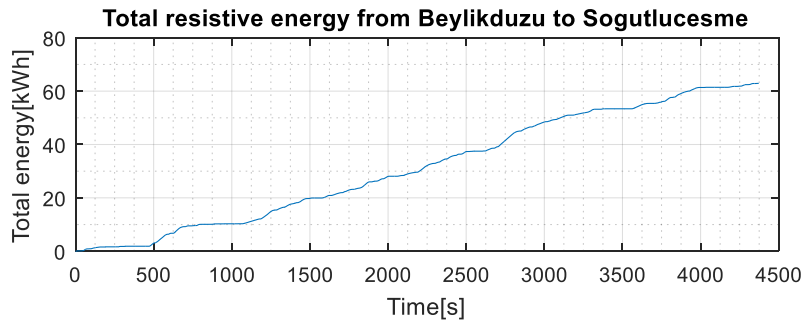
Figure 4-19 Total resistance of the vehicle at morning peak hour
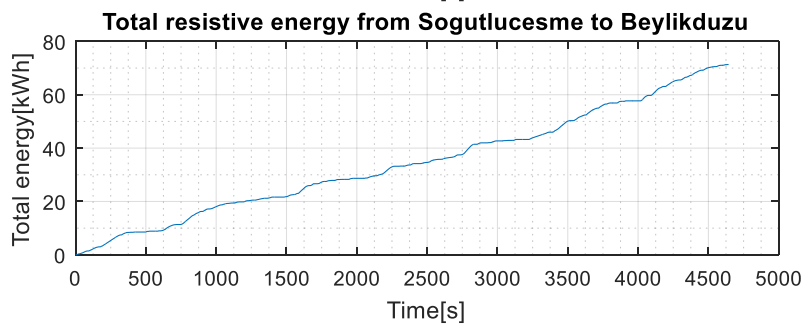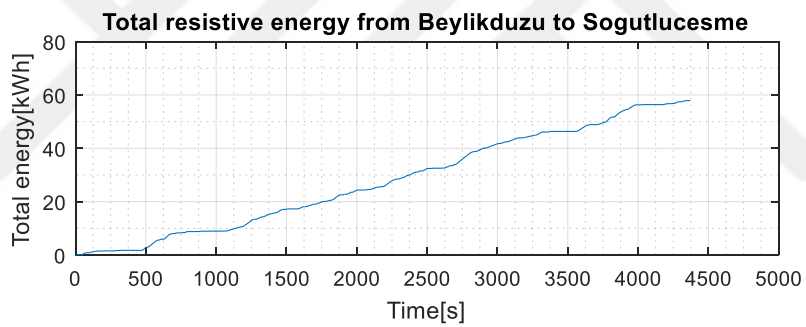
Figure 4-20 Total resistance of the vehicle at afternoon peak hour
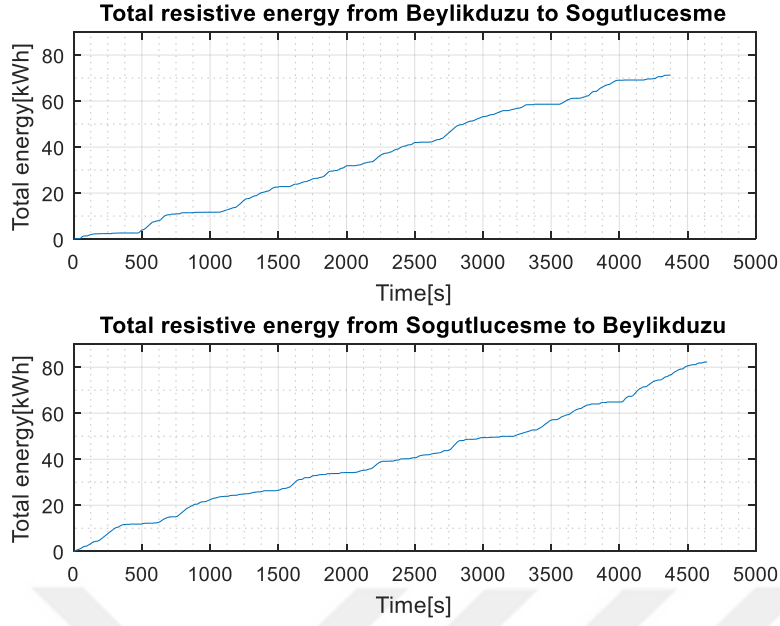
Figure 4-21 Total resistive energy of fully loaded vehicle

The average energy amount per km to be supplied to traction system for overcoming the resistive forces in Söğütlüçeşme and Beylikdüzü directions are tabulated in Table 4-1.

Table 4-1 Average energy consumption of the vehicle

Direction	Load	Consumption (kWh/km)
Söğütlüçeşme	Empty	0.91
	Peak hour (morning)	1.32
	Peak hour (afternoon)	1.22
	Full	1.50
Beylikdüzü	Empty	1.04
	Peak hour (morning)	1.34
	Peak hour (afternoon)	1.46
	Full	1.70

4.1.2 Auxiliary consumptions

4.1.2.1 HVAC

The HVAC power requirement of Istanbul Metrobus Network is calculated in detail by taking into account the annual hourly passenger density, the hourly position of the sun, the location of the bus line and the bus working hours. Hourly passenger density data for one year between each stations of the Metrobus Network was obtained from the bus service operator.

4.1.2.1.1 Metabolic heat load

According to a health survey of Turkish Statistical Institute, average height of in Turkey is 1.67 m and average weight is 71.5 kg [40]. Thus, from equation (4.9) A_{DU} of an average Turkish people is calculated as follows.

$$A_{DU} = 0.202 \; x \; 71.5^{0.425} \; x \; 1.672^{0.725} = 1.80 \; m^2 \tag{4.9}$$

With the help of equation (4) and (6) metabolic heat generation rate of a driver, sitting passenger and a standing passenger is calculated easily in equation (4.10), (4.11) and (4.12).

$$\dot{Q}_{Driver} = 120 \; \frac{W}{m^2} \; x \; 1.80 \; m^2 = 216 \; W \tag{4.10}$$

$$\dot{Q}_{Sitting} = 60 \; \frac{W}{m^2} \; x \; 1.80 \; m^2 = 108 \; W \tag{4.11}$$

$$\dot{Q}_{Standing} = 70 \; \frac{W}{m^2} \; x \; 1.80 \; m^2 = 126 \; W \tag{4.12}$$

Finally, total metabolic heat generation rate in bus cabin can be calculated from equation (4.13).

$$\dot{Q}_{Met} = 216 \; W + n_{Sitting} \; x \; 108 \; W + n_{Standing} x \; 126 \; W \tag{4.13}$$

It is assumed that passengers prefer to sit in the bus when there is empty space. There are only 43 seats for passengers in the Metrobus but the passenger capacity is 181.

Heat map of metabolic heat load with period of one day is shown in Figure 4-22.
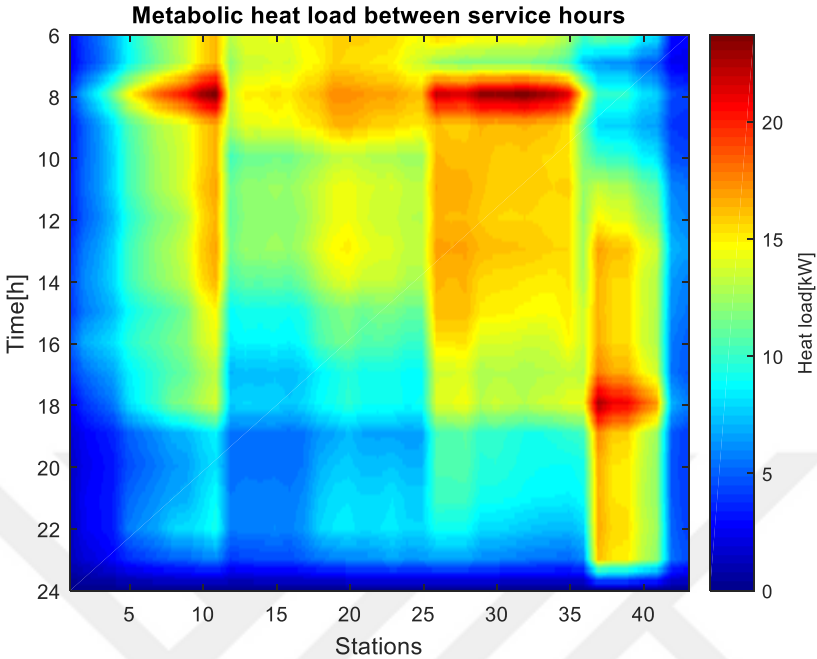
Figure 4-22 Metabolic heat load for one day

Heat map of metabolic heat load with period of one year is shown in Figure 4-23. Since Metrobus is not working at night, there is no metabolic heat load between night hours.
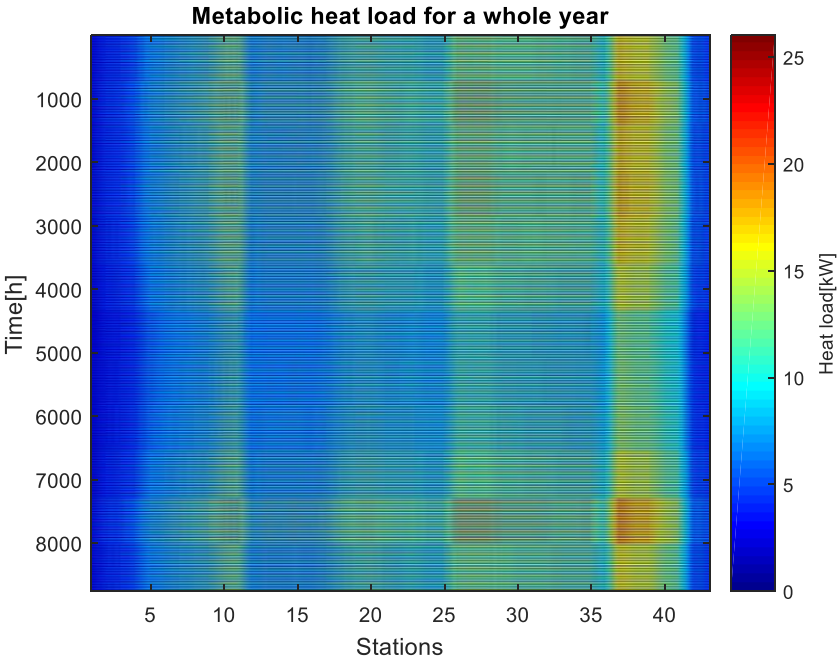
Figure 4-23 Metabolic heat load for a whole year

4.1.2.1.2 Solar Heat Loads

As it is stated in Introduction, the Metrobus network is mainly established on the east-west direction. For calculation of solar heat load, it is assumed that the Metrobus operates only from west to east direction.

Hourly incidence angle of each surface for 1 year, which are calculated from equation (11), are shown in Figure 4-24.
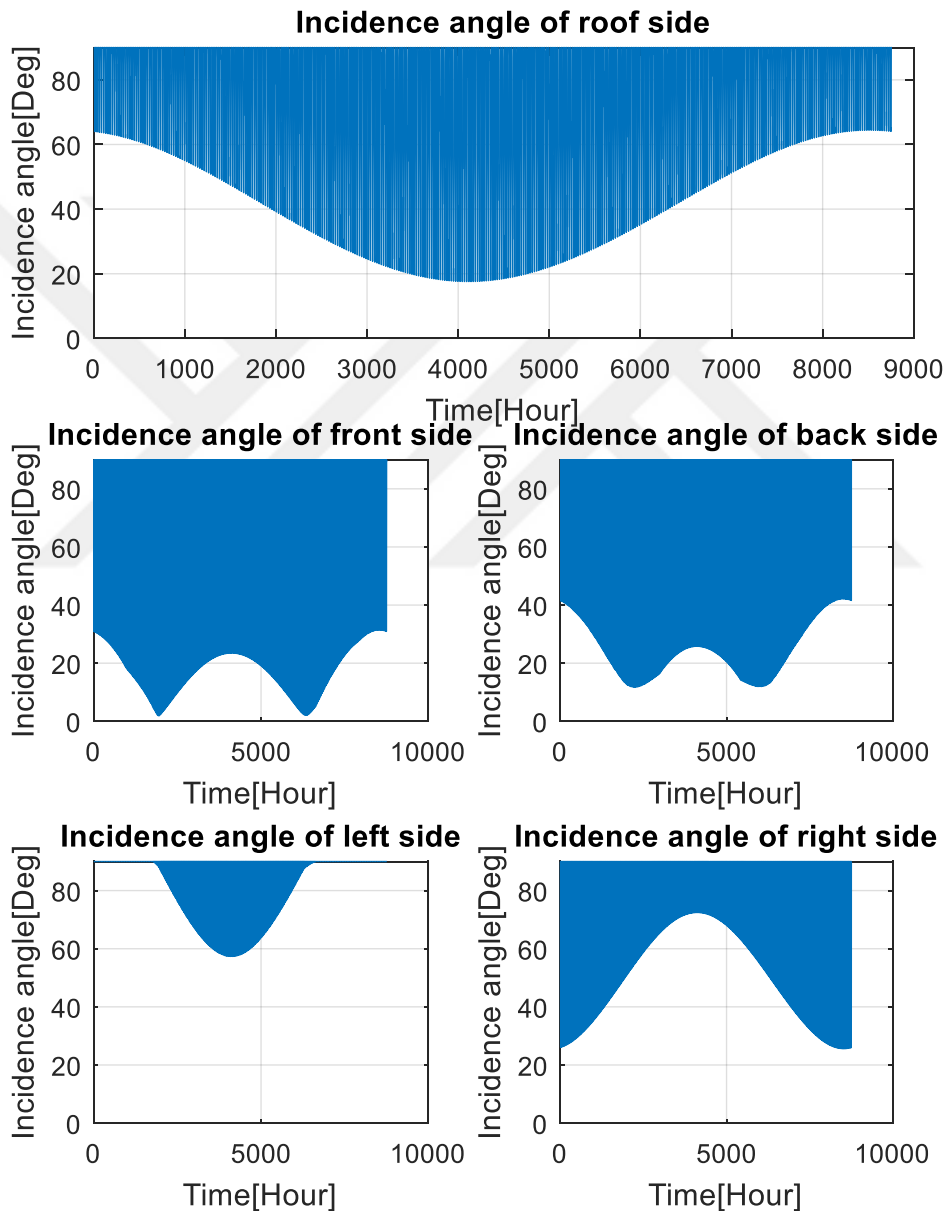
Figure 4-24 Incidence angle of all surfaces

Hourly altitude angles of all surfaces for one year period, which are calculated from equation (11), are shown in Figure 4-25.
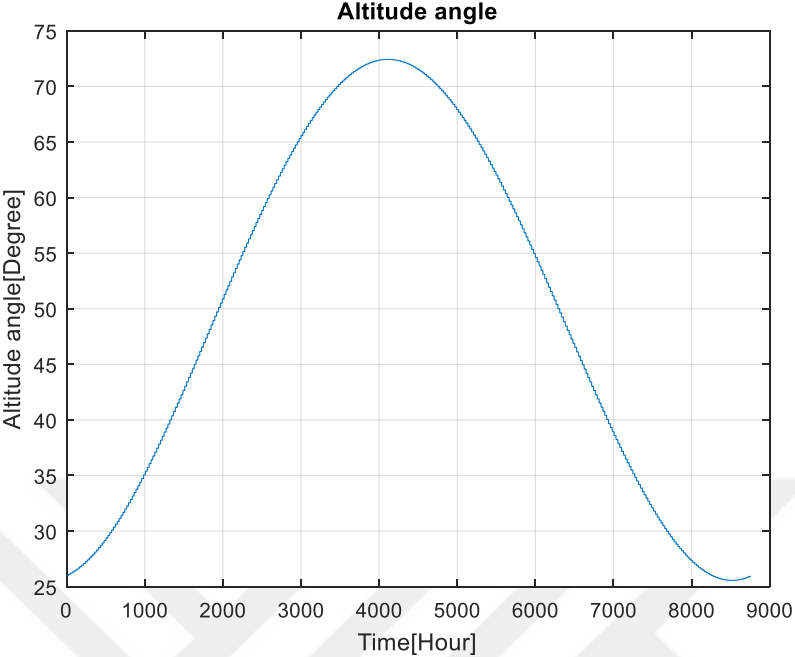
Figure 4-25 Altitude angles

4.1.2.1.2.1 Direct Radiation Heat Load

Direct radiation heat loads for each hour are calculated from equation (11). Transmissivity values and surface areas, which are required in order to calculate direct radiations, are obtained from Table 3-8. Result of calculation shown in Figure 4-26.
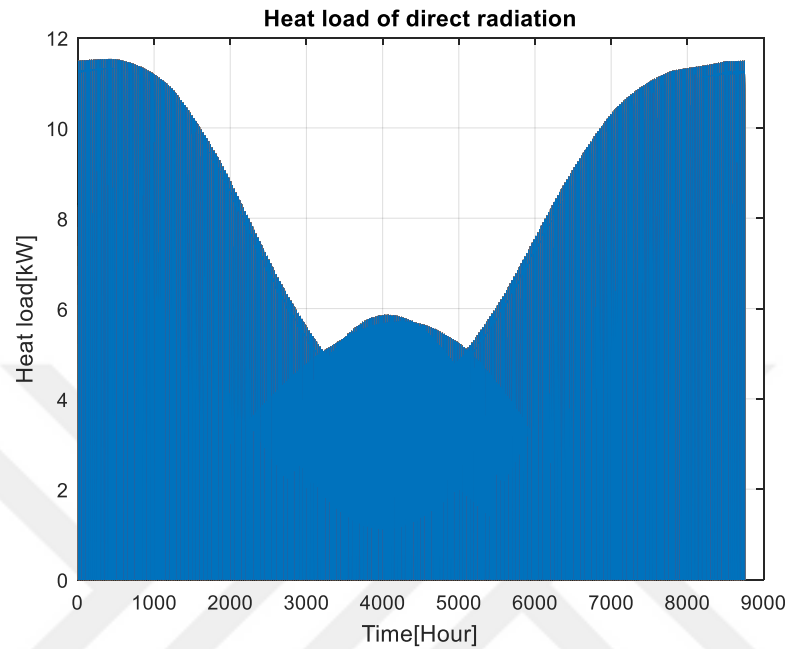
Figure 4-26 Heat load of direct radiation

4.1.2.1.2.2 Diffused Radiation Heat Load

Heat loads of diffused radiation are obtained from equation (18). Heat load that is generated by diffused radiation for each hour of a year are shown in Figure 4-27.
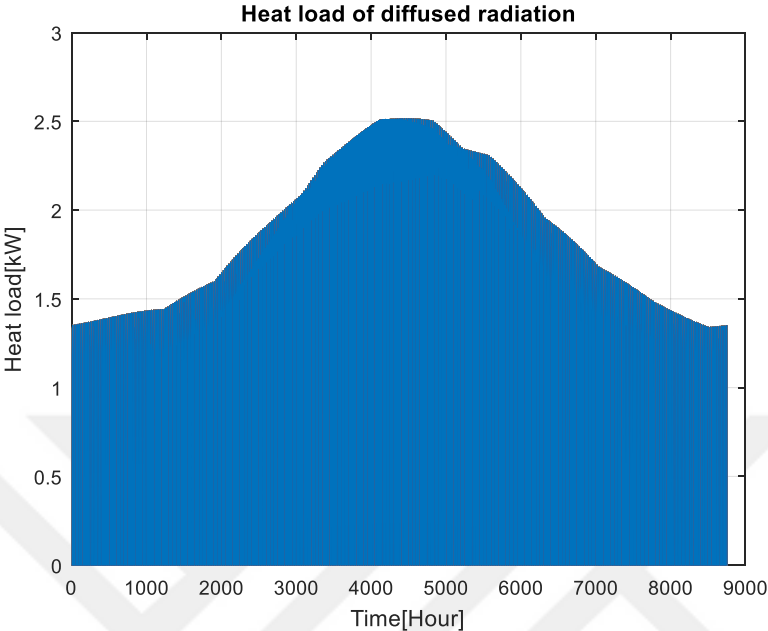
Figure 4-27 Heat load of diffused radiation

4.1.2.1.2.3 Reflected Radiation Heat Load

Heat load due to reflected radiation is calculated from equation (20). It is assumed that sunlight is reflected only from the ground (asphalt) and, reflectivity coefficient of the ground (asphalt), ρ_g, is 0.2 [41]. Results are shown in Figure 4-28.
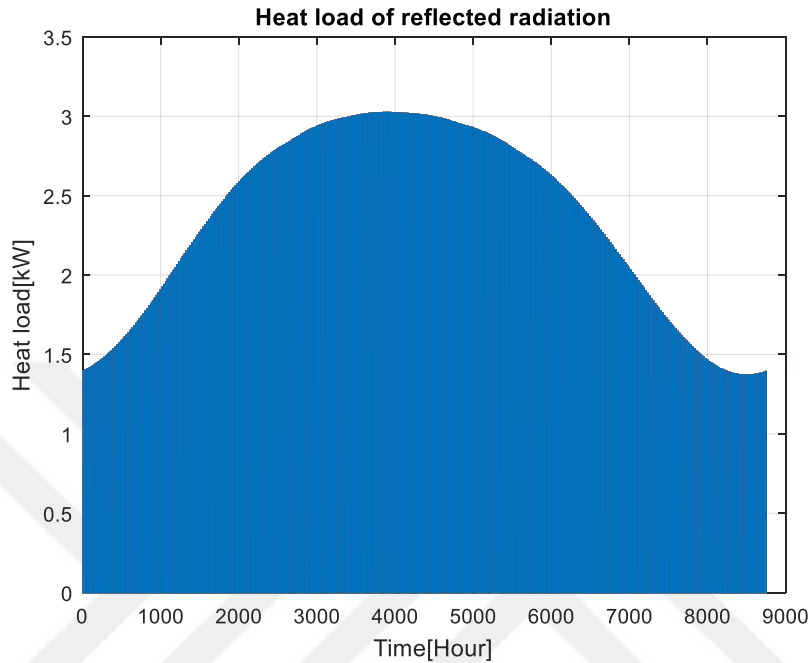
Figure 4-28 Heat load of reflected radiation

4.1.2.1.3 Ambient Heat Load

Thickness of the body and glass, λ, may vary from vehicle to vehicle and it is easy to measure. In that case vehicle body thickness is assumed to be 15mm and glass thickness is assumed to be 5mm. Thermal conductivity of the glass is 1.05 W/mK and thermal conductivity of the body is 0.2 W/mK. [22].

For the calculation of ambient heat load, inner temperature of the Metrobus is required. For practical reasons, inner temperature of the bus is assumed to be always in comfortable ranges. Comfortable inner temperature and relative humidity ranges were tabulated in Table 4-2.

In addition to inner temperature, outer temperatures are also required. Hourly outside temperature data are obtained from Turkish State Meteorological Service. Temperature difference between outside and inside of the Metrobus for a year are given in Figure 4-29.
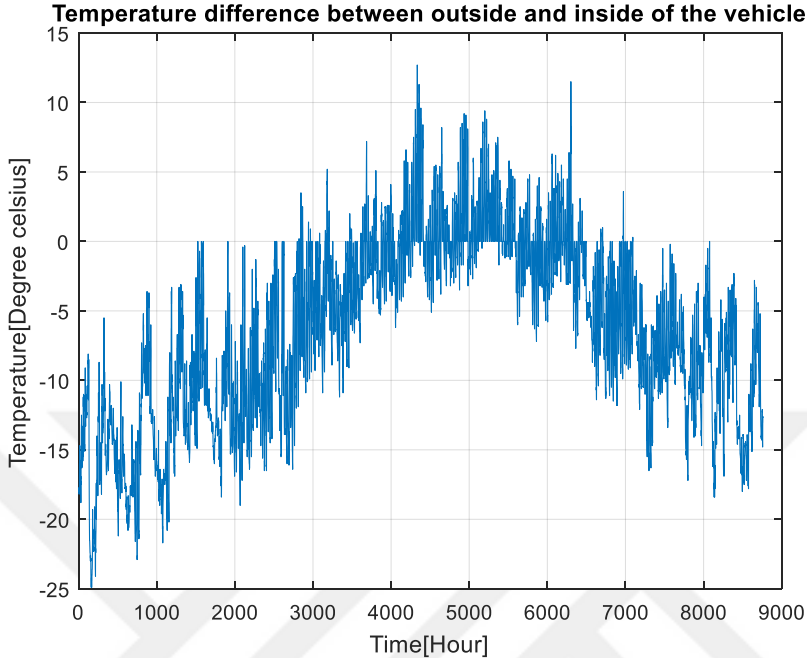
Figure 4-29 Temperature difference between outside and inside of the vehicle

Convection coefficient of the outer, h_o, and inner, h_i, surfaces are calculated from equation (24). Velocity of the inside air is assumed to be zero and the velocity air on the outer surfaces of the Metrobus is assumed to be 11.33 m/s which is the average velocity of the Metrobus according the driving cycle obtained by tests with zero wind speed assumption.

Ambient heat load due to conductive and convective heat transfer through body and windows for each hour of a year is calculated from equation (22) and result are shown Figure 4-30. Negative values means, outside of the Metrobus is colder and heating is required to maintain comfortable conditions.
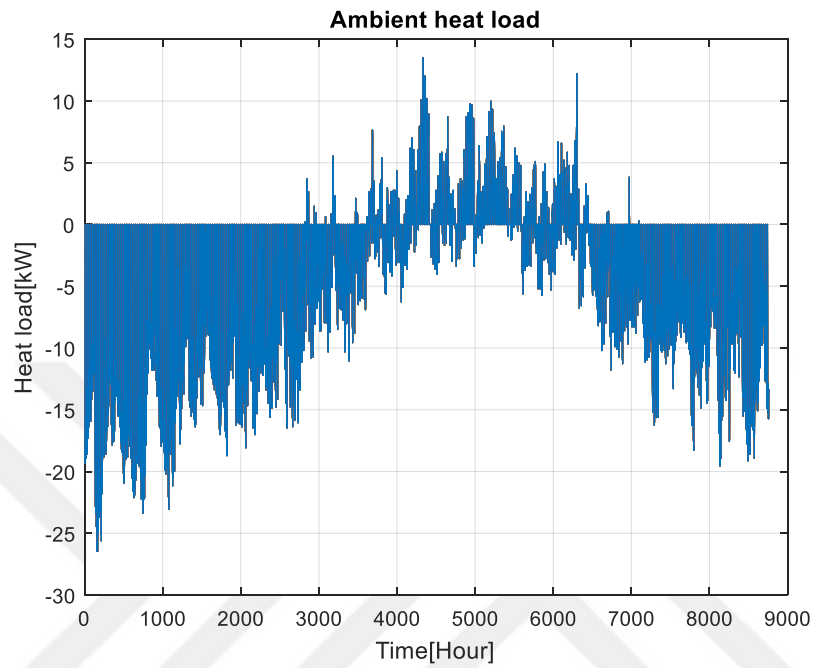
Figure 4-30 Ambient heat load

4.1.2.1.4 Ventilation Heat Load

The temperature and relative humidity must be changed according to thermal comfort requirements so as to keep inside of the bus in comfortable thermal conditions. Target inner temperature and relative humidity ranges are tabulated in Table 4-2.

Table 4-2 Target comforttemperatre and relative humidity values

Season	Temperature range	Humidity range
Winter	20.5-23 ^{o}C	30%-60%
Spring	22-24.5 ^{o}C	30%-60%
Summer	23.5-26 ^{o}C	30%-60%
Fall	22-24.5 ^{o}C	30%-60%

For the calculation of ventilation load, hourly outside temperature and humidity data are considered. Outdoor temperature and target inside temperature are shown in Figure 4-31.
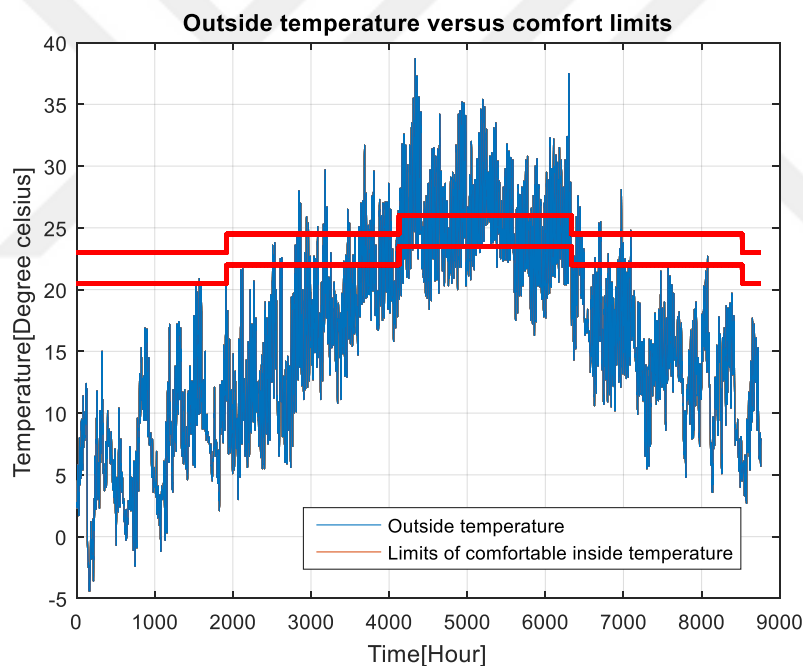
Figure 4-31 Outside temperature and comfortable inside temperature

In addition to temperature, another important data for thermal comfort, target relative humidity and inside relative humidity are shown in Figure 4-32.
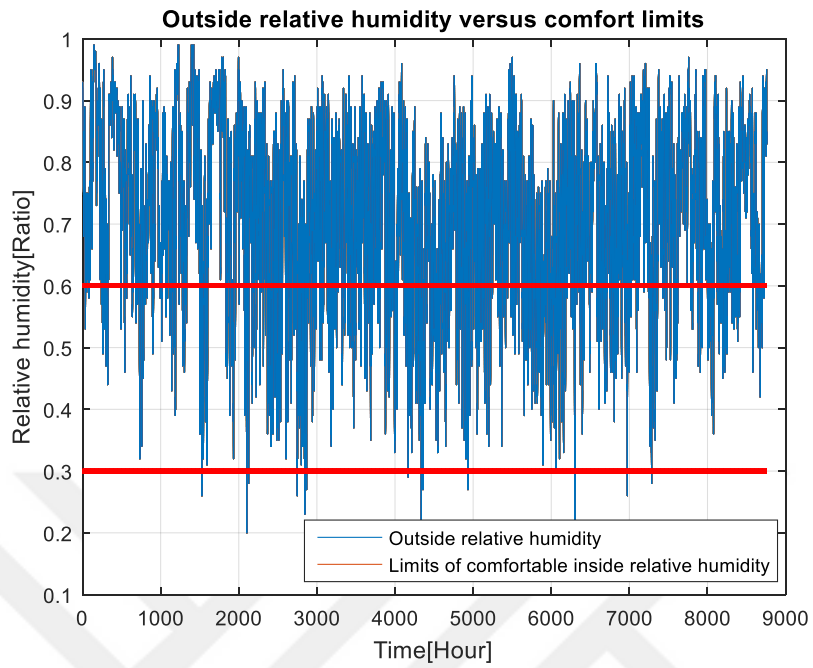
Figure 4-32 Outside relative humidity and comfortable inside relative humidity

Since the ventilation requirements are directly dependent on the number of passenger, hourly passenger occupancy rate of each station for one year are considered in calculations. Ventilation heat load of the Metrobus are calculated for each hour of the year by equation (25). Result of the calculation is shown in Figure 4-33.
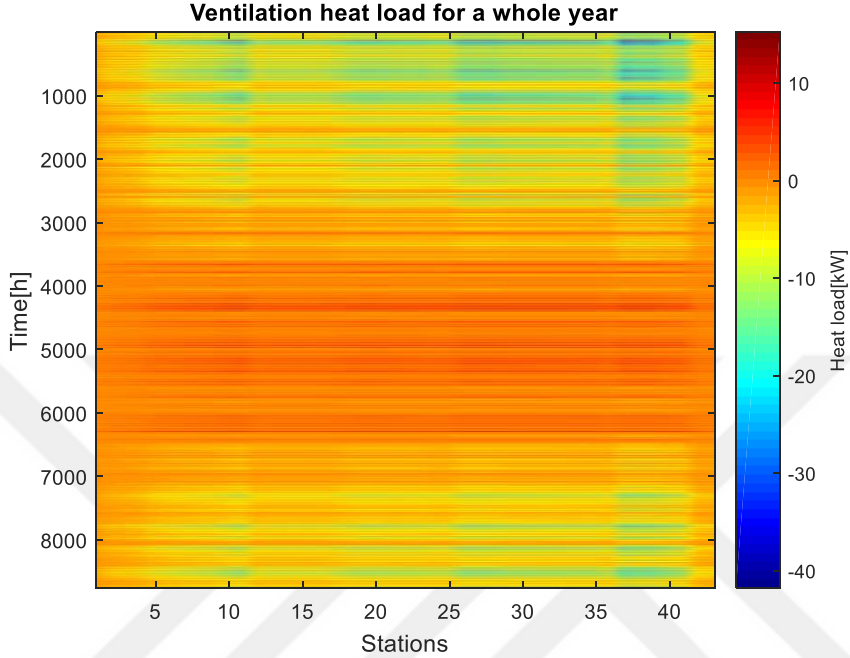
Figure 4-33 Ventilation heat load

As it can be observed from Figure 4-33, heat load changes between -42 kW and 13 kW. Negative values of heat load mean that, outside of the bus is colder and to fresh air supplied from outside the bus must be heated to the passenger comportment comfortable.

4.1.2.1.5 Results

Total heat load of the Metrobus for each hour for one year and for each station is shown in Figure 4-34. Total heat load of the Metrobus for each service hour for one year and for each station is shown in Figure 4-35. The maximum amount of heat flow into the cabin is 37.92 kW and the maximum amount of heat dissipates from the cabin is 68.25 kW.
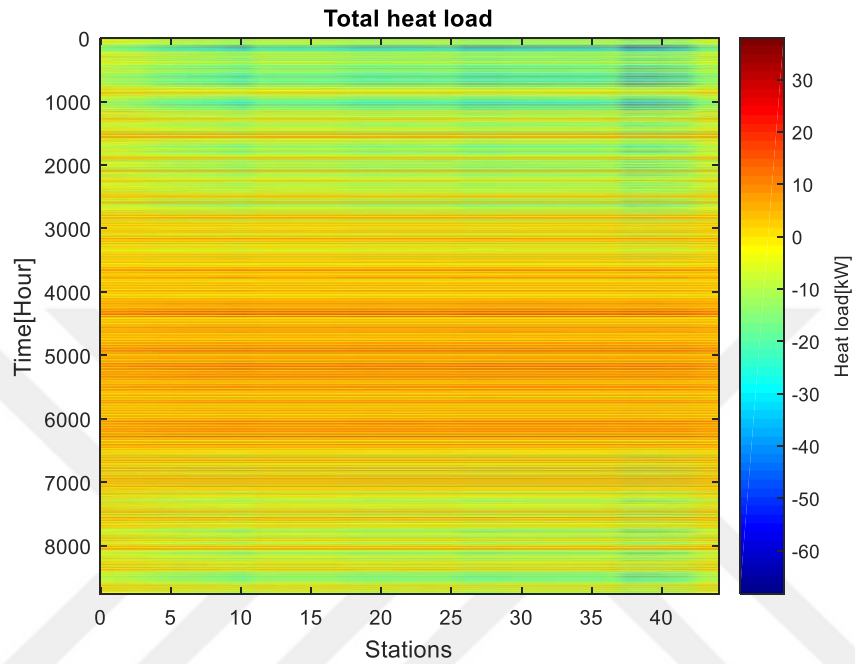
Figure 4-34 Total heat load
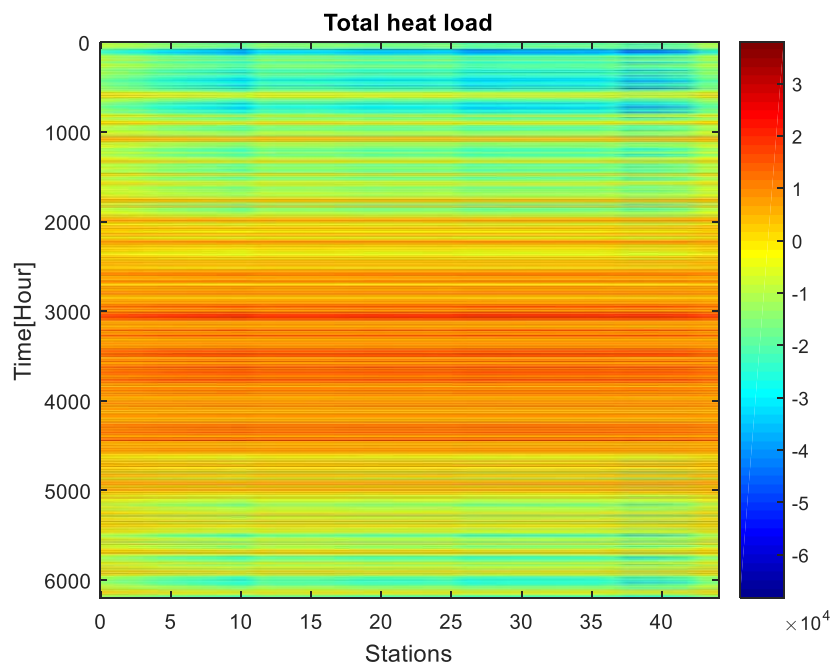
Figure 4-35 Total heat load in service hours

In order to simplify the hourly data, daily average heat load of the Metrobus is shown in Figure 4-36.
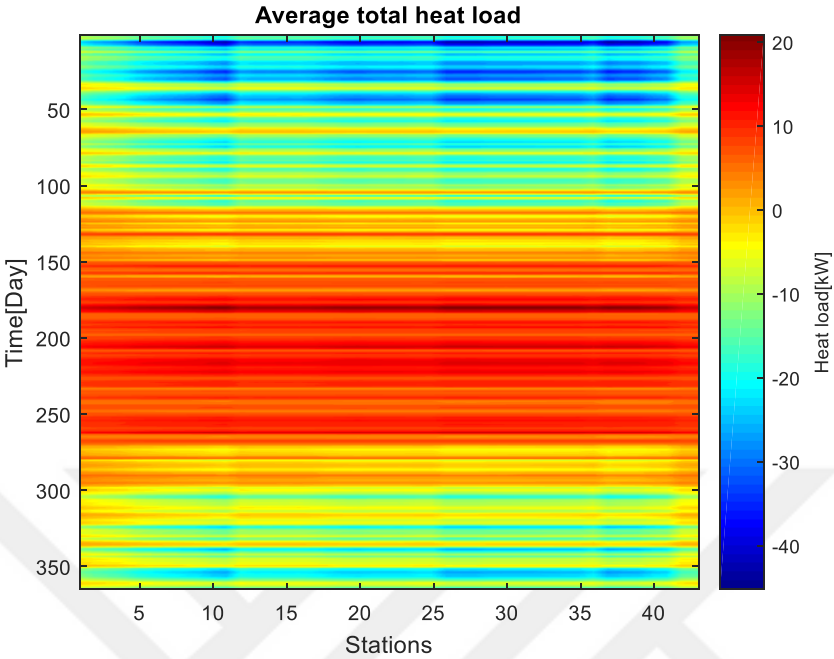
Figure 4-36 Average total heat load

Daily average heat load per kilometer is shown in Figure 4-37.As it can be seen from the figure average heat load per kilometer changes between -1.1 kWh/km and 0.5 kWh/km.
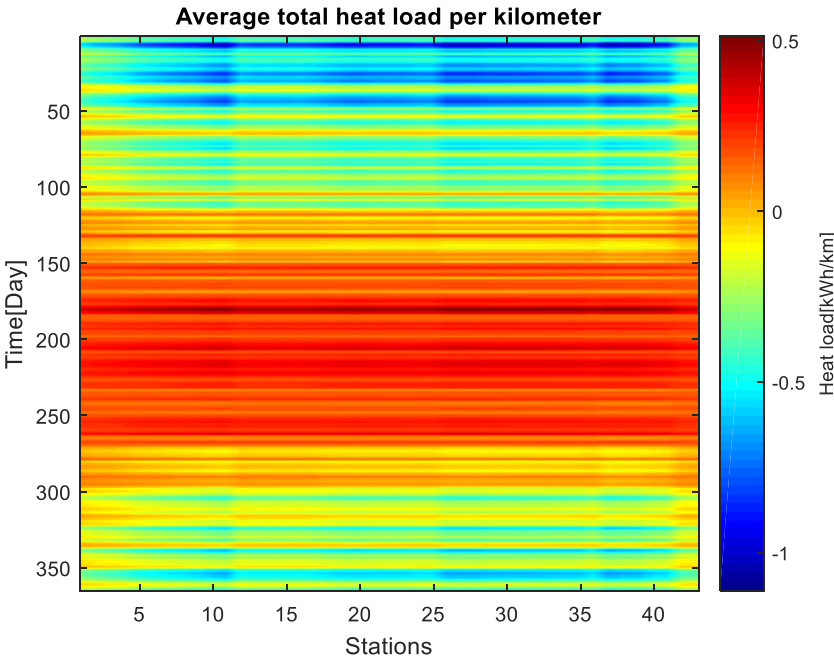
Figure 4-37 Daily average heat load per kilometer

4.1.2.2 Thermal management system of the battery

The performance of EVs is greatly dependent on the battery pack. Temperatures of the cells in a battery pack need to be maintained within its optimum operating temperature range in order to achieve maximum performance, safety and reliability under various operating conditions. Poor thermal management will affect the charging and discharging power, cycle life, cell balancing, capacity and fast charging capability of the battery pack. Hence, a thermal management system is needed in order to enhance the performance and to extend the life cycle of the battery pack [42].

Thermal management system of a battery should be capable to remove heat from the battery, to heat the battery so as to improve the battery temperature when the temperature is too low, insulate to prevent sudden temperature changes and ventilate to exhaust the potentially hazardous gases from the battery [43].

It is difficult to estimate the consumption of the battery thermal management system of the vehicle because of the difference in battery composition, capacity, charge and discharge rate. Kriger et al. investigated the energy consumption of battery cooling system for different type of refrigerant in different driving cycle. According to results of the study it can be assumed that battery cooling system generates 3.5% additional consumption for a general urban cycle [44]. So, the consumption of the thermal management system of the battery of Metrobus can be assumed to be between 0.04 kWh/km and 0.1 kWh/km.

In order to cope with the heat load of a large battery, a powerful cooling system is needed like secondary loop liquid cooling system which is widely used in electric vehicles. Secondary loop liquid cooling system has a good cooling performance thanks to the high heat transfer coefficient of cooling liquid [45].

4.1.2.3 Other auxiliary systems

In addition to HVAC system of the vehicle and thermal management system of the battery, there are other auxiliary systems that consume energy. These systems are;

- Steering system
- Braking system
- Internal and external lights
- Compressors
- Water pumps
- Electronic control systems

It is difficult to estimate the consumption of these systems, because the usage rate of these systems depends on the unpredictable factors such as driver, time, road quality, driving cycle etc. For this reason according to studies conducted for 9 meter minibus [46] [47] and according the measurement in Avenue EV, it is assumed that average consumption of these systems is 6 kW or for the average speed obtained from driving cycle it is 0.15kWh/km.

4.1.3 Inefficiencies

In efficiencies of subcomponents of the traction system must be considered in order to estimate correct energy consumption estimation. In this section source of inefficiencies are presented and after the selection of the components their exact values are presented in 5.

There two type of inefficiency in battery, the first one is the inefficiency due to internal resistance and the second one is the charging/discharging inefficiency. They are not considered as a factor that reduces the capacity of the battery because the capacities of batteries are generally presented as nominal capacity of the battery in product catalogues by suppliers.

Nominal capacity of the battery is the amount of energy that can be withdrawn from the battery at a particular constant current, starting from a fully charged state. [48] While the maximum capacity (or theoretical capacity) of a battery is the total amount of energy it contains when fully charged. Nominal capacity and maximum capacity of a battery is represented in Figure 4-38.
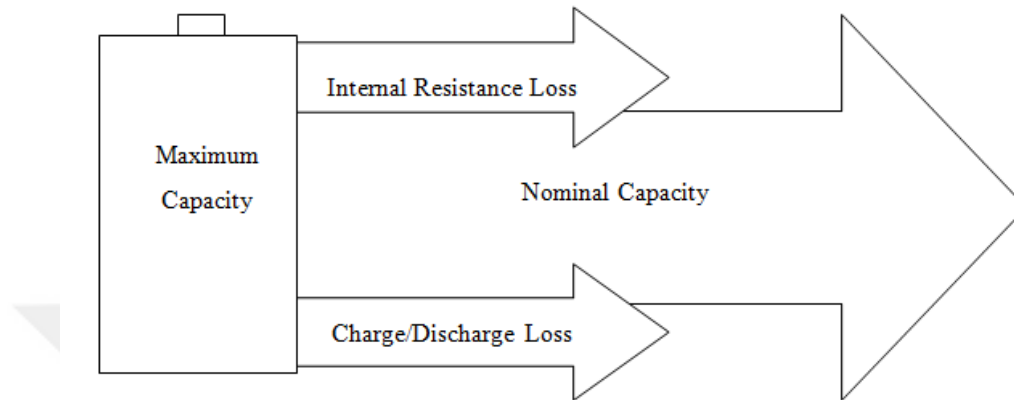
Figure 4-38 Loss in battery

Electric traction sub-system consists of electric engine, inverter and final drive. Although, electric traction systems are more efficient than internal combustion engines, there are still inefficiencies that should be considered.

Efficiency of the final drive, which is the last part of the electric traction sub-system, is assumed to be 95 % [49]. The efficiency of engine and inverter are considered together, because tests to determine the efficiency are conducted together. Even tough efficiency of the engine and inverter may reach up to 98%, this value can be obtained only in one point at the torque versus speed graph. The efficiency map of coupled engine-inverter subsystem is shown in Figure 4-39.
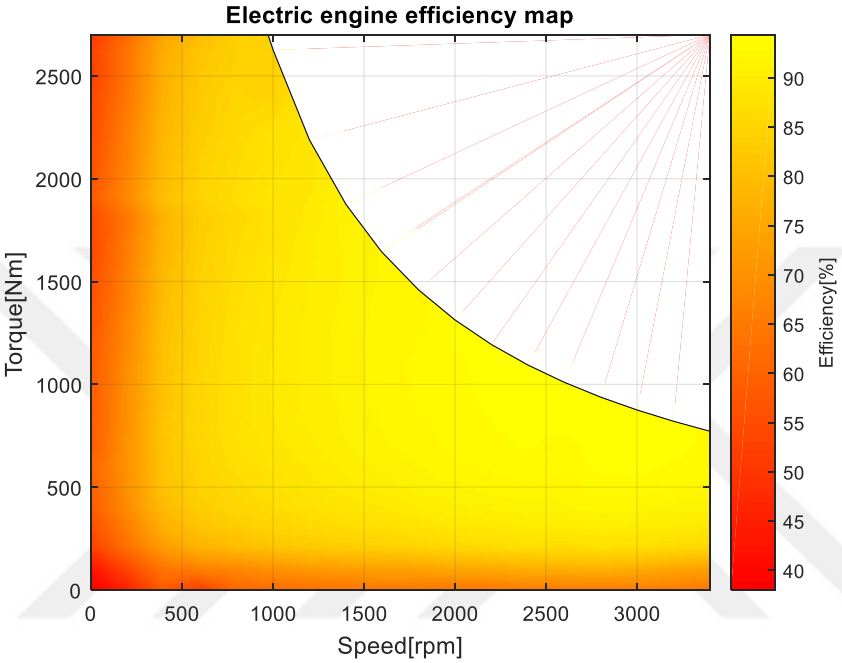
Figure 4-39 Efficiency map of the electric engine

Driving cycle is considered to determine the efficiency of the engine and inverter, results are shown in 5.2.

Since the amount of consumption of auxiliary systems such as HVAC, cooling system of battery, air compressors are small compared to the traction system, their inefficiencies are omitted.

4.1.4 Overall energy consumption

Since the component and sub-systems of the vehicle are not selected, the calculation of the total consumption is difficult. But the maximum and minimum consumption can be predicted according to values calculated in previous sections.

For the calculation of HVAC load and load of the thermal management system of the battery, it is assumed that the coefficient of performance of heating/cooling system as 3. The coefficient of performance defined as the ratio of the heat gain to the compressor electric power [50]. Additionally, inefficiencies of components and subsystems are neglected.

Prediction of minimum and maximum consumptions per kilometer is shown in Table 4-3.

Table 4-3 Prediction of minimum and maximum consumptions

Consumption	Minimum [kWh/km]	Maximum [kWh/km]
Traction (efficiency assumed 100%)	0.91	1.70
HVAC	0	0.37
Thermal management of battery	0.04	0.08
Other auxiliary systems	0.2	0.2
Overall average consumption	1.15	2.35

5 SYSTEM DESIGN

5.1 Vehicle body

Istanbul Metrobus Network was first put into service in 2007 and all details of the network such as stations, parking areas, connection roads are designed for current vehicles. For this reason, bus operator want to keep the vehicle body same. So, the body type of the electric Metrobus is selected as 18m articulated bus and the capacity of the electric Metrobus is 181 similar to the present vehicle.

The weight of the present vehicle is 18500 kg, and the weight of the electric metrobus is expected as 18000kg (battery excluded) because the internal combustion engine with a weight of 1065 kg will be replaced by approximately 550 kg of electrical traction [29].

And all other properties related to body such as, wheels, tires, drag resistance, roll resistance are assumed to be same.

5.2 Traction sub-system (engine, inverter and gearbox)

Engine, inverter and gearbox are considered as the traction sub-system. In this section components of this sub-system are selected. Since the characteristic of a component of this sub-system affects the selection process of the other component, they are not considered individually. And the selection of the components is started with the engine.

5.2.1 Engine

The engine and inverter of ASELSAN are evaluated for this project. Peak power of the engine and inverter, which are used in Avenue EV, is 250 kW. However, the engine and inverter, which are evaluated for the Metrobus project, have a similar structure but the peak power of this traction sub-system is 270kW. Torque-speed curve of the engine is shown in Figure 5-1.
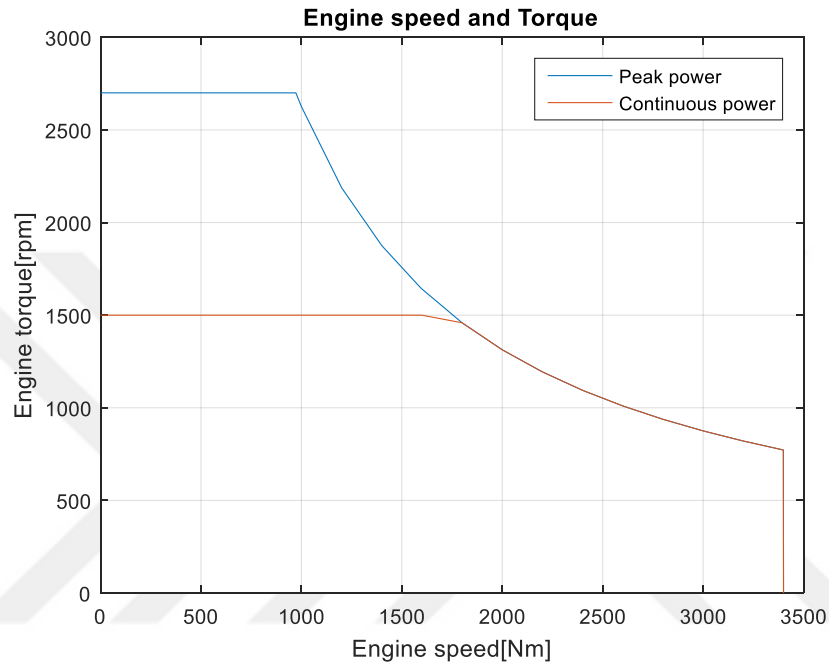
Figure 5-1 Torque-speed curve of the engine

The maximum torque of the engine is 2700 Nm and the maximum speed of the engine 3400rpm. In Figure 5-1, the blue line represents the maximum torque of the engine at peak power, while the red line represents the de-rated continuous power.

ASELSAN's 270kW traction sub-system is a nine phase permanent magnet synchronous motor. In Figure 5-2, classification of the electric engines is shown, and the place of the ASELSAN's engine is represented with red circle.
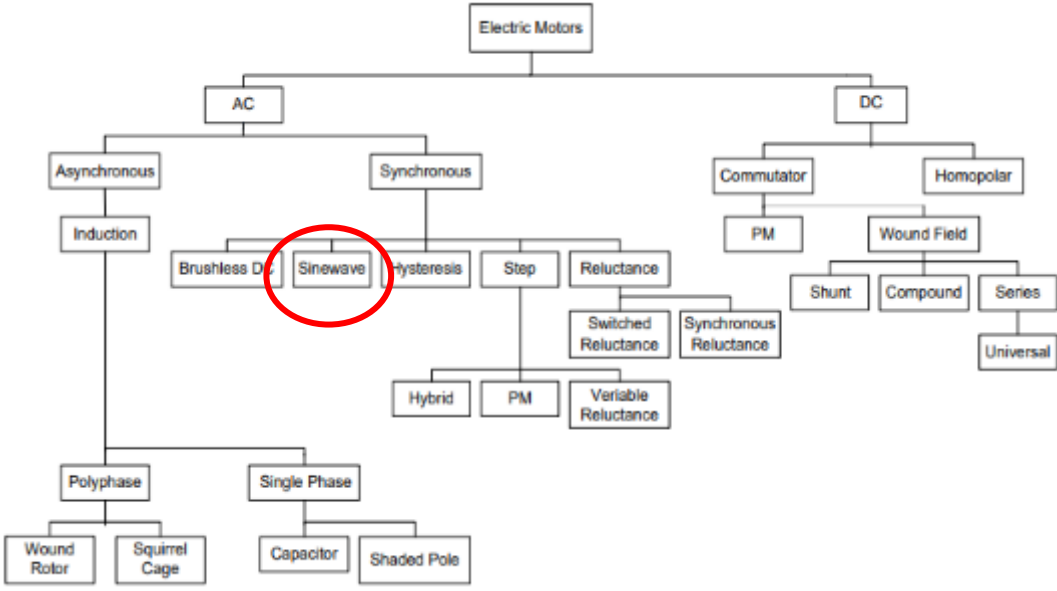
Figure 5-2 Classification of electric engines

Actually, the current that is supplied from the battery into the inverter is DC, however, since the current is converted from DC to AC by the inverter, it is an AC electric engine. Nine phase electric engine consists of 3 parallel 3 phases. The current is controlled by the inverter according to the torque request of the drive. The inverter switches the current in order to supply it with a phase difference of 120 degrees to a, b and c phases of the engine. In Figure 5-3, circuit diagram of the single phase and three-phase equivalent are shown.
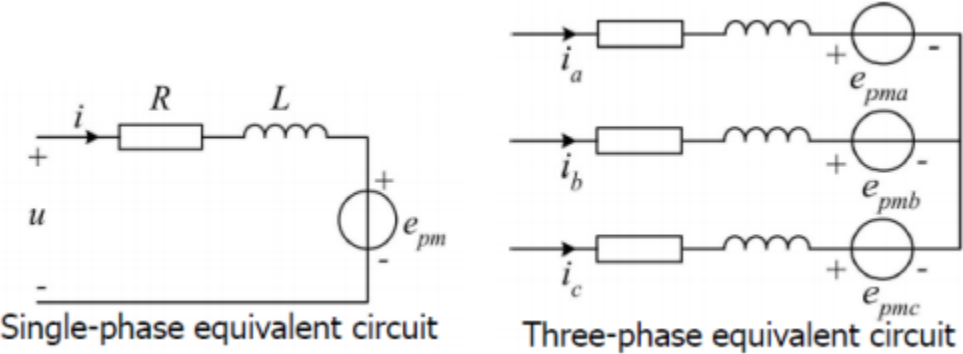
Figure 5-3 Circuit of the electric engine

Phases a, b and c can be calculated from equation (5.1).

$$\emptyset_a = \emptyset_{PM}\cos(\frac{\pi}{\tau_p x}) \tag{5.1}$$

$$\emptyset_b = \emptyset_{PM}\cos(\frac{\pi}{\tau_p x} - \frac{2\pi}{3}) \tag{5.2}$$

$$\emptyset_c = \emptyset_{PM}\cos(\frac{\pi}{\tau_p x} + \frac{2\pi}{3}) \tag{5.3}$$

In traction case the current flows in direction as shown in Figure 5-3, however in regenerative braking case, engine starts to generate current. The current that is generated by the engine, flow in the opposite direction to the current i. When, the current generated by the engine is greater than the current i, engine acts like a generator and charges the battery. Regenerative braking torque can be controlled by increasing or decreasing the current i.

5.2.2 Gearbox ratio

To determine the gearbox ratio several properties are investigated. These are;

- Maximum speed requirement
- Maximum torque requirement
- Grade-ability requirement
- Acceleration requirement
- Available adhesion coefficient

5.2.2.1 Maximum speed requirement

To determine upper limit of the range of the gearbox ratio, maximum speed of the engine and maximum speed of the driving cycle are considered. The maximum speed of the engine is 3400 rpm while the maximum speed of the driving cycle is 18.9 m/s. From equation (5.4), maximum gear ratio is determined.

$$\varphi_{gearbox} = \frac{2\pi\, r_{wheel\,eff}}{v_{\max vehicle} \times 60} \times \omega_{max\,engine} \tag{5.4}$$

where $\omega_{max\,engine}$ is the engine speed in rpm, $v_{\max vehicle}$ is the maximum speed of the vehicle in meter per second according to driving cycle, $r_{wheel\,eff}$ is the effective tire radius

and $\varphi_{gearbox}$ is the gear box ratio. The radius of the tire is 0.475 m but the effective tire radius is less than this value. Since the effective tire radius is depends on several unpredictable factors such as, pressure and tire wear and to design the vehicle for worst conditions the effective radius is assumed as (5% less than the tire radius).

From equation (5.1) upper limit of the gearbox ratio is determined as 8.50. Metrobus with gearbox that has any ratio higher than 8.50 is not capable to reach the maximum speed of the driving cycle.

5.2.2.2 Maximum torque requirement

To determine the lower limit of the range of the gearbox ratio, maximum torque of the engine and maximum traction force obtained from driving cycle are considered. From equation (5.5), maximum gear ratio is determined.

$$\varphi_{gearbox} = \frac{F_{max\,traction\,vehicle} \times r_{wheel\,eff}}{T_{max\,engine} \times \eta_{gearbox}} \tag{5.5}$$

where $T_{max\,engine}$ is the engine's maximum torque in Nm, $F_{max\,traction\,vehicle}$ is the maximum traction force of the vehicle according to driving cycle, $r_{wheel\,eff}$ is the radius of wheel which is 0.475 m, $\eta_{gearbox}$ is the efficiency of the gearbox (assumed to be 0.95) [49] and $\varphi_{gearbox}$ is the gear box ratio. $F_{max\,traction\,vehicle}$ can be obtained from equation (5.6).

$$F_{max\,traction\,vehicle} = \frac{P_{max\,traction\,vehicle}}{v_{vehicle\,max\,traction}} \tag{5.6}$$

where $P_{max\,traction\,vehicle}$ is the maximum traction power of the vehicle according to driving cycle and $v_{vehicle\,max\,traction}$ is the vehicle's speed at maximum traction.

From equation (5.6) the lower limit of the gearbox ratio is determined as 8.01. Metrobus with gearbox that has any ratio lower than 8.01 is not able to reach the required acceleration of the driving cycle.

5.2.2.3 Grade-ability

Grade-ability is the ability of the Metrobus to climb a slope. In this section the grade-ability of the vehicle and the acceleration of the vehicle at different speeds for different gearbox ratio are investigated. Additionally, abilities of the vehicle are compared with other vehicles. In the end of the section range of the gearbox ratio is reevaluated according to results.

Although the maximum slope of the Metrobus Network is 4.29 degree (7.5%), grade-ability is evaluated according to allowable maximum slope of Turkish roads which is 7.5 degree (9%) [51]. From equation(5.7) it is obtained that, fully loaded Metrobus with gearbox that has any ratio lower than 7.72 is not able to climb 9% slope and with a gearbox ratio greater than 4.41 it can climb 7.5% slope. With a gearbox ratio higher than 7.72 Metrobus is able to climb the slope with any speed lower than 22.5 kph.

$$\varphi_{gearbox} = \frac{m_{vehicle\,loaded} \times g \times r_{wheel\,eff} \times \sin(7.5)}{T_{max\,engine} \times \eta_{gearbox}} \tag{5.7}$$

5.2.2.4 Available adhesion coefficient

Metrobus has 4 axles which are front axle, center axle, drive axle and trailer axle. Metrobus is driven from the third axle which is the drive axle.

Typical adhesion coefficient factors for various roads are given in Table 5-1.

Table 5-1 Adhesion coefficient factors for various road [45]

Road type	Concrete of Asphalt
Dry	0.76-0.85
Wet	0.48-0.52

The third axle has 4 tires and the fourth axle has 2 tires. It is assumed that third axle and fourth axle share the load in the ratio of the number of tire. In other word, third axle carry two times more weight than the forth axle. Additionally, it is assumed that third and fourth axle only carry the load of the articulation.

According to these assumptions the maximum available force that can be delivered to the road can be calculated from equation (5.8).

$$F_{available} = m_{articulation} \times g \times \mu_{dry} \times \frac{2}{3} \tag{5.8}$$

where $F_{available}$ is the maximum available, $m_{articulation}$ is the mass of the articulated part of the vehicle, g is the gravitational acceleration and μ_{dry} is the adhesion coefficient of the dry asphalt.

On the other hand maximum traction force of the engine can be calculated from equation (5.9).

$$F_{max\ traction} = \frac{T_{max} \times \varphi_{gearbox} \times \eta_{gearbox}}{r_{wheel\ eff}} \tag{5.9}$$

where $F_{max\ traction}$ is the maximum traction for that can be produced by the engine, T_{max} is the maximum torque of the engine, $\varphi_{gearbox}$ is the gearbox ratio, $\eta_{gearbox}$ is the efficiency of the gearbox and $r_{wheel\ eff}$ is the effective tire radius.

Since $F_{available}$ is the maximum traction force that can be delivered to the road, values of $F_{max\ traction}$ that is greater than $F_{available}$ is unnecessary. In other word, to prevent the slip at maximum adhesion coefficient $F_{max\ traction}$ must be less than $F_{available}$.

By combining equation (5.8) and (5.9), the gearbox ratio that is sufficient to supply $F_{available}$ can be calculated from equation (5.10) .

$$\varphi_{gearbox} = \frac{2 \times r_{wheel\ eff} \times F_{z_r} \times \mu_{dry}}{3 \times \eta_{gearbox} \times T_{max}} \tag{5.10}$$

Where, F_{z_r} is the vertical force due to the weight of the articulation. From the equation (5.10), it is found out that, gearbox ratio bigger than 8.40 is unneeded because the traction force at maximum torque is greater than the available traction force. For this calculation, load transfer between wheels due to acceleration is neglected.

5.2.2.5 Selection of the gearbox ratio

Available gearbox ranges are tabulated in Table 5-2 according to four criteria.

Table 5-2 Gearbox ratio selection criteria

Criteria	Lower limit	Upper
Maximum speed	-	8.50
Maximum torque	8.01	-
Grade-ability	7.72	-
Adhesion		8.40

As it can be seen from Table 5-2 gearbox ratio must be between 8.01 and 8.50 in order to work at all torques and at all speeds required by the driving cycle. And, to be able to climb 9% slope, it must have a gearbox ratio higher than 7.72 which is already satisfied by the minimum gearbox ratio 8.01. Additionally, to prevent slip at maximum traction, gearbox ratio 8.40 is enough. To sum up, gearbox ratio must be between 8.01 and 8.5.

At this point to find the optimum gearbox ratio in terms of efficiency, different gearbox ratios are investigated. Driving cycle efficiency of the engine is calculated for different gearbox ratios between 8.01 and 8.5, and it is found out that maximum efficiency can be achieved with 8.32 gearbox ratio. Speed-torque points of the driving cycle on efficiency map of the engine are shown in Figure 5-4.
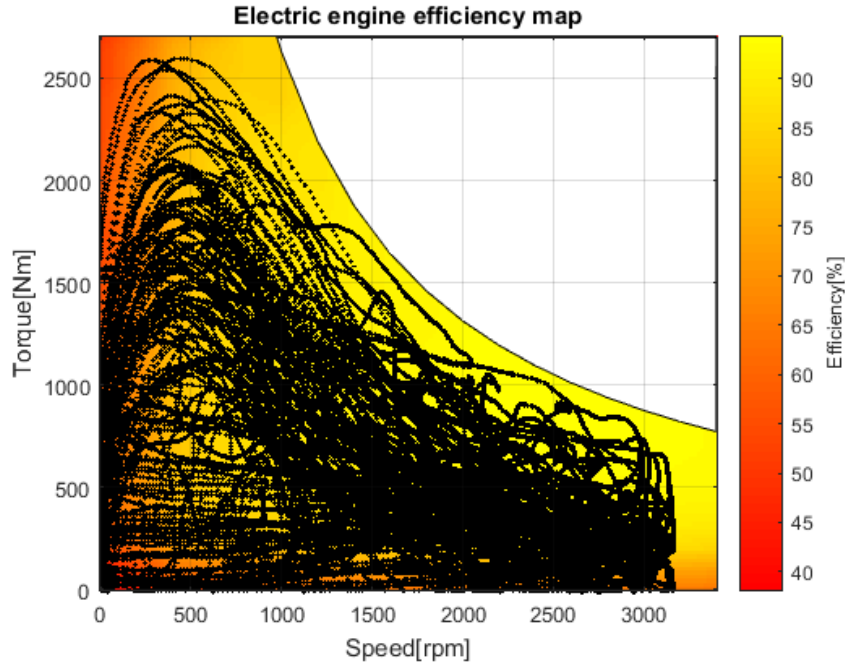
Figure 5-4 Efficiency map of the engine (Gearbox ratio: 8.32)

Thus, the ratio of the gearbox selected as 8.32. With this ratio the efficiency of the engine-inverter couple is 84.8% for Söğütlüçeşme direction and 81.6% for Beylidüzü direction. It should be noted that, depending on the availability in market the ratio can be between 8.01 and 8.40, but if the most efficient gearbox ratio is needed, the ratio should be 8.32 and in this study it is considered as 8.32.

5.2.3   De-rating

In this engine, de-rating is applied to prolong the life of the engine and to prohibit failure in the inverter. In the inverter there are insulated gate bipolar transistors (IGBT), which are used for switching. IGBTs of the inverter are cooled with a cold plate. Cooling capacity of the cold plate may be insufficient of long duration high power working condition of IGBTs. In order to prohibit possible failure in IGBTs, inverter is controlled by an algorithm that de-rates the maximum power of the traction system. The algorithm de-rates the maximum power to continuous power after 60 seconds of working above the continuous power curve. So, de-rating situation must be evaluated at fully loaded case.

For the evaluation of the engine, curve of engine's maximum torque and speed is plotted. Then, the torque and speed points that are obtained from the driving cycle at fully loaded condition are plotted into this graph for maximum and minimum gear ratios. The plot for 8.32 gearbox ratio can be seen in Figure 5-5.
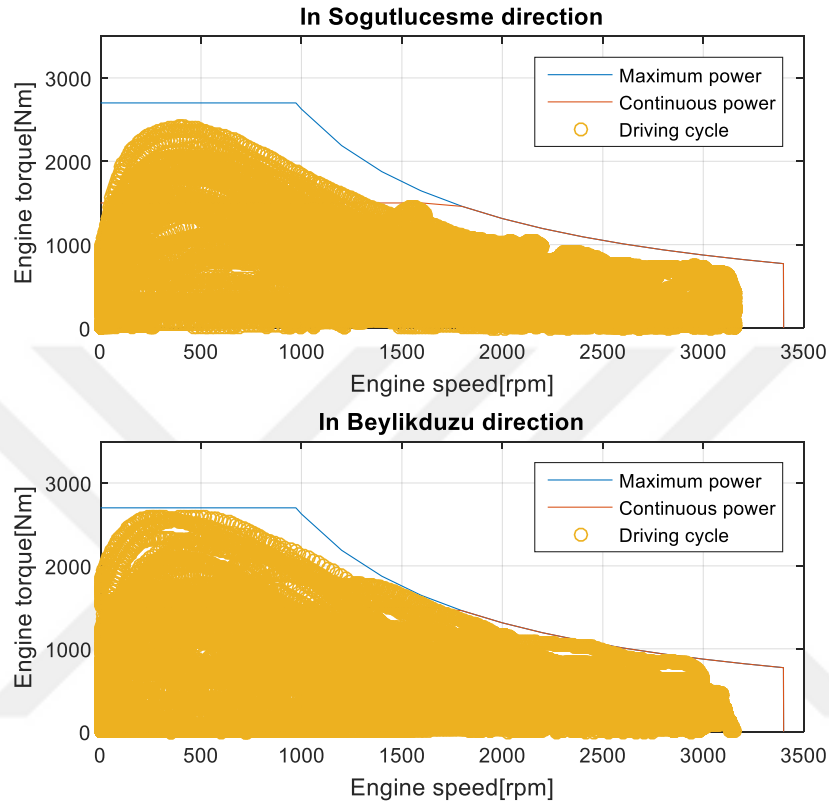
Figure 5-5 Engine torque and speed curve (gearbox ratio: 8.32)

From Figure 5-5, it can be observed that all torque-speed points of driving cycle are involved by the maximum power curve of the engine. To finalize the engine selection derating case must be checked. When the time spent in the high power zone is examined, there is no traction above the continuous power lasting more than 20 seconds. Thus it can be said that the engine is suitable for gearbox ratio 8.32.

5.2.4 Overall efficiency and performance

In order to use the engine's most efficient areas different gearbox ratios were examined. The most efficient gearbox ratio for the traction sub-system is selected as 8.32. Efficiency map of the traction sub-system and the corresponding points of the driving cycle are shown in Figure 5-4.

To sum up, the engine and inverter of ASELSAN are suitable for electrification of the Metrobus Network. The average efficiency of the traction sub-system for the driving cycle in both directions is 83.2% and the efficiency of the gearbox is assumed to be 95% [49] . Thus, the total efficiency of gearbox-engine-inverter becomes 79%.

Acceleration performance of the vehicle with this engine can be obtained from equation (5.11).

$$\Delta t = m_{vehicle} \int_{v_{initial}}^{v_{final}} \frac{\partial v}{F_{net}} \qquad (5.11)$$

where, $m_{vehicle}$ is the mass of the vehicle, v_{final} is the final speed, $v_{initial}$ is the initial speed, which is 0 for this case, F_{net} is the net tractive effort and Δt is the required duration to reach to the final speed. Results obtained for different final speeds from this equation are shown in Table 5-3.

Table 5-3 Acceleration perfomance of the vehicle

Scenario	Duration
Empty vehicle from 0 kph to 30 kph	2.6 seconds
Empty vehicle from 0 kph to 50 kph	7.2 seconds
Empty vehicle from 0 kph to 70 kph	14.1 seconds
Loaded vehicle from 0 kph to 30 kph	4.7 seconds
Loaded vehicle from 0 kph to 50 kph	13.1 seconds
Loaded vehicle from 0 kph to 70 kph	25.6 seconds

5.3 HVAC

Thermal loads of the Metrobus cabinet at comfortable temperature and humidity are calculated in section 4.1.2.1. Peak thermal power requirement to keep the cabinet comfortable of one year period and maximum daily average cooling and heating requirement are tabulated in Table 5-4. These are the maximum cooling and maximum heating requirements, so the HVAC system to be selected must be capable to supply enough cooling and heating power.

Table 5-4 Thermal load of the Metrobus

	Maximum cooling	Maximum heating
Peak thermal power	37.92 kW	68.25 kW
Daily average thermal power	0.5 kWh/km	1.1 kWh/km

The energy-based efficiency measure of the refrigeration unit, COP can be defined as follows;

$$W_{Comp} = \frac{\dot{Q}_{HVAC}}{COP} \tag{5.12}$$

$\dot{Q}_{HVAC}$ is the thermal load and W_{Comp} is the minimum power that is needed to be supplied to the compressor. COP (coefficient of performance) may vary according to different months, temperature and air mixture ratios. Typical coefficient of performance of an air conditioning system of a bus is assumed to be 3 [19]. The power requirement of the HVAC compressor is calculated from equation (5.12) and the results are shown in Table 5-5.

Table 5-5 HVAC power consumption

	Maximum cooling	Maximum heating
Peak HVAC power	12.64 kW	22.75kW
Daily average HVAC consumption	0.166 kWh/km	0.366 kWh/km

The capacity and discharge rate of the battery must be able to supply the required power of the HVAC system in addition to the traction power requirement. Furthermore the average annual consumption of the HVAC system is 0.1 kWh/km, regardless of station and time.

5.4 Regenerative Braking

One of the most important features that distinguish electric vehicles from other vehicles is their regenerative braking system. With regenerative braking, electric vehicles can recover some of the energy lost during braking. Deceleration profile and energy consumed by braking of a fully loaded Metrobus are shown in Figure 5-6and Figure 5-7, respectively.
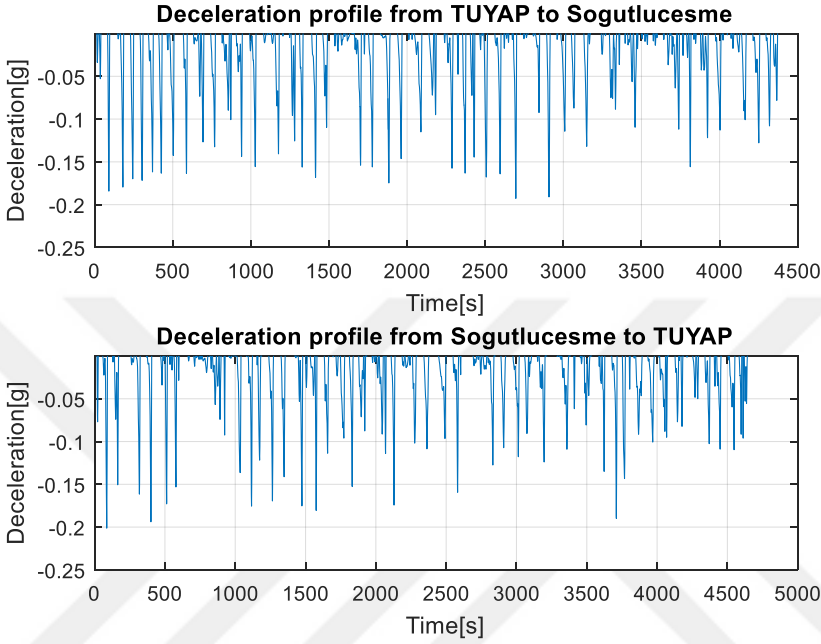
Figure 5-6 Deceleration profile of the vehicle
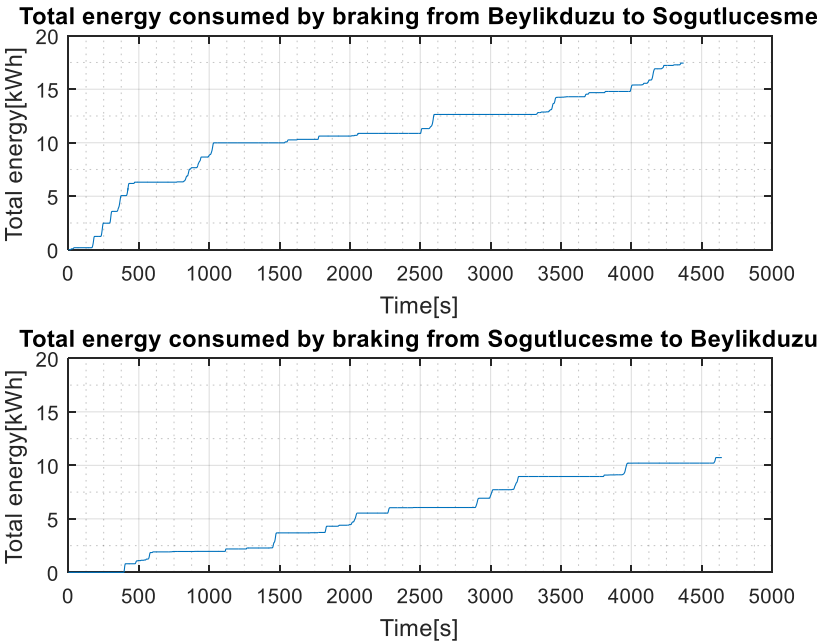
Figure 5-7 Energy consumed by braking

94

5.4.1 Brake force distribution

Braking energy consumption that is shown in Figure 5-7 is the potential energy that can be recuperated by the regenerative braking system but generally it is not possible to recuperate all the energy because, there are some limitation due to vehicle stability and charging inefficiencies.

Probably the most important safety/stability characteristic of a vehicle is its braking performance. Stability and safety of buses, especially articulated buses, are very important and very complex issues. Tractor/trailer systems can be inherently unstable in certain conditions, such as high speed hard braking. In such conditions, stability is not always maintained by passive braking systems, even if they are in perfect operating condition [53].

When a lock occurs in the tractor steering axle, the tractor moves only to the direction of progress, which is plow-out. When a lock occurs in the tractor tandem axle, tractor tandem axle is rotated excessively, which is Jackknife so it is impossible to recover its posture. Also when the lock occurs in the semitrailer axle, the semitrailer is out of trajectory, which is trailer swing [54]. Trailer swing and jackknifing are illustrated in Figure 5-8.
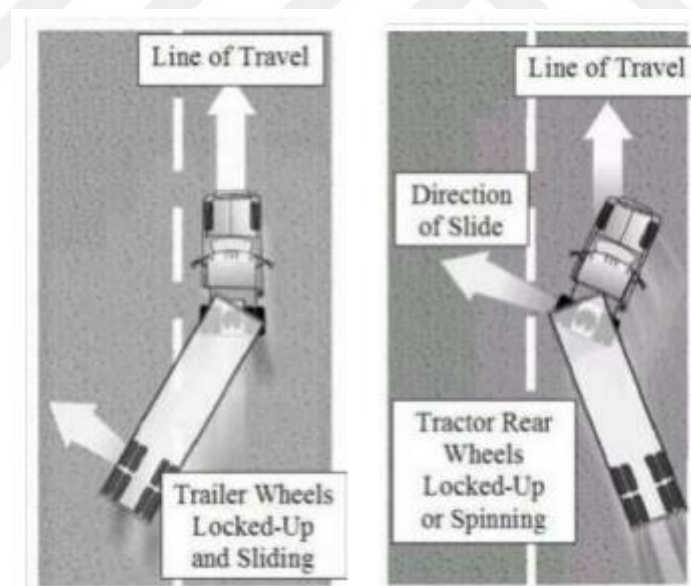
Figure 5-8 Trailer Swing (Left), Tractor Jackknife (Right) [48]

The tests conducted by the NHTSA clearly showed the safety benefits of locking front brakes first in terms of shorter stopping distance and improved stability, even when braking on slippery roadway while the vehicle is turning [56].

As it can be seen from Figure 3-1, Metrobus has 4 axles which are front axle, center axle, drive axle and trailer axle. Metrobus is driven from the third axle which is the drive axle. Second, center axle, and the drive axle have double tires while the first and fourth axle have one tire. During the braking there are load transfers between axles however, since the distance between third and fourth axle is too small to transfer load, they are considered as one axle for the calculation of brake force distribution.

The force and moment equilibrium balance of the Metrobus [56];

$$F_{z_r} = W_2 m_2 - W_2 a (x_2 - z_2) - F_{x_r} z_2 \tag{5.13}$$

$$F_{z_m} = W_1 m_1 - W_2 (1 - m_2) y + a\left(-W_1 x_1 - W_2 z_1 + W_2 y (x_2 - z_2)\right) + F_{x_r}(z_1 \tag{5.14}$$
$$+ y z_2)$$

$$F_{z_f} = W_1 (1 - m_1) + W_2 (1 - m_2)(1 - y) \tag{5.15}$$
$$+ a\left(W_1 x_1 + W_2 z_1 + W_2 (1 - y)(x_2 - z_2)\right) + F_{x_r}(z_2 - (z_1$$
$$+ y z_2))$$

By the using the terminology of equations 5.13, 5.14 and 5.15, geometric and load configurations are illustrated in Figure 5-9.
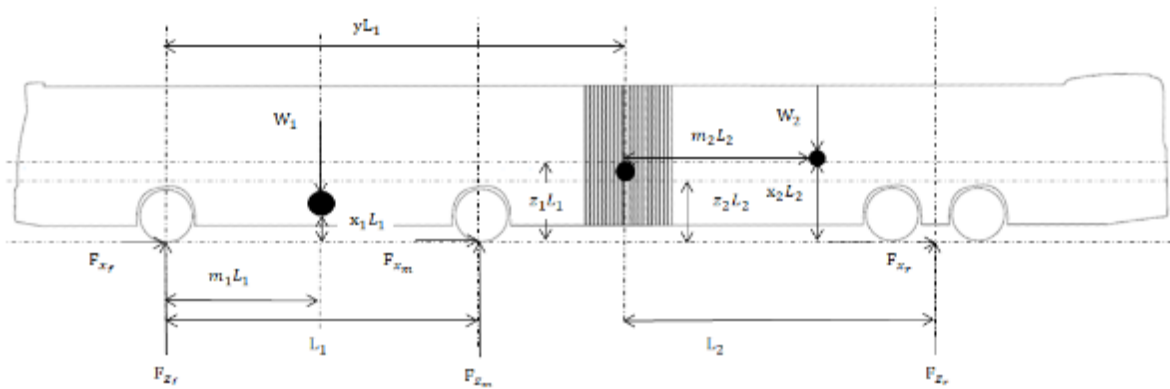
Figure 5-9 Geometric and load configuration of Metrobus

In ideal condition where the deceleration divided by the gravitational acceleration is equal to the adhesion force, brake force on each axle of the Metrobus can be determined from the following equations;

$$\frac{F_{x_f}}{W_1} = a(1 - m_1 + ax_1) + a\frac{W_2}{W_1}(1 - y + az_1)\frac{1 - m_2 + ax_2}{1 + az_2} \tag{5.16}$$

$$\frac{F_{x_m}}{W_1} = a(m_1 - ax_1) + a\frac{W_2}{W_1}(y - az_1)\frac{1 - m_2 + ax_2}{1 + az_2} \tag{5.17}$$

$$\frac{F_{x_r}}{W_2} = a\frac{m_2 + a(z_2 - x_2)}{1 + az_2} \tag{5.18}$$

Results of equation (5.16), (5.17) and (5.18) are represented in Figure 5-10 for different weight conditions.
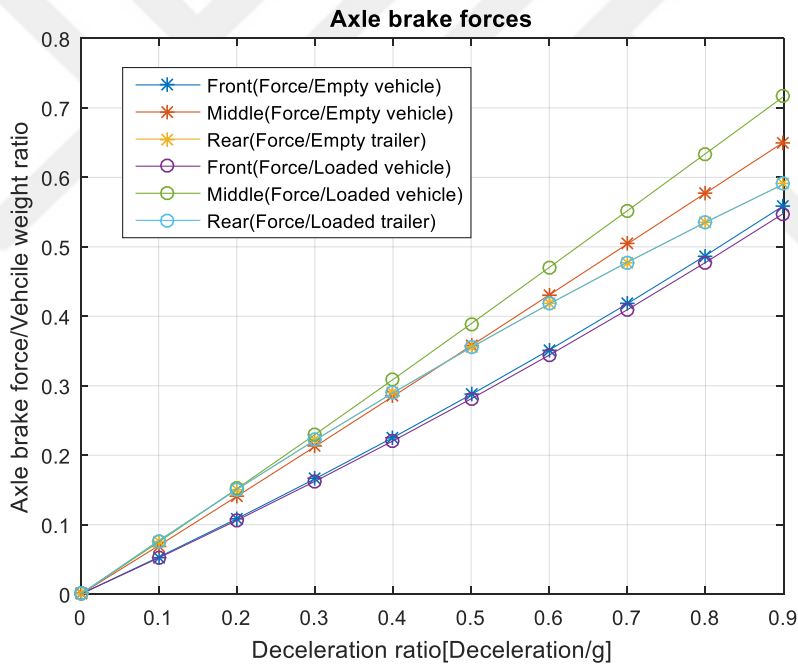
Figure 5-10 Axle brake forces

97

The ideal braking force distribution curves are shown in Figure 5-11. To design a braking system to lock up all axles at the same time, the braking force on all axles must follow these curves.
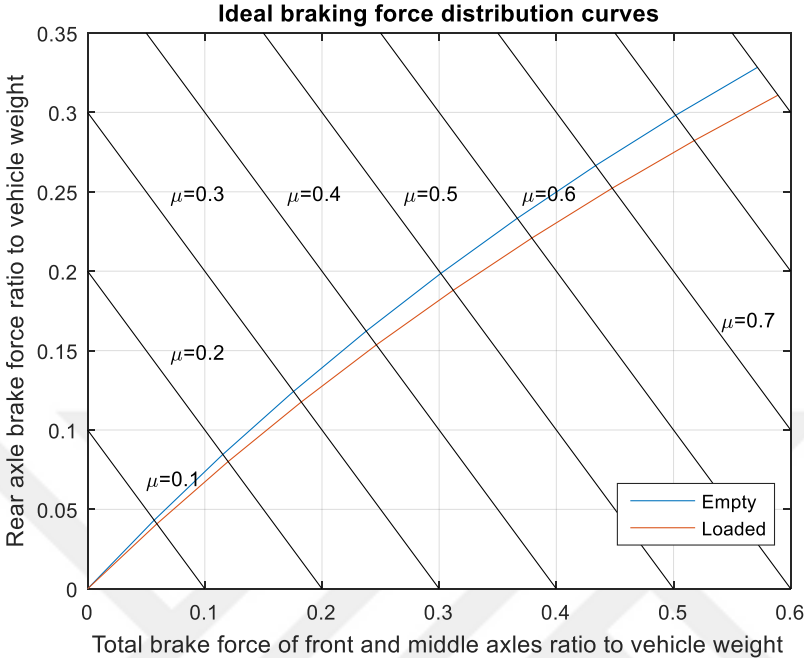
Figure 5-11 Ideal braking force distribution

In addition to ideal braking force distribution, available braking force on the drive axle must be investigated. For the investigation it should be noted that, trailer has two axles, first one is the drive axle with 4 wheels and the second one is the carrier axle with 2 wheels. For the ease of calculation, these two axes in the calculation of the ideal brake distribution were considered as one axle, however, in order to calculate the available braking force on the drive axle it is considered separately because they share the vertical forces.

For the calculation of vertical load, the vertical load is assumed to be directly proportional to the number of wheels. In Figure 5-12the vertical force distribution is illustrated.
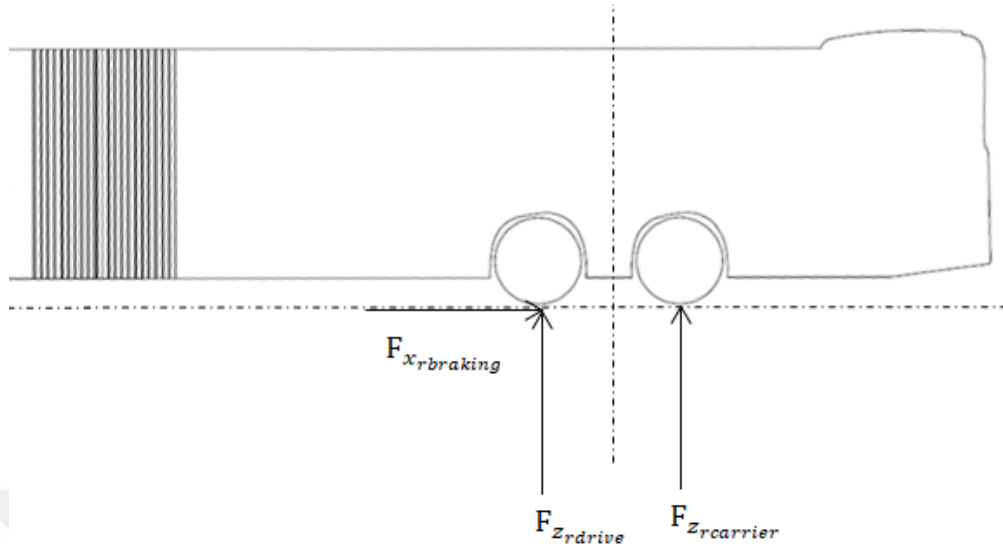
Figure 5-12 Verticale force distribution of trailer's axles

The relation between these two axles and total vertical load is shown in equation (5.19) and (5.20)

$$F_{z_{rdrive}} = 2 \times F_{z_{rcarrier}} \tag{5.19}$$

$$F_{z_r} = F_{z_{rdrive}} + F_{z_{rcarrier}} \tag{5.20}$$

Available braking force of drive axle can be calculated from equation (5.21)

$$F_{x_{rbraking}} = \mu_{avaliable} \times F_{z_{rdrive}} \tag{5.21}$$

Finally, from equations (5.13), (5.18) (5.19), (5.20) and (5.21) available braking force of drive axle can be calculated from equation (5.22).

$$F_{x_{rbraking}} = \mu_{avaliable} \times \frac{2}{3} \times (W_2 m_2 - W_2 a (x_2 - z_2)$$
$$- a \frac{m_2 + a(z_2 - x_2)}{1 + az_2} z_2 W_2) \tag{5.22}$$

Available braking force depends on available adhesion coefficient ($\mu_{avaliable}$), weight of the trailer (W_2) and the position of the center of the gravity of the vehicle.

In order to calculate the minimum available braking force various scenario is considered. The worst road condition is the icy road and the worst load distribution is that all passengers are on the front and the rear is empty. In this study regenerative braking system is designed for the most probable case which is the dry road and normal passenger distribution. Adhesion coefficient of the dry road is 0.85 [52].

On the other hand total braking force required braking force for a certain deceleration can be obtained from equation (5.23).

$$F_{x_{braking}} = a \times m_{vehicle} \tag{5.23}$$

where, $F_{x_{braking}}$ is the total braking force, a is the deceleration of the vehicle and $m_{vehicle}$ is the mass of the vehicle. For the analysis of the worst case it is assumed that all passengers are on the front and the rear is empty.

Required braking force of the vehicle and available braking force of the drive axle are shown in Figure 5-13.
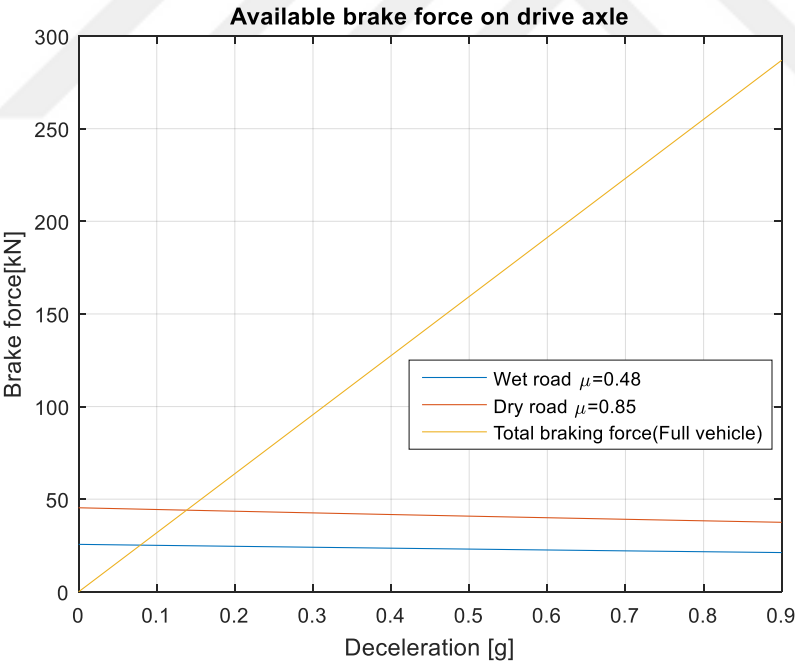
Figure 5-13 Available brake force on drive axle

So, in order to prevent the rear wheel from locking at wet road, regenerative braking force must be under the blue line shown in Figure 5-13. And the available brake force on the drive axle is able to supply total braking until 0.08g deceleration. Similarly for the dry road condition, drive axle is able to supply total braking power until 0.14g.

5.4.2   Brake control strategies

Distribution of the total braking forces between front and rear axles in order to minimize the stopping distance and distribution of the total braking forces between regenerative braking and mechanical brake so as to recover the kinetic energy of the vehicle as much as possible are two important problems in designing the regenerative braking system [24]. In his book M.Ehsani proposed three different regenerative brake strategies [57].

5.4.2.1   Series brake – optimal feel

This control objective is to minimize the stopping distance and optimize driver and passenger comfort. In this method, regenerative braking is applied as long as the deceleration from the brake pedal is below a certain acceleration value, for example 0.2g. When the deceleration above this certain acceleration value is desired, mechanical brakes in addition to the regenerative braking are activated to provide this deceleration. This method simulates the deceleration caused by the engine friction torque in internal combustion engine vehicles.

5.4.2.2   Series brake – optimal energy recovery

This control objective is to recover the braking energy as much as possible. In this method, the deceleration request from the brake pedal is provided by regenerative braking, as long as the coefficient of friction of the road is sufficient. At the point where the friction force is insufficient, mechanical brakes are activated and the desired deceleration is achieved.

5.4.2.3   Parallel brake

In this method, the mechanical braking and regenerative braking are applied in parallel and simultaneously. In vehicle design, the actual braking forces on the axles are usually designed to have a fixed linear proportion. [57]. Mechanical brake part of this system has a fixed braking force distribution ratio. Total mechanical braking force is proportional to the brake pedal position. Since the regenerative braking torque capacity of the engine depends on engine speed and since almost no kinetic energy can be covered at low engine speed, in order to maintain braking balance, braking force at high deceleration is designed to be zero.

When the desired deceleration is below a certain value, only the regenerative braking is active. When the deceleration is higher, the regenerative braking brakes up to a certain force. If too high deceleration is requested, the motor stops regenerative braking and all the deceleration is achieved by mechanical brakes. This strategy is illustrated in Figure 5-14.
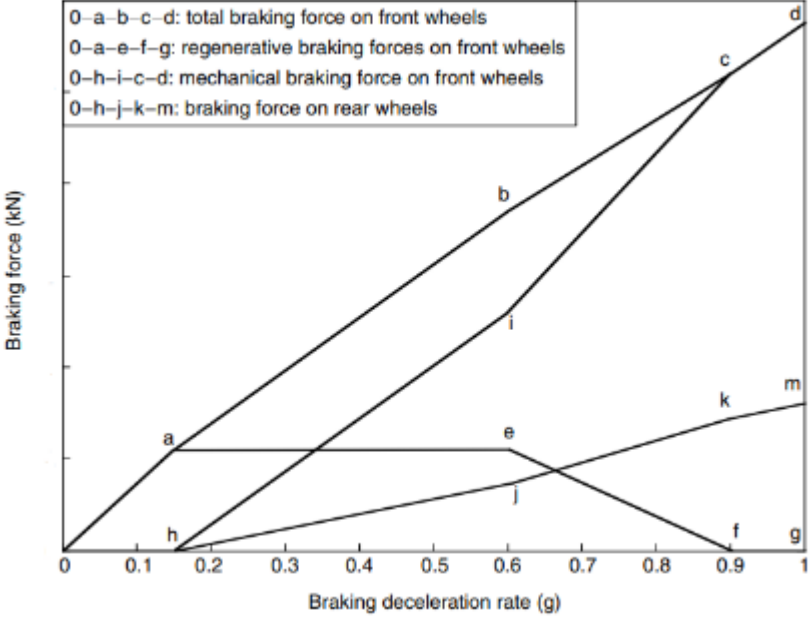
Figure 5-14 Braking force varying with deceleration rate [57]

5.4.2.4 Selection of the brake control strategy

For the selection of the regenerative braking strategy, braking decelerations and regenerative braking points on the engine's torque-speed curve must be investigated. In Figure 5-6, deceleration profile of the Metrobus in both directions is shown. Since Metrobus Network has a separated road without any disturbance from other vehicle such as sudden slowdown, improper lane change etc. and since it has a driving procedure, there is not deceleration higher than 0.25g as shown in Figure 5-6.

The reflection of this deceleration profile on the engine map is in Figure 5-15.
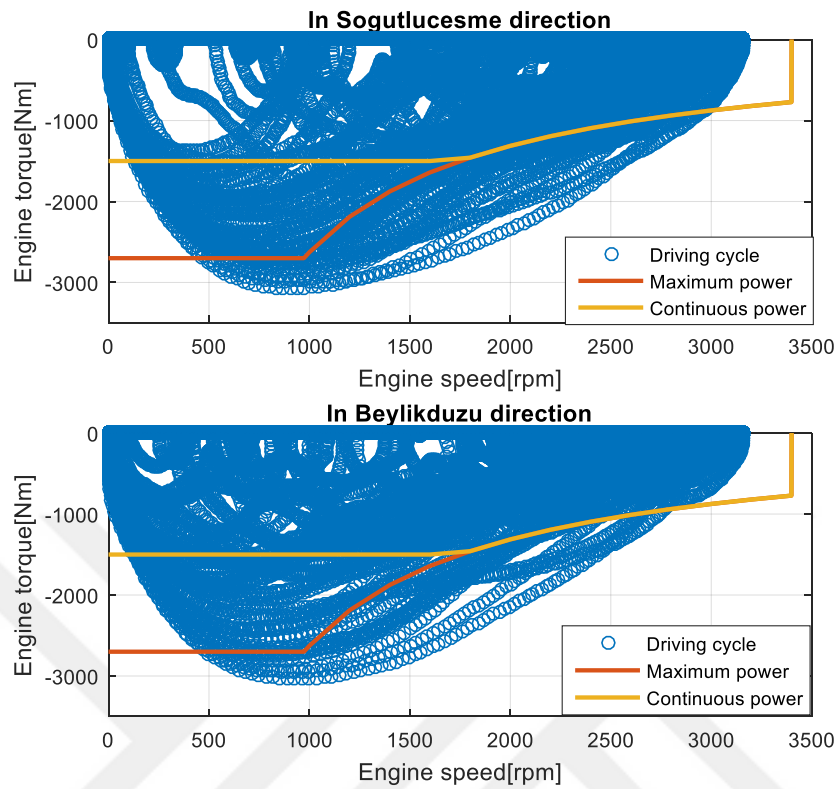
Figure 5-15 Engine torque and speed curve for regenerative braking

From Figure 5-15, it is observed that engine is not capable regain all braking; at some point of the driving cycle required braking torque exceeds maximum torque of the engine. In addition to this situation, it should be remembered from Figure 5-13, at average road and passenger distribution conditions, wheels of the drive axle is not able to transfer the braking force for a deceleration more than 0.14g.

In Figure 5-16, torque-speed points of the deceleration profile is evaluated again for decelerations less than 0.14g.
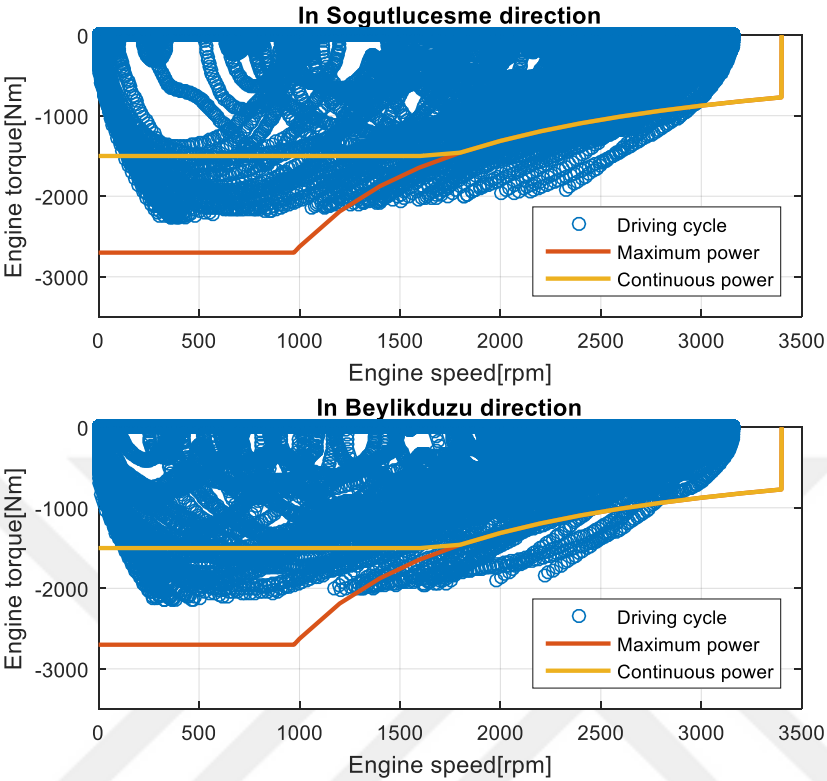
Figure 5-16 Engine torque and speed curve for regenerative braking (<0.14g)

From Figure 5-16, it is observed that at higher deceleration than 0.14g engine is not able to supply required braking force.

In Figure 5-16, torque-speed points of the deceleration profile is evaluated again but now for decelerations less than 0.1g.
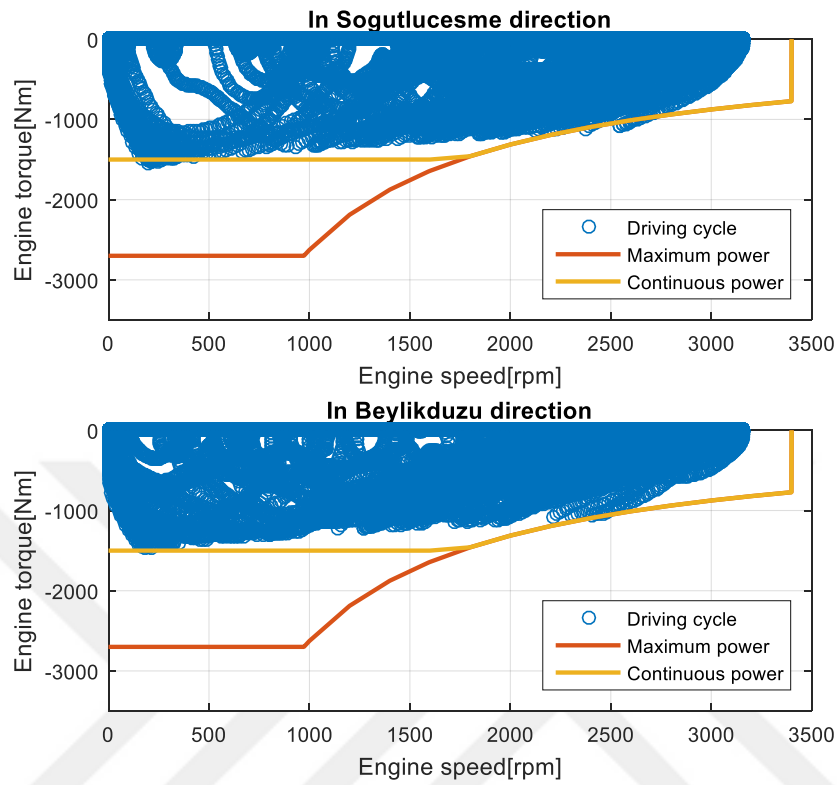
Figure 5-17 Engine torque and speed curve for regenerative braking (<0.1g)

From Figure 5-16, it is observed that at higher deceleration than 0.1g engine is not able to supply required braking force. Now it is became clear that the strategy of the regenerative braking should be series braking because drive axle has enough adhesion force to stop the vehicle for deceleration request less than 0.1g. Furthermore, since the selected deceleration (0.1g) is not high, both series braking strategies, optimal energy recovery and optimal feel, are giving the same result.

In this strategy, regenerative braking torque simulates the friction of an internal combustion engine or a retarder. But the difference is that regenerative braking torque is independent from the engine speed or vehicle speed. When the deceleration request is less than 0.1g all braking force is applied by the electric engine, when the deceleration request is greater than 0.1g mechanical brakes help electric engine to supply the requested total braking force. Brake forces of different axles are distributed according to linear brake distribution. The linear brake line is a line that is under the ideal brake curve and is similar to the ideal brake curve. With this line, the total brake force is distributed linearly close to the ideal brake curve. Linear brake distribution line and ideal brake force distribution curve are shown in Figure 5-18.
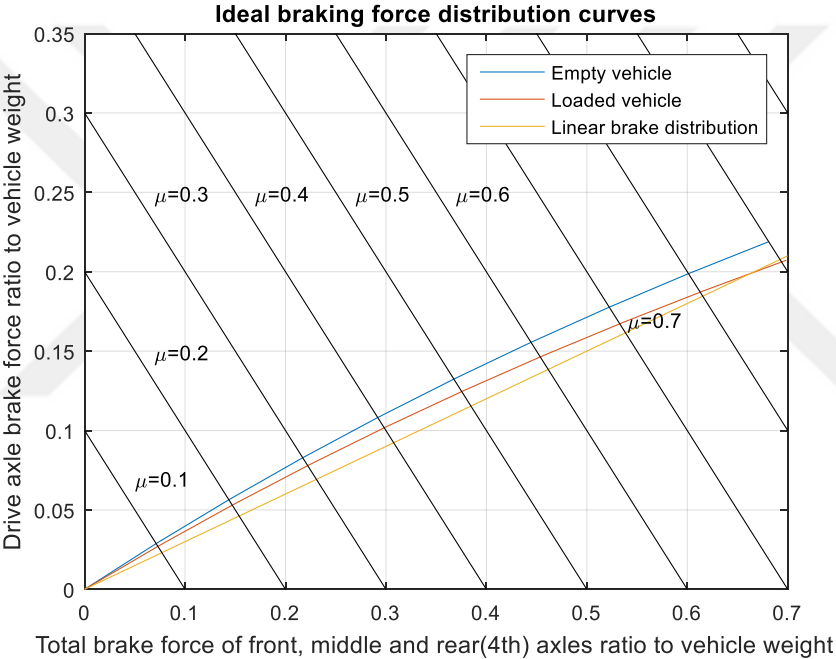
Figure 5-18 Linear and ideal brake force distributions

The strategy is illustrated in Figure 5-19.
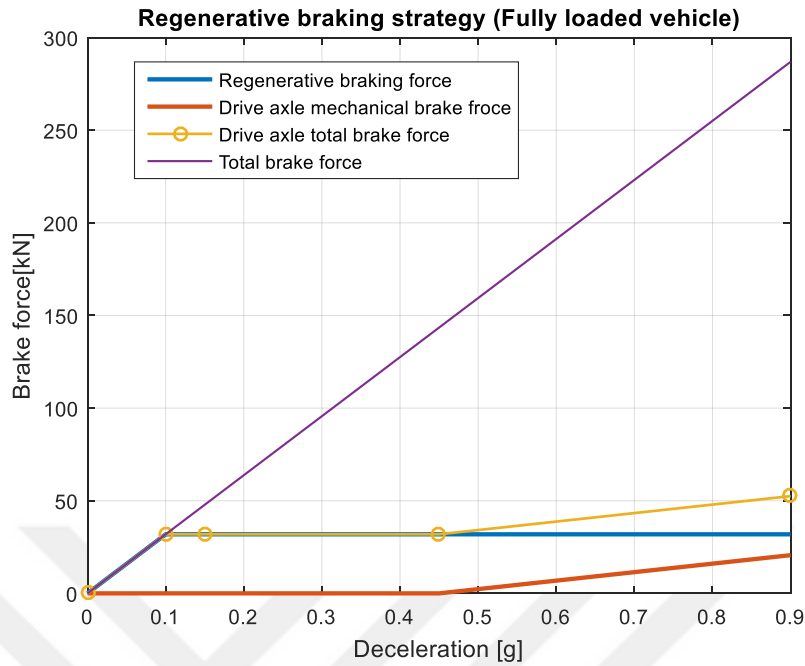
Figure 5-19 Regenerative braking strategy

5.4.3 Energy recuperated from regenerative braking system

In Figure 5-20, energy recuperated with parallel braking system and brake energy consumption is shown. In Söğütlüçeşme direction 68.5% of the braking energy can be recuperated and in Beylikdüzü direction this value is 70.7%.
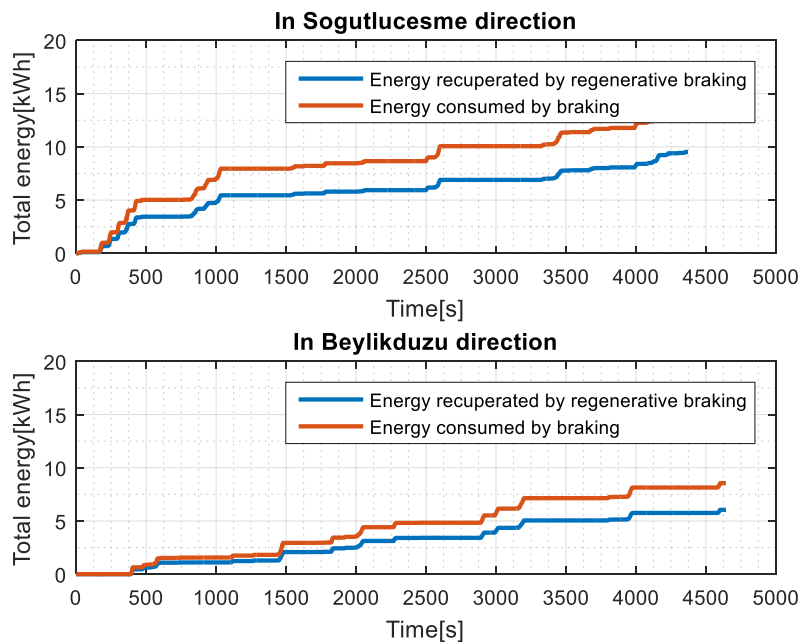
Figure 5-20 Brake energy consumption versus energy recuperation

In Figure 5-21, energy recuperation of the regenerative braking system is compared with the total energy consumption. The vehicle is assumed to be fully loaded and it is find out that 13.35% percent of the total energy consumption in Söğütlüçeşme direction can be recuperated while in Beylikdüzü direction, 7.8% of the total energy consumption can be recuperated.

In Sogutlucesme direction

In Beylikduzu direction
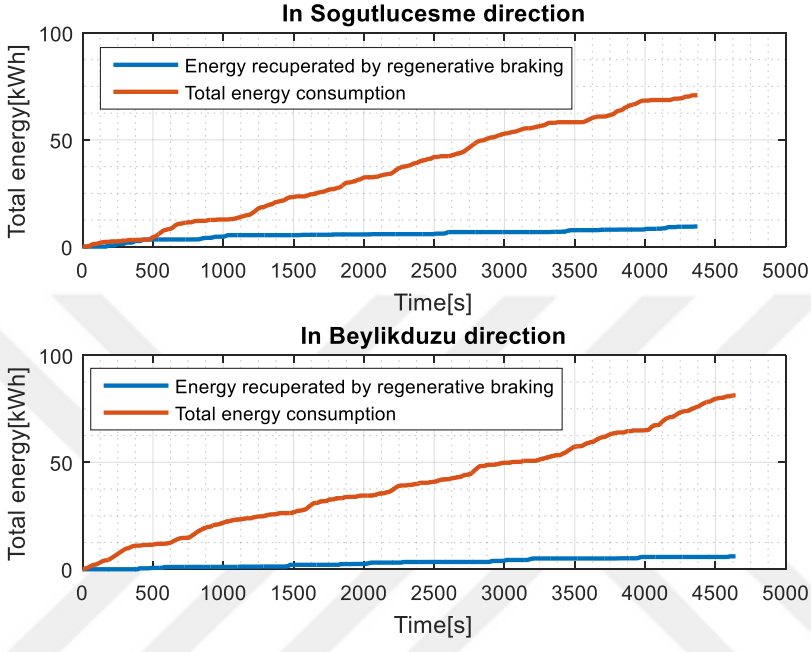
Figure 5-21 Total energy consumption versus energy recuperation

It should be noted that inefficiencies of the engine, gearbox and charge/discharge efficiencies are considered for the calculation of the recuperation. Charge/discharge efficiency of the battery is assumed to be 90% [58].

5.5 Battery and charging unit

5.5.1 Battery capacity

In order to determine the capacity of the battery, worst cases to obtain maximum energy consumption must be investigated. The following assumptions are considered to be the worst conditions for the energy consumption of the Metrobus;

- The vehicle is fully loaded.
- Maximum HVAC consumption.

The consumption calculations in the previous sections are made for the whole network, from Beylikdüzü to Söğütlüçeşme. In this work, five main lines (34, 34Z, 34AS, 34BZ, 34C) of the Metrobus Network are considered. The average consumptions for different weight conditions are calculated for the whole network and it is tabulated in Table 4-1, but it may change for different lines of the network. Average energy consumption per kilometer and length of each line are tabulated in Table 5-6, different than previous calculations, inefficiencies of the gearbox (95%) and engine (83.2%) are considered.

Table 5-6 Energy consumption of different lines

Line	Length (km)	Consumption (kWh)		Consumption per km (kWh/km)	
		Söğütlüçeşme	Beylikdüzü	Söğütlüçeşme	Beylikdüzü
34	28.97	54.94	56.56	1.90	1.95
34Z	11.47	18.28	20.52	1.6	1.79
34AS	40.18	78.25	76.56	1.94	1.91
34BZ	38.75	77.21	81.71	1.99	2.11
34C	27.53	45.06	56.69	1.63	2.05

In addition to the traction consumption there are other consumptions due to auxiliary systems. The maximum consumption of the HVAC system can reach up to 0.366 kWh/km on a cold day. In addition to the HVAC system, other auxiliary systems such as, steering system, braking system, internal and external lights, compressors, water pumps, electronic control systems consumes 0.15kWh of energy per kilometer. Finally, the thermal management system of the battery consumes additional 3.5% of total energy. On the other hand, regenerative braking system is able to recuperate 13.35% and 7.8% of the total traction energy (it should be noted that; not the overall energy, only the traction energy) in Söğütlüçeşme and Beylikdüzü directions, respectively. To determine the required battery capacity, maximum energy consumptions budget of each Metrobus line are tabulated in Table 5-7and Table 5-8. It should be noted that charging/discharging efficiencies are not included in these values and the consumption due to addition mass of the battery. The mass difference of the newly added electric traction system with the mass of the removed internal combustion engine is assumed to be 1500kg. And, the mass of the battery is assumed to be 1500kg, if the mass of the battery is greater than 1500 kg, the extra consumption due to the battery mass should be recalculated.

In Table 5-7 and Table 5-8, maximum energy consumptions of the vehicle are shown in both directions

Table 5-7 Maximum energy consumption of Metrobus in Söğütlüçeşme direction

Söğütlüçeşme direction					
Line	34	34Z	34AS	34BZ	34C
Length (km)	28.97	11.47	40.18	38.75	27.53
Traction consumption (kWh)	54.94	18.28	78.25	77.21	45.06
BTMS (kWh)	2.45	0.85	3.46	3.40	2.07
Regenerative braking (kWh)	0.00	0.00	0.00	0.00	0.00
HVAC (kWh)	10.60	4.20	14.71	14.18	10.08
Auxiliary (kWh)	4.35	1.72	6.03	5.81	4.13
Overall (kWh)	72.33	25.05	102.45	100.61	61.34

Table 5-8 Maximum energy consumption of Metrobus in Söğütlüçeşme direction

Beylikdüzü direction					
Line	34	34Z	34AS	34BZ	34C
Length (km)	28.97	11.47	40.18	38.75	27.53
Traction consumption (kWh)	56.56	20.52	76.56	81.71	56.69
BTMS (kWh)	2.50	0.93	3.41	3.56	2.48
Regenerative braking (kWh)	0.00	0.00	0.00	0.00	0.00
HVAC (kWh)	10.60	4.20	14.71	14.18	10.08
Auxiliary (kWh)	4.35	1.72	6.03	5.81	4.13
Overall (kWh)	74.01	27.36	100.70	105.26	73.38

In Table 5-9 and Figure 5-9, average consumptions of the vehicle are shown.

Table 5-9 Average energy consumption of Metrobus in Söğütlüçeşme direction

Söğütlüçeşme direction					
Line	34	34Z	34AS	34BZ	34C
Length (km)	28.97	11.47	40.18	38.75	27.53
Traction consumption (kWh)	40.33	14.70	51.62	50.98	33.11
BTMS (kWh)	1.68	0.54	2.17	2.14	1.41
Regenerative braking (kWh)	-5.38	-1.64	-6.89	-6.81	-4.42
HVAC (kWh)	3.19	1.26	4.42	4.26	3.03
Auxiliary (kWh)	4.35	1.72	6.03	5.81	4.13
Overall (kWh)	44.15	16.34	57.35	56.39	37.25

Table 5-10 Average energy consumption of Metrobus in Söğütlüçeşme direction

Beylikdüzü direction					
Line	34	34Z	34AS	34BZ	34C
Length (km)	28.97	11.47	40.18	38.75	27.53
Traction consumption (kWh)	33.25	15.89	50.65	53.95	40.98
BTMS (kWh)	1.43	0.58	2.14	2.24	1.68
Regenerative braking (kWh)	-2.59	-1.06	-3.95	-4.21	-3.20
HVAC (kWh)	3.19	1.26	4.42	4.26	3.03
Auxiliary (kWh)	4.35	1.72	6.03	5.81	4.13
Overall (kWh)	39.62	18.29	59.29	62.06	46.63

There may be different approaches to determine the battery capacity. In this study, three criteria are considered for selection of the battery capacity. The first criterion, the vehicle should be able to complete the corresponding line in case of maximum consumption. The second criterion, the capacity of the battery should be 25% higher than the average energy consumption because the vehicle will be charged in the range of 90% to 10%. Reason of this charging range is that using a larger battery increases the lifetime of the battery [59]. Furthermore, after the battery is recharged, there must be empty capacity in the battery for the regenerative braking. The final criterion the battery should be able to supply the required energy during its life time where the capacity of the battery is reached 80% of its first capacity. So, additional 25% battery capacity is required for the compensation of its deterioration. According to these design requirements, capacity need of the battery are obtained, results shown in Table 5-11. Consumptions that are used for the design are shown in bold.

Table 5-11 Battery capacity requirements

Line	34	34Z	34AS	34BZ	34C
Söğütlüçeşme direction					
Maximum energy consumption (kWh)	**72.33**	25.05	**102.45**	**100.61**	**61.34**
Average consumption with additional capacity (kWh)	68.98	**25.52**	89.60	88.10	58.20
Beylikdüzü direction					
Maximum energy consumption (kWh)	**74.01**	27.36	**100.70**	**105.26**	**73.38**
Average consumption with additional capacity (kWh)	61.90	**28.58**	92.63	96.96	72.85

5.5.2 Battery features

There are three main properties of a battery cell, these are energy density, charge rate, cycle life.

Energy density of the battery is the energy capacity in weight. Generally, it is represented with kWh per kg. Batteries with high density are more preferred because they do not increase the weight of the vehicle much, thus reducing the consumption of the vehicle.

Charge rate or C-rate specifies the charging speed or discharge. A 1C rate battery is able to discharge the entire battery in 1 hour, similarly, a 5C rate battery discharges the battery in 12minutes or a 0.5C battery discharges the battery in 2 hours.

Cycle life is the maximum number of discharge-charge that the battery is able to experience during its life before failure. Cycle life of a battery is measured for specific charge and discharge conditions. The actual operating life of the battery is affected by conditions such as temperature and humidity. On the other hand, depth of discharge is an important parameter for the cycle life, the higher the depth of discharge during its life the lower the life cycle.

5.5.3 Battery chemistry

Most common cell types in electric buses market are lithium iron phosphate (LFP), lithium titanium oxide (LTO) and lithium nickel manganese cobalt oxide (NMC) [14].

Properties of these cell types are tabulated in Table 5-12 according to data sheets of battery manufacturer.

Table 5-12 Main properties of different cell types

Cell type	LFP [53]	NMC [54]	LTO [55]
Cell voltage	3.2 V	3.65 V	2.3 V
Cell capacity	45 Ah	27 Ah	23 Ah
Energy density	146 Wh/kg	260 Wh/kg	96 Wh/kg
Energy density	-	-	202 Wh/l
Specific Power	-	-	-
Charge rate	1C	2C	6C
Cycle life (80% SOC)	5000 @25C w/1C	7000 @25C w/1C	160000 @25C w/2C
Charge temperature	-10 and 60	0 and 40	
Discharge temperature	-30 and 60	-30 and 55	-30 and 45
Cell mass	0.99 kg	0.38 kg	0.55kg

Since the cycle life depends on several conditions such as charging rate and temperature it is given in Table 5-12 for one specific point and the exact cycle life should be determined after the selection of the operation and charging system.

5.5.4 Charging strategies

Although there are several charging strategies such as battery swapping, opportunity charging, two charging strategies may be accepted by the bus operator, overnight charging and fast charging.

5.5.4.1 Overnight charging

In this strategy, vehicles are charged generally at night from 00.00 to 06.00 when they are not in service but if there are enough time vehicles can be charged at daytime. Advantages of this strategy are;

- Buses do not need to wait for charging during service hours.
- Longer range than fast charging.
- Flexibility during service hours.

Disadvantages of this strategy are;

- Expensive vehicle due to bigger batteries

5.5.4.2 Fast charging

In this strategy, vehicles are charged at start point of lines when they are in service. Advantages of this strategy are;

- Smaller battery is enough.
- Lower energy consumption.

Disadvantages of this strategy are;

- Smaller range than overnight charging.
- Generally more vehicles are required.

5.5.5 Selection of the battery

Two types of battery are selected for different charging strategies. The first one is for fast charging strategy and the second is for overnight charging.

5.5.5.1 Fast charging battery

5.5.5.1.1 Chemistry of the battery

For a fast charging infrastructure the chemistry of the battery should be LTO because it has the highest charge rate among other type of battery chemistry.

5.5.5.1.2 Capacity of the battery

In Table 5-11, consumption of each line is tabulated. The highest consumption is observed in line 34AS in Söğütlüçeşme direction which is 105.26kWh. So, the capacity of the battery should be 105 kWh.

5.5.5.1.3 Mass of the battery

Energy density of the LTO cell is 96Wh/kg, so for 105kWh battery 1094kg of cell is needed. For the cooling system, electronic devices and for packaging 66% additional weight is required [14]. So the mass of the battery system became 1815 kg. At the beginning of the calculation of the consumption, the mass of the battery was assumed to be 1500kg, but the mass of the battery is 1815kg. So, there are 315kg of additional battery than previous predication. The additional mass increases the consumption of the vehicle however, additional consumption due to battery is neglected because the addition mass of is small compared to the vehicle mass.

5.5.5.1.4 Module configuration

The working voltage range of ASELSAN traction system is between 500V and 750V, so the voltage of the battery should be in this range. The number of cells connected in series and parallel should be selected accordingly.

The nominal voltage of one cell is 2.3 V and its energy is 53Wh. In Figure 5-22, typical voltage curve of the battery is given. Since the working range of the battery is selected between 10% and 90%, green region is considered. So, minimum voltage of the battery is 2V because the traction system will be turned off at the battery voltage lower than 2V. On the other hand, maximum voltage of the battery is 2.4V when the capacity is 90% and 2.6V when the capacity is 100%. In normal operation the vehicle will be charged until 90% of the capacity, but the battery can be reach up to 100% of capacity with regenerative braking so for this calculation the maximum voltage of the battery is considered as 2.6 V.
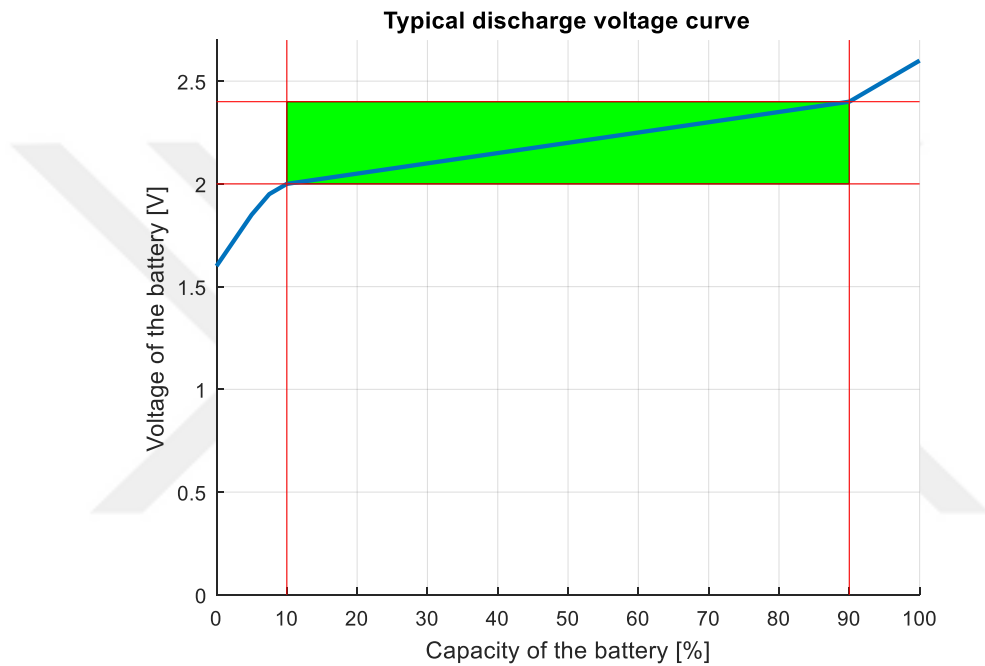
Figure 5-22 Typical voltage curve of the battery cell

Maximum and minimum numbers of cells in one serial line are tabulated in Table 5-13.

Table 5-13 Number of cell in one serial line

	System voltage (V)	Cell voltage (V)	Number of cell	Energy (kWh)
Maximum	750	2.6	288	15.26
Minimum	500	2	250	13.25

The capacity in one serial line is between 13.25kWh and 15.26kWh, and the requirement is 105kWh. So, there should be 7 or 8 parallel line to reach to the required capacity.

In this phase some requirements are defined to design the module and the battery.

- The mass of one module should be less than 50kg for the ease of transportation.
- To reduce the weight of the packaging, as many cells as possible should be placed into one module.
- To be able to place the modules in two rows on the vehicle, the number of modules in a serial line must be even.

These requirements are useful for integration and manufacturing process. According to these, it is decided that a module should consist of 25 cells and a serial line should consist of 10 modules.

To verify the selection in terms of dimensions, a cell, a module and the battery is drawn with the help of CAD software. Furthermore, in Figure 5-23, cells, modules and the battery placed on the bus is illustrated.
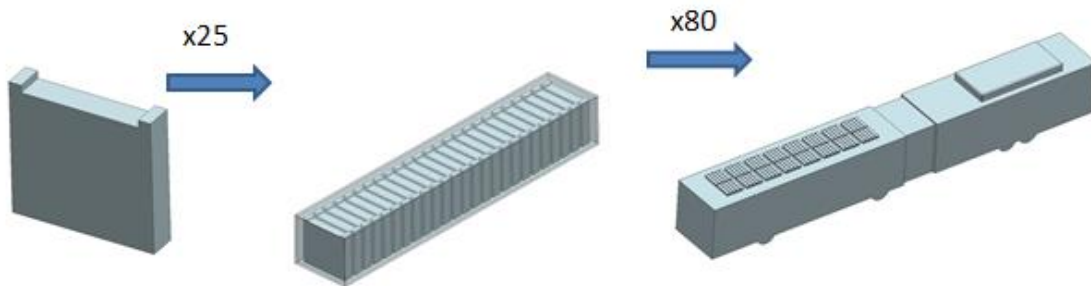
Figure 5-23 Drawing of a cell, a modules and the battery

With this configuration, there are 2000 cells and the total energy of the battery is 106 kWh which is a little higher than the required battery capacity.

5.5.5.1.5 Charging method and charging time

There are different charging/refueling methods such as battery swapping, induction, pantograph and manual charging with plug. Battery swapping is not considered because it is an expensive method because there should be additional batteries and the price of the battery is a large part of the bus price. So, it is not economically feasible. On the other hand, due to large space between transmitter and receiver coils induction charging is not efficient for application like electric bus charging [63]. Pantograph and manual charging are suitable for this application.

C-rate of the LTO battery is 6C, so one cell can be charged with 360A in 10 minutes. For this, a charger with 636 kW charging power is required, any charger with a power less 636kW is also suitable but it increases the charging time. In market, chargers with 600 kW are available [64] [65]. So, the charging time of the battery with a 600kW charger is 10.5 minutes. In addition to the charging time, there are processes such as opening/closing the pantograph (for pantograph charging) or plugging/unplugging the plug (for manual charging) and communication of charger and vehicle for starting to charge process. It is assumed that these additional procedures will last for 4.5 minutes and increase the total charging time to 15 minutes. The charging interface is selected as pantograph for simplicity.

5.5.5.2 Overnight charging battery

5.5.5.2.1 Chemistry of the battery

For a fast charging infrastructure the chemistry of the battery should be NMC because the energy density of NMC batteries are higher than the LFP batteries and the other features are almost equal.

5.5.5.2.2 Capacity of the battery

In Table 5-11, consumption of a round trip of each line is tabulated. In order to determine the capacity of the battery the number of round trip with one overnight charge should be considered. Lines 34AS and 34BZ are in service from 6h to 24h, so vehicles of these lines can be charged only nights. On the other hand, lines 34, 34Z and 34C are working part-time. Service hours of each line are tabulated in Table 5-14.

Table 5-14 Working hours of each line

Line	Working hours	Travel time (round trip)	Maximum number of trip
34	6h-10h and 15.30h-21.30h	120 minutes	3
34Z	6h-10h and 15h-21h	48 minutes	8
34AS	6h-24h	180 minutes	6
34BZ	6h-24h	180 minutes	6
34C	6h-10h and 15h-21h	120 minutes	3

According to number of round trip, required battery capacities are tabulated in Table 5-15.

Table 5-15 Battery capacity requirements

Line	34	34Z	34AS	34BZ	34C
Energy consumption for a round trip (kWh)	146.36	54.10	203.15	205.87	134.38
Number of round trip	3	8	6	6	3
Energy consumption for one day(kWh)	439	433	1219	1235	404

Thus, the capacity of the battery should be at least 1235kWh for lines 34AS and 34BZ. On the other hand, for lines 34,34Z and 34C a battery with 439kWh capacity is enough.

5.5.5.2.3 Mass of the battery

Energy density of the NMC cell is 260Wh/kg, so for a 1235kWh battery 4750kg of cell is needed. For the cooling system, electronic devices and for packaging 66% additional weight is required [14]. So the mass of the battery system became 7885 kg. At the beginning of the calculation of the consumption, the mass of the battery was assumed to be 1500kg, but the mass of the battery is 7854kg. So, there are 6385kg of additional battery than previous predication. The additional mass increases the consumption of the vehicle. Furthermore, with the weight of the batteries the vehicle becomes inappropriate for the Turkish roads due to maximum axle weight limitation. Thus, overnight charging strategy is not suitable for lines 34AS and 34BZ that are working full-time.

On the other hand, for the vehicle working on lines 34, 34Z and 34C 1688kg of NMC cell is needed. With the additional weight due to cooling system, electronic devices and for packaging the weight of the battery becomes 2802kg. So it means 1302kg of additional mass. The additional mass increases the consumption of the vehicle but it negligible. Thus, overnight charging strategy may be a suitable solution for lines 34, 34Z and 34C which are working part-time.

5.5.5.2.4 Module configuration

The working voltage range of ASELSAN traction system is between 500V and 750V, so the voltage of the battery should be in this range. The number of cells connected in series and parallel should be selected accordingly.

The nominal voltage of one cell is 3.65 V and its energy is 98.5Wh. In Figure 5-22, typical voltage curve of the battery is given [66]. Since the working range of the battery is selected between 10% and 90%, green region is considered. So, minimum voltage of the battery is 3.4V because the traction system will be turned off at the battery voltage lower than 3.4V. On the other hand, maximum voltage of the battery is 4.1V when the capacity is 90% and 4.2V when the capacity is 100%. In normal operation the vehicle will be charged until 90% of the capacity, but the battery can be reach up to 100% of capacity with regenerative braking so for this calculation the maximum voltage of the battery is considered as 4.2 V.
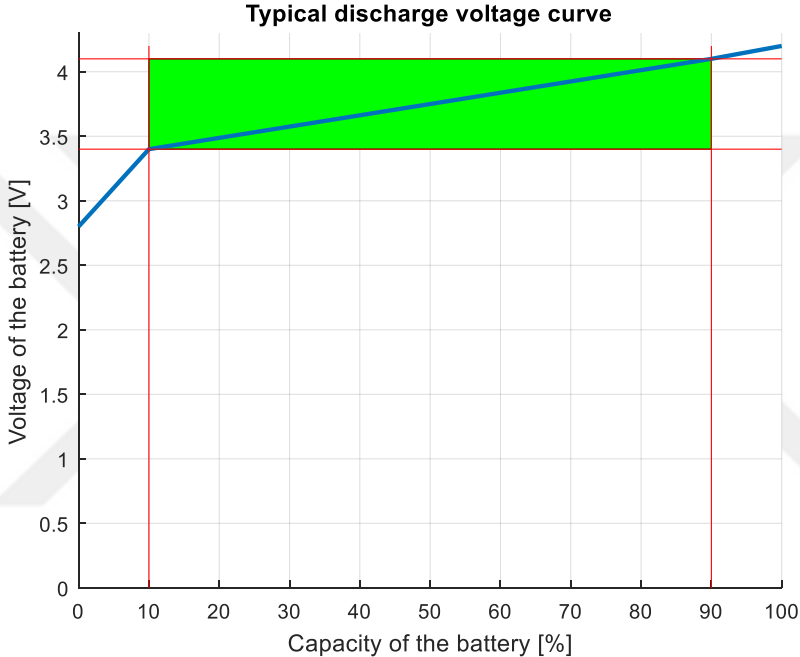
Figure 5-24 Typical voltage curve of the battery cell [66]

Maximum and minimum numbers of cells in one serial line are tabulated in Table 5-13.

Table 5-16 Number of cell in one serial line

	System voltage (V)	Cell voltage (V)	Number of cell	Energy (kWh)
Maximum	750	4.2	178	17.53
Minimum	500	3.4	148	14.57

The capacity in one serial line is between 14.57kWh and 17.53kWh, and the requirement is 439kWh. So, the number of parallel line is between 26 and 31.

In this phase some requirements are defined to design the module and the battery.

- The mass of one module should be less than 50kg for the ease of transportation.
- To reduce the weight of the packaging, as many cells as possible should be placed into one module.
- To be able to place the modules in two rows on the vehicle, the number of modules in a serial line must be even.

These requirements are useful for integration and manufacturing process. According to these, it is decided that a module should consist of 75 cells and a serial line should consist of 2 modules, the battery should consist 45 parallel lines.

To verify the selection in terms of dimensions, a cell, a module and the battery is drawn with the help of CAD software. Furthermore, in Figure 5-25, cells, modules and the battery placed on the bus is illustrated.
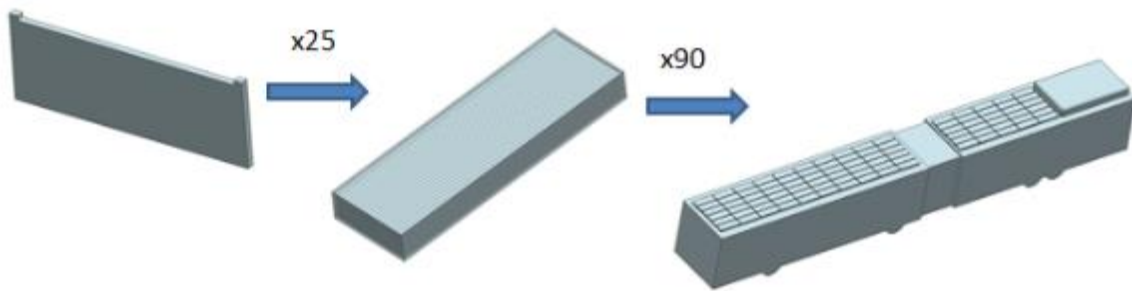
Figure 5-25 Drawing of a cell, a modules and the battery

With this configuration, there are 4500 cells and the total energy of the battery is 443.25 kWh which is a little higher than the required battery capacity.

5.5.5.2.5 Charging method and charging time

There are different charging/refueling methods such as battery swapping, induction, pantograph and manual charging with plug. Battery swapping is not considered because it is an expensive method since there should be additional batteries and the price of the battery is a large part of the bus price. So, it is not economically feasible. On the other hand, due to large space between transmitter and receiver coils induction charging is not efficient for application like electric bus charging [63]. Pantograph and manual charging are suitable for this application. However, as shown in Figure 5-25, there is not much space for the pantograph son the charging method is selected as manual charging with plug.

C-rate of the NMC battery is 2C, so one 27Ah cell can be charged with 54A in 30 minutes. These are maximum values, charging the battery with lower power has several benefits;

- Reduction in temperature rise of battery, cables and charger.
- Reduction in charger cost because smaller charger will be sufficient.

Thus, in order to profit from these benefits the minimum c-rate should be determined. The minimum time interval of lines 34, 34C and 34Z for charging process is from 10:00 to 15:00. The first and last hour is reserved for the arrangement of the vehicles; 3 hours left for charging process. So, the charging rate should be 0.33C which means 9A charging current for each cell.

For this, a charger with at least 144.8 kW charging power is required. In market, chargers with 150 kW are available [67] [68]. So, the charging time of the battery with a 150 kW charger is 182 minutes.

On the other hand, charging with 0.33C requires more chargers. So, to reduce the initial cost for charger and to use the same charger of fast charging system 600kW charger is selected, in this way vehicle with LTO battery are able to be charged with these chargers. The c-rate becomes 1.37C and the charging time is 44 minutes. It is assumed that these additional procedures will last for 6 minutes and increase the total charging time to 50 minutes. Charging time intervals of lines 34, 34C and 34Z are generally from 10:00 to 15:00 at daytime and it is from 24:00 to 06:00 at nighttime. So vehicles could be charged with 4, 5 and 6 shifts according to their time table.

On the other hand, the charging interface of the overnight charging vehicles are selected as manual charging with plug due to lack of place on the top of the vehicle for pantograph and it is mentioned that the charging interface of the fast charging vehicles can be manual charging or pantograph. Since it is decided to use same charger, the charging interface of the fast charging vehicles should be manual charging with plug as well.

5.6 Fleet and grid

Two different fleets are possible for the Metrobus Network. The first fleet is composed of fast charging vehicles and the second one is hybrid solution. In hybrid solution, lines 34AS and 34BZ are composed of fast charging vehicles while other lines are composed of overnight charging vehicles. These two solution is technically possible and suitable for the network, however to find out the most suitable solution it should be evaluated economically after the design of the fleet.

5.6.1 Fleet with fast charging batteries

5.6.1.1 Line 34AS

Average travel time in one direction is 90 minutes. There should be 146 vehicles and there should be additional 17 vehicles for each direction because, in 15minutes (charging duration) 17 vehicles are given in the line at peak hours. Thus, 180 vehicles are needed for this line. In addition to 180 vehicles, 34 chargers are required. The battery should be charged 12 times a day.

5.6.1.2 Line 34BZ

Average travel time in one direction is 90 minutes. There should be 152 vehicles and there should be additional 15 vehicles for each direction because, in 15minutes (charging duration) 15 vehicles are given in the line at peak hours. Thus, 182 vehicles are needed for this line. In addition to 182 vehicles, 30 chargers are required. The battery should be charged 12 times a day.

5.6.1.3 Line 34

Average travel time in one direction is 60 minutes. There should be 100 vehicles and there should be additional 12 vehicles for each direction because, in 15minutes (charging duration) 12 vehicles are given in the line at peak hours. Thus, 124 vehicles are needed for this line. In addition to 124 vehicles, 24 chargers are required. The battery should be charged 6 times a day.

5.6.1.4 Line 34C

Average travel time in one direction is 60 minutes. There should be 120 vehicles and there should be additional 13 vehicles for each direction because, in 15minutes (charging duration) 13 vehicles are given in the line at peak hours. Thus, 146 vehicles are needed for this line. In addition to 146 vehicles, 26 chargers are required. The battery should be charged 6 times a day.

5.6.1.5 Line 34Z

Average travel time in one direction is 24 minutes. Different than other lines maximum consumption of this line is less the half of the battery capacity, namely a vehicle is able to complete a round trip in this line. Thus, it is enough to place charger at only at only one end of the line.

There should be 62 vehicles and there should be additional 18 vehicles because, in 15minutes (charging duration) 18 vehicles are given in the line at peak hours. Thus, 80 vehicles are needed for this line. In addition to 80 vehicles, 18 chargers are required. The battery should be charged 8 times a day.

5.6.2 Hybrid fleet

In hybrid solution, lines 34AS and 34BZ are composed of fast charging vehicles and they are represented in previous section. Other lines are investigated in this section.

5.6.2.1 Line 34

Average travel time in one direction is 60 minutes. There should be 100 vehicles and the battery should be charged 2 times a day. The minimum time interval for charging is from 10:00 to 15:30 so there are 330 minutes for charging however it is assumed that 60 minutes are needed to make all vehicles ready for charging. Thus, vehicles can be charged in 5 shifts. So, the number of charger for this line is 20.

5.6.2.2 Line 34C

Average travel time in one direction is 60 minutes. There should be 120 vehicles and the battery should be charged 2 times a day. The minimum time interval for charging is from 10:00 to 15:00 so there are 300 minutes for charging however it is assumed that 60 minutes are needed to make all vehicles ready for charging. Thus, vehicles can be charged in 4 shifts. So, the number of charger for this line is 30.

5.6.2.3 Line 34Z

Average travel time in one direction is 24 minutes. There should be 62 vehicles and the battery should be charged 2 times a day. The minimum time interval for charging is from 10:00 to 15:00 so there are 300 minutes for charging however it is assumed that 60 minutes are needed to make all vehicles ready for charging. Thus, vehicles can be charged in 4 shifts. So, the number of charger for this line is 16.

5.7   Overview of the designed system

Life cycle of a battery depends on many parameters such as temperature, charge/discharge rate. In catalogues life cycle values are given for special conditions. In Table 5-12, properties of NMC and LTO batteries are shown. Life of LTO and NMC cell are given as 1600 and 7000, respectively, however it is valid when the depth of discharge is 80%. In this study the depth of discharge is less than catalogue values of batteries, so greater life cycle is expected. The relationship between depth of discharge and life cycle is given in Figure 5-26 it hold true for most lithium-ion batteries [69].
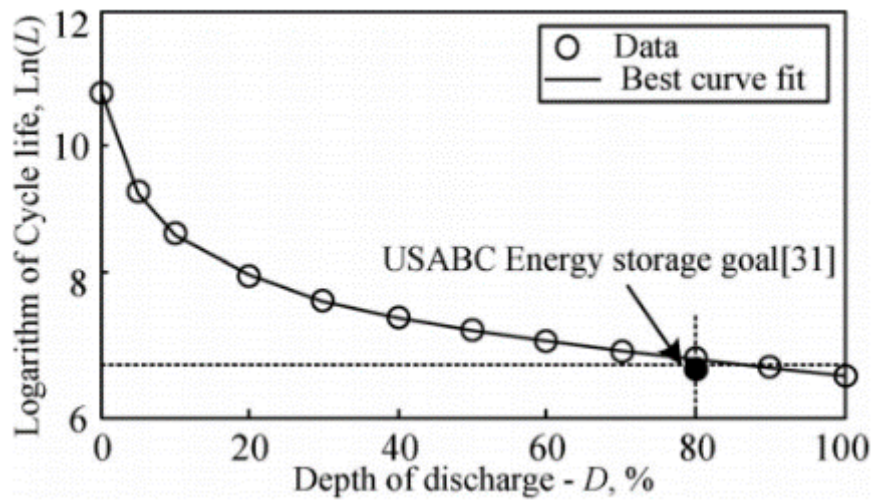
Figure 5-26 Depth of discharge versus life cycle [69]

Since the regenerative braking consists of micro cycles compared to charging process, effect of the regenerative braking on the cycle life of the battery is neglected [15].

In Table 5-17, overview of the fast charging network is tabulated.

Table 5-17 Overview of the fast charging network

Fast Charging Network					
Line	34AS	34BZ	34	34C	34Z
Length (km)	40.18	38.75	28.97	27.53	11.47
Charge type	Fast	Fast	Fast	Fast	Fast
C-rate (C)	6				
Battery capacity (kWh)	106				
Available battery capacity(kWh)	84.8				
Max.consumption (kWh)	102.45	105.26	74.01	73.38	28.58
Avg.consumption (kWh) (one way)	58.32	59.22	41.88	41.94	17.31
Average depth of discharge	55%	56%	40%	39%	33%
Number of vehicle	180	182	124	146	80
Additional number of vehicle	34	30	24	26	18
Number of charger	34	30	24	26	18
Charging time (min)	15				
Number of charge per day	12	12	6	6	8
Cycle life	16000				
Cycle life at line	22400	22352	29600	29568	36000
Expected life (year)	6.31	6.11	13.52	13.50	12.33
Expected life (km)	900,032	866,140	691,542	669,047	606,740
Total km per day (km)	391.09	388.35	140.18	135.76	134.83
Charge/discharge efficiency	90%				
Charging time	From 6h to 24h				
Peak charge power (mW)	24.03	21.20	16.96	18.37	12.72

In Table 5-18, overview of the hybrid network which is composed of fast and slow charging buses is tabulated.

Table 5-18 Overview of hybrid network

Hybrid Network					
Line	34AS	34BZ	34	34C	34Z
Length (km)	40.18	38.75	28.97	27.53	11.47
Charge type	Fast	Fast	Slow	Slow	Slow
C-rate (C)	6		1.7		
Battery capacity (kWh)	106		439		
Available battery capacity(kWh)	84.8		351.2		
Max.consumption (kWh)	102.45	105.26	222.03	220.14	228.64
Avg.consumption (kWh) (one way)	58.32	59.22	41.88	41.94	34.62
Average depth of discharge	55%	56%	50%	50%	52%
Number of vehicle	180	182	100	120	62
Additional number of vehicle	34	30	0	0	0
Number of charger	34	30	20	30	16
Charge time (min)	15		40		
Number of charge per day	12		2	2	2
Cycle life (Catalogue value)	16000		7000		
Cycle life at line	22400	22352	10150	10150	10080
Expected life (year)	6.31	6.11	13.90	13.90	13.81
Expected life (km)	900,032	866,140	882,137	838,289	924,941
Total km per day (km)	391.09	388.35	173.82	165.18	183.52
Charge/discharge efficiency	90%				
Charging time	From 6h to 24h		From 10h30 to 15h		
Peak charge power (mW)	24.03	21.20	16.58	24.88	13.27

6 COMPARISON

6.1 Economic feasibility

There are many studies on economic analysis of electric buses in the literature. The price information that are used in these analyzes depends on many parameters such as time, product, technology, region and number of buses. Therefore, it is very difficult to make economic analysis. For a more accurate analysis, battery manufacturers, bus manufacturers and the market were reviewed to share project-specific price information. The analysis was made according to prices that are obtained from these manufacturers. Furthermore, prices obtained from literature are shared.

For economic analysis, the electric bus is evaluated in four basic sections. These sections are battery, body, traction system and charging station.

All prices are in Euro. The Euro U.S. Dollar parity and the Euro Turkish Lira parity were accepted as 1.15 and 6.5, respectively.

6.1.1 Initial cost

6.1.1.1 Battery

For the Metrobus fleet, there are two battery options, LTO and NMC. The capacity of the NMC battery is 439 kWh while the capacity of the LTO battery is 106 kWh. Prices of the battery per kWh are tabulated in Table 6-1.

Table 6-1 Price of LTO and NMC batteries

Type	Price [€/kWh]	Source	Year
LTO	640	Market Research	2019
	950 [14]		2018
	1130 [70]		2016
	2000 [71]	Literature	2013
NMC	460	Market Research	2019
	540 [70]		2016
	792 [72]		2015
	800 [14]	Literature	2018

The main reasons of the difference between literature and research are the number of order and year. The price of the battery for high volume order shows a serious decline [15]. For the low number of orders, the producers were quoted close to the prices mentioned in the literature.

6.1.1.2 Body

The body type of the Metrobus is selected as 18 meter articulated bus. The price of the body includes the carcass, auxiliary systems, brakes, wheels etc. The price may change according to several factors but during the market research it is aimed to estimate the price of a bus very similar to the current diesel vehicle. Prices of the body are tabulated in Table 6-2.

Table 6-2 Price of articulated bus body

Price [€]	Source
320000	Market Research
247000 [73] 360000 [74] 500000 [75]	Literature

6.1.1.3 Traction system

ASELSAN traction system is selected. The price of the traction system includes the engine, the inverter and the gearbox. Price estimation for the traction system is 70000 €. According to prices that are found in literature the price is calculated as 63700 € [72]. Additionally, the heating and cooling system of the batteries is considered as a part of the traction system. The price of the battery cooling system is 10000 €. So, the total price of the traction system is 80000 €.

6.1.1.4 Charger and other costs

Prices of the fast charger infrastructure and charger are tabulated in Table 6-3. Price includes, the charger, infrastructure and man work.

Table 6-3 Price of the charger

Price [€]	Source
152000	Market Research
243000 [72] 320000 [14]	Literature

6.1.1.5 Diesel bus cost

The price of diesel Metrobus vehicles used in the current Metrobus network is 440000€ [76].

6.1.2 Expenses

6.1.2.1 Electric price

According to the interview with the bus operator, the electricity price is 0.06 €/kWh. In equation (6.1), electric consumption of the one vehicle per km for each line is calculated.

$$E_{electric} = \frac{c_{avg\ electric}}{\eta_{charger}} e_{electric} \tag{6.1}$$

Where $E_{electric}$ is the average electric consumption per km of one vehicle in Euro, $c_{avg\ electric}$ is the average electric consumption per km of one vehicle in kWh, $e_{electric}$ is the electricity price and $\eta_{charger}$ is the efficiency of the charger which is 0.96 [64].

Average electric consumptions of each line are tabulated in Table 6-4. Since average electric consumptions and electricity prices are same, results are same for hybrid charging and fast charging networks.

Table 6-4 Average electric consumptions

Line	34AS	34BZ	34	34C	34Z
Length [km]	40.18	38.75	28.97	27.53	11.47
Energy consumption[kWh/km]	1.51	1.59	1.51	1.59	1.57
Energy cost[EUR/km]	0.091	0.096	0.090	0.095	0.094

6.1.2.2 Diesel price

According to the interview with the bus operator, the diesel fuel purchase price is 0.87€/l. In equation (6.2), electric consumption of the one vehicle per km for each line is calculated.

$$E_{fuel} = c_{avg\ fuel} e_{electric} \tag{6.2}$$

Where E_{fuel} is the average fuel consumption per km of one vehicle in Euro, $c_{avgfuel}$ is the average fuel consumption per km of one vehicle in liter, which is 0.6 l/km, and e_{fuel} is the fuel price.

Average fuel consumptions of each line are tabulated in Table 6-5.

Table 6-5 Average fuel consumptions

Line	34AS	34BZ	34	34C	34Z
Length [km]	40.18	38.75	28.97	27.53	11.47
Fuel consumption[l/km]	0.6	0.6	0.6	0.6	0.6
Fuel cost[EUR/km]	**0.522**	**0.522**	**0.522**	**0.522**	**0.522**

6.1.2.3 Maintenance

Vehicle maintenance costs are very variable because of the different vehicle, material costs and labor costs. The electric bus is expected to have lower maintenance costs, because the regenerative braking reduces the brake disc wear, no oil change, no air and fuel filter changes are required. The maintenance cost of the bus operator and the cost in the literature are listed in Table 6-6. Maintenance cost of electric Metrobus was estimated according to the ratio of maintenance costs of diesel and electric bus given in the literature. It is assumed that the maintenance cost of the electric Metrobus is %40 lower than the diesel one.

Table 6-6 Maintenance cost of different buses

Electric bus	Diesel bus	Source
0.276 €/km [77]	0.71 €/km [77]	Literature
0.183 €/km [70]	0.292 €/km [70]	
	0.25 €/km [15]	
168000€/life	365000€/life [78]	
	0.24 €/km	Market Research

Thus it is predicted that the maintenance cost of the electric Metrobus is 0.144 €/km.

Average maintenance costs of electric Metrobus network are tabulated in Table 6-7.

Table 6-7 Average maintenance costs of electric Metrobus network

Line	34AS	34BZ	34	34C	34Z
Maintenance cost[EUR/km]	0.144	0.144	0.144	0.144	0.144

Average maintenance costs of diesel Metrobus network are tabulated in Table 6-8.

Table 6-8 Average maintenance cost of diesel Metrobus network

Line	34AS	34BZ	34	34C	34Z
Maintenance cost[EUR/km]	0.24	0.24	0.24	0.24	0.24

6.1.2.4 Depreciation

6.1.2.4.1 Battery

In the design of the system, it is assumed that when the capacity of the battery drops to 80 percent, it will become unusable and complete its life. Therefore, the depreciation of the battery is considered a regular expense.

For buses to be used on some lines, the life of the battery is longer than the life of other systems. On the other hand, the life of the battery in some lines is shorter than the life of other systems. Therefore, the battery needs to change after a certain period of time.

In fact, the battery that completed its life cycle, has still an energy capacity of 80 percent. So it can still be used for some applications. Also the materials used in the battery are valuable. Therefore, in terms of transportation, the batteries that have completed their life have an economic value.

Batteries that have been used on the electric buses and whose capacity has dropped to 80% can be sold again for use in other applications. Today, there are some companies that use, used batteries of electric vehicle for energy storage. Currently, however, the batteries used on the vehicle do not have a clear price and market [79]. Again, there are prices calculated over the feasibility studies related to the usage situation in other applications. The batteries mentioned in this study will complete the life after 5-6 years, so it is very hard to predict the situation of the battery market. Developments in battery technology may reduce the price of used batteries or, on the other hand, the increase in renewable energy applications can increase the energy storage requirement and then can increase the prices of used batteries, additionally this can lead to the formation of a large used battery market. The

estimated price of second hand batteries is between 33€/kWh and 115€/kWh that are calculated in feasibility studies [80]. In this study it is assumed that the price of used battery is 70€/kWh.

In equation (6.3), battery depreciation per km is calculated.

$$E_{battery} = \frac{(C_{battery\ inital} - C_{battery\ final})Q_{battery}}{L_{total}} \tag{6.3}$$

Where, $E_{battery}$ is the depreciation of battery per km for one vehicle, L_{total} is the total travelled distance in its life time, $Q_{battery}$ is the capacity of the battery in kWh, $C_{battery\ inital}$ and $C_{battery\ final}$ are the initial and final battery price per kWh.

Depreciation costs of batteries per km of electric fast charging Metrobus network are tabulated in Table 6-9.

Table 6-9 Depreciation costs of batteries (Fast charging network)

Line	34AS	34BZ	34	34C	34Z
Battery capacity[kWh/bus]	106	106	106	106	106
Life of battery[years]	6.31	6.11	13.52	13.5	12.33
Number of battery used(12 years)	2	2	1	1	1
Battery total cost[EUR/bus](12 years)	135680	135680	67840	67840	67840
Income (used battery)[EUR/bus](12y.)	14840	14840	7420	7420	7420
Depreciation cost[EUR/bus](12 years)	120840	120840	60420	60420	60420
Depreciation cost[EUR/km]	0.071	0.071	0.098	0.102	0.102

Depreciation costs of batteries per km of electric hybrid charging Metrobus network are tabulated in Table 6-10.

Table 6-10 Depreciation costs of batteries (Hybrid charging network)

Battery capacity[kWh/bus]	106	106	439	439	439
Life of battery[years]	6.31	6.11	13.9	13.9	13.81
Number of battery used(12 years)	2	2	1	1	1
Battery total cost[EUR/bus](12 years)	135680	135680	201940	201940	201940
Income(used battery)[EUR/bus](12 y.)	14840	14840	30730	30730	30730
Depreciation cost[EUR/bus](12 years)	120840	120840	171210	171210	171210
Depreciation cost[EUR/km]	0.071	0.071	0.225	0.237	0.213

6.1.2.4.2 Body

Depreciation of the bus is generally calculated based on the economic life of the bus. Life for public buses is generally accepted between 10 and 15 years [73] [78] [81] [82]. In this study, bus life is accepted as 12 years according to the feedback received from bus operator and studies in literature. Furthermore at the end of its life, residual value of the bus is assumed to be 10% [73]. Thus the depreciation of the bus body is assumed to be 7.5% of its initial price per year.

In equation (6.4), body depreciation per km is calculated.

$$E_{body} = \frac{0.9 \times C_{body}}{L_{total}} \tag{6.4}$$

Where, E_{body} is the depreciation of the body per km for one vehicle, L_{total} is the total travelled distance in its life time and C_{body} is the initial price of one articulated bus body without the battery and the traction system.

It is expected that the traction system is able to work until 1.5 million km or 12 years. Depreciation of the traction system is assumed to be in direct proportion of these limit values.

Depreciation costs of bus body per km of electric fast charging Metrobus network are tabulated in Table 6-11.

Table 6-11 Depreciation costs of bus body (Fast charging network)

Bus body cost [EUR]	320000	320000	320000	320000	320000
Life [years]	12	12	12	12	12
Depreciation cost[EUR/bus](12 y.)	288000	288000	288000	288000	288000
Depreciation cost[EUR/km]	0.168	0.169	0.469	0.484	0.488

Depreciation costs of bus body per km of electric hybrid charging Metrobus network are tabulated in Table 6-12.

Table 6-12 Depreciation costs of bus body (Hybrid charging network)

Bus body cost [EUR]	320000	320000	320000	320000	320000
Life [years]	12	12	12	12	12
Depreciation cost[EUR/bus](12 y)	288000	288000	288000	288000	288000
Depreciation cost[EUR/km]	0.168	0.169	0.378	0.398	0.358

6.1.2.4.3 Charger

According to interviews with manufacturers, the life of the charger is assumed to be 12 years.

In equation (6.5), body depreciation per km is calculated.

$$E_{charger} = \frac{C_{charger} \times \dfrac{n_{charger}}{n_{vehicle}}}{L_{total}} \qquad (6.5)$$

Where, $E_{charger}$ is the depreciation of the charger per km for one vehicle, L_{total} is the total travelled distance in its life time, $C_{charger}$ is the initial price of one charger, $n_{charger}$ is the number of charger that is assigned for the corresponding line and $n_{vehicle}$ is the number of vehicle that is assigned for the corresponding line.

Depreciation costs of chargers per km of electric fast charging Metrobus network are tabulated in Table 6-13.

Table 6-13 Depreciation costs of chargers (Fast charging network)

Charger cost[EUR]	152000	152000	152000	152000	152000
Life [years]	12	12	12	12	12
Number of charger	34	30	24	26	18
Number of charger per vehicle	0.189	0.165	0.194	0.178	0.225
Charger price per vehicle[EUR/bus]	28711	25055	29419	27068	34200
Depreciation cost[EUR/bus](12 y.)	28711	25055	29419	27068	34200
Depreciation cost[EUR/km]	0.017	0.015	0.048	0.046	0.058

Depreciation costs of chargers per km of electric hybrid charging Metrobus network are tabulated in Table 6-14.

Table 6-14 Depreciation costs of chargers (Hybrid charging network)

Charger cost[EUR]	152000	152000	152000	152000	152000
Life [years]	12	12	12	12	12
Number of charger	34	30	20	30	16
Number of charger per vehicle	0.189	0.165	0.200	0.250	0.258
Charger price per vehicle[EUR/bus]	28711	25055	30400	38000	39226
Depreciation cost[EUR/bus](12 years)	28711	25055	30400	38000	39226
Depreciation cost[EUR/km]	0.017	0.015	0.040	0.053	0.049

6.1.2.4.4 Diesel bus

Depreciation of the bus is generally calculated based on the economic life of the bus. Life for public buses is generally accepted between 10 and 15 years [73] [78] [81] [82]. In this study, bus life is accepted as 12 years according to the feedback received from bus operator and studies in literature. Furthermore at the end of its life, residual value of the bus is assumed to be 10% [73]. Thus the depreciation of the bus body is assumed to be 7.5% of its initial price per year.

In equation (6.6), diesel bus depreciation per km is calculated.

$$E_{body} = \frac{0.9 \times C_{body}}{L_{total}} \tag{6.6}$$

Where, $E_{diesel\,bus}$ is the depreciation of the body per km for one vehicle, L_{total} is the total travelled distance in its life time and $C_{diesel\,bus}$ is the initial price of one complete articulated diesel bus.

Depreciation costs of bus per km of diesel Metrobus network are tabulated in Table 6-15Table 6-11.

Table 6-15 Depreciation costs of diesel bus

Bus body cost [EUR]	440000	440000	440000	440000	440000
Life [years]	12	12	12	12	12
Depreciation cost[EUR/bus](12 years)	396000	396000	396000	396000	396000
Depreciation cost[EUR/km]	0.188	0.194	0.416	0.411	0.366

6.1.3 Total cost of ownership

Total cost of ownership is calculated for 12 years period and the interest is omitted.

6.1.3.1 Diesel Fleet

Total investments of diesel Metrobus fleet of each line are shown in Table 6-16.

Table 6-16 Total investment of diesel Metrobus fleet

Line	34AS	34BZ	34	34C	34Z
Bus body cost [mioEUR]	64.24	66.88	44.00	52.80	27.28
Total investment [mioEUR]	64.24	66.88	44.00	52.80	27.28

All regular expenses of the diesel Metrobus line are tabulated in Table 6-17.

Table 6-17 Total expenses of diesel Metrobus fleet

Line	34AS	34BZ	34	34C	34Z
Number of bus	146	152	100	120	62
Fuel cost[EUR/km]	0.522	0.522	0.522	0.522	0.522
Maintenance cost[EUR/km]	0.240	0.240	0.240	0.240	0.240
Depreciation of body[EUR/km]	0.188	0.194	0.520	0.547	0.520
Cost of one bus[EUR/km]	0.950	0.956	1.282	1.309	1.282
Cost of one bus[EUR/bus](1 y.)	167,105	162,330	81,345	78,940	81,387
Cost of the fleet[mioEUR](1y.)	24.40	24.67	8.13	9.47	5.05
Cost of one bus[EUR/bus](12y.)	2,005,257	1,947,959	976,145	947,280	976,649
Cost of the fleet[mioEUR](12y.)	292.77	296.09	97.61	113.67	60.55

Total cost of ownership of the diesel Metrobus lines are shown in Table 6-18. The period of total cost of ownership is 12 years.

Table 6-18 Total cost of ownership of diesel Metrobus fleet

Line	34AS	34BZ	34	34C	34Z
Total cost of the fleet [mioEUR](12years)	267.12	267.91	123.93	146.03	79.30
Total investment [mioEUR]	64.24	66.88	44.00	52.80	27.28
Total cost of ownership [mioEUR](12 y.)	331.36	334.79	167.93	198.83	106.58

6.1.3.2 Fast charging electric fleet

Total investments of fast charging electric Metrobus fleet of each line are shown in Table 6-19.

Table 6-19 Total investment of fast charging electric Metrobus fleet

Line	34AS	34BZ	34	34C	34Z
Bus body cost [mioEUR]	57.60	58.24	32.00	38.40	19.84
Traction system cost [mioEUR]	14.40	13.65	7.50	9.00	4.65
Battery cost [mioEUR]	24.42	24.69	6.78	8.14	4.21
Charger cost [mioEUR]	5.17	4.56	3.65	3.95	2.74
Total investment [mioEUR]	101.59	101.14	49.93	59.49	31.43

All regular expenses of the fast charging electric Metrobus line are tabulated in Table 6-20.

Table 6-20 Total expenses of fast charging electric Metrobus fleet

Line	34AS	34BZ	34	34C	34Z
Number of bus	180	182	124	146	80
Energy cost[EUR/km]	0.091	0.096	0.090	0.095	0.094
Maintenance cost[EUR/km]	0.144	0.144	0.144	0.144	0.144
Depreciation of body[EUR/km]	0.168	0.169	0.469	0.484	0.488
Depreciation of trct.sys.[EUR/km]	0.047	0.044	0.122	0.126	0.127
Depreciation of battery [EUR/km]	0.071	0.071	0.098	0.102	0.102
Depreciation of charger[EUR/km]	0.017	0.015	0.048	0.046	0.058
Cost of one bus[EUR/km]	0.54	0.54	0.97	1.00	1.01
Cost of one bus [EUR/bus](1 y.)	76,635	76,359	49,727	49,394	49,864
Cost of the fleet [mioEUR](1y.)	13.79	13.90	6.17	7.21	3.99
Cost of one bus [EUR/bus](12y.)	919,615	916,305	596,729	592,732	598,362
Cost of the fleet [mioEUR](12y.)	165.53	166.77	73.99	86.54	47.87

Total cost of ownership of the fast charging electric Metrobus lines are shown in Table 6-21. The period of total cost of ownership is 12 years.

Table 6-21 Total cost of ownership of fast charging electric Metrobus fleet

Line	34AS	34BZ	34	34C	34Z
Total cost of the fleet [mioEUR](12y.)	165.53	166.77	73.99	86.54	47.87
Total investment [mioEUR]	101.59	101.14	49.93	59.49	31.43
Total cost of ownership[mioEUR](12 y.)	267.12	267.91	123.93	146.03	79.30

6.1.3.3 Hybrid charging electric fleet

Total investments of fast charging electric bus fleet of each line are shown in Table 6-22.

Table 6-22 Total investment of hybrid charging electric Metrobus fleet

Line	34AS	34BZ	34	34C	34Z
Bus body cost [mioEUR]	57.60	58.24	32.00	38.40	19.84
Traction system cost [mioEUR]	14.40	13.65	7.50	9.00	4.65
Battery cost [mioEUR]	24.42	24.69	20.19	24.23	12.52
Charger cost [mioEUR]	5.17	4.56	3.04	4.56	2.43
Total investment [mioEUR]	101.59	101.14	62.73	76.19	39.44

All regular expenses of the fast charging electric Metrobus line are tabulated in Table 6-23.

Table 6-23 Total expenses of hybrid charging electric Metrobus fleet

Line	34AS	34BZ	34	34C	34Z
Number of bus	180	182	100	120	62
Energy cost[EUR/km]	0.091	0.096	0.090	0.095	0.094
Maintenance cost[EUR/km]	0.144	0.144	0.144	0.144	0.144
Depreciation of body[EUR/km]	0.168	0.169	0.378	0.398	0.358
Depreciation of trct.sys.[EUR/km]	0.047	0.044	0.099	0.104	0.093
Depreciation of battery [EUR/km]	0.071	0.071	0.225	0.237	0.213
Depreciation of charger[EUR/km]	0.017	0.015	0.040	0.053	0.049
Cost of one vehicle per km[EUR/km]	0.54	0.54	0.98	1.03	0.95
Cost of one vehicle [EUR/bus](1y.)	76,635	76,359	61,919	62,107	63,750
Cost of the fleet [mioEUR](1y.)	13.79	13.90	6.19	7.45	3.95
Cost of one vehicle [EUR/bus](12y.)	919,615	916,305	743,030	745,279	765,003
Cost of the fleet [mioEUR](12y.)	165.53	166.77	74.30	89.43	47.43

Total cost of ownership of the fast charging electric Metrobus lines are shown in Table 6-24. The period of total cost of ownership is 12 years.

Table 6-24 Total cost of ownership of hybrid charging electric Metrobus fleet

Line	34AS	34BZ	34	34C	34Z
Total cost of the fleet [mioEUR](12y.)	165.53	166.77	74.30	89.43	47.43
Total investment [mioEUR]	101.59	101.14	62.73	76.19	39.44
Total cost of ownership [mioEUR](12y.)	267.12	267.91	137.04	165.63	86.87

6.1.3.4 Results of TCO

6.1.3.4.1 Line 34AS

Total cost of ownership is calculated for a 12-year period. The change of TCO of diesel, fast charging electric bus fleets against time are shown in Figure 6-1.
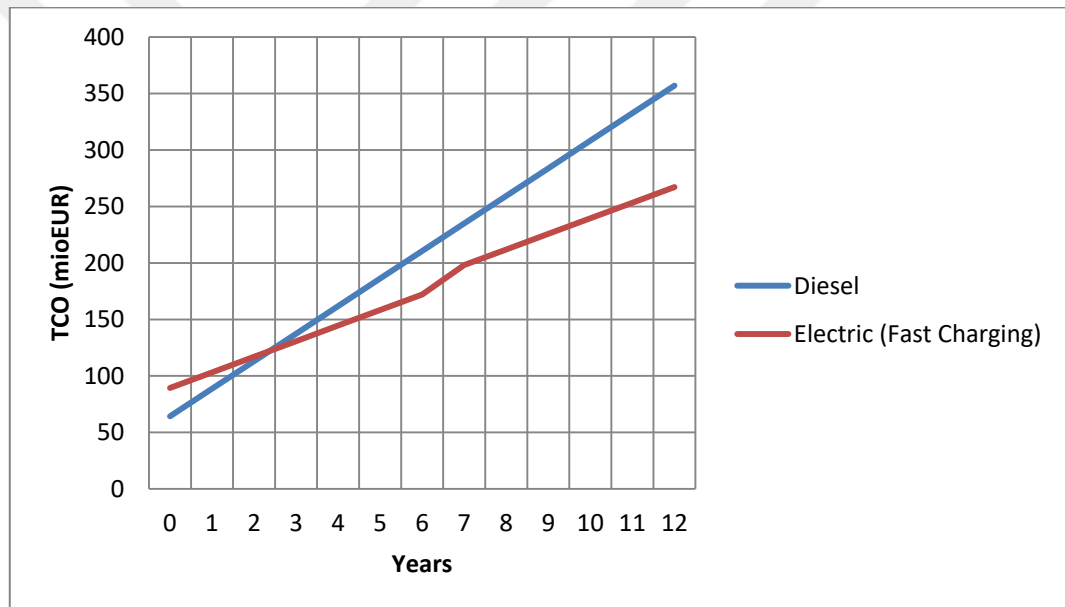
Figure 6-1 Total cost of ownership comparision of Line 34AS

There is a dramatic change in electric bus TCO. The reason for this change is at the end of the 6th year, the battery completes its life cycle and a new battery is installed.

Thanks to the fast charging feature, a small battery is sufficient for the system. This reduces the initial investment cost of the battery. Thus, in less than 3 years electric bus system becomes economically more feasible.

Slow charging system is not considered for this line, because, due to its battery weight it is not technically feasible.

6.1.3.4.2 Line 34BZ

Total cost of ownership is calculated for a 12-year period. The change of TCO of diesel, fast charging electric bus fleets against time are shown in Figure 6-2.

Figure 6-2 Total cost of ownership comparision of Line 34BZ

There is a dramatic change in electric bus TCO. The reason for this change is at the end of the 6th year, the battery completes its life cycle and a new battery is installed.

Thanks to the fast charging feature, a small battery is sufficient for the system. This reduces the initial investment cost of the battery. Thus, in less than 3 years electric bus system becomes economically more feasible.

Slow charging system is not considered for this line, because, due to its battery weight it is not technically feasible.

6.1.3.4.3 Line 34

Total cost of ownership is calculated for a 12-year period. The change of TCO of diesel, fast and slow charging electric bus fleets against time are shown in Figure 6-3.

Figure 6-3 Total cost of ownership comparision of Line 34

Thanks to the fast charging feature, a small battery is sufficient for the system. This reduces the initial investment cost of the battery. Thus, in less than 3 years fast charging electric bus system becomes economically more feasible. On the other hand, slow charging electric bus becomes economically more feasible in 10years because of it higher initial cost due to its big battery.

6.1.3.4.4 Line 34C

Total cost of ownership is calculated for a 12-year period. The change of TCO of diesel, fast and slow charging electric bus fleets against time are shown in Figure 6-4.
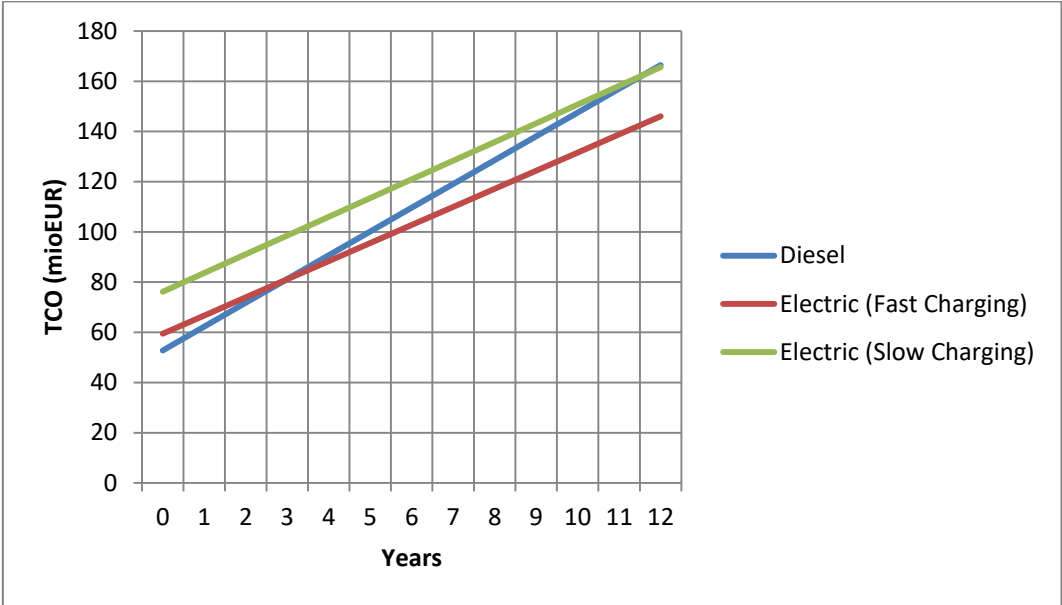
Figure 6-4 Total cost of ownership comparision of Line 34C
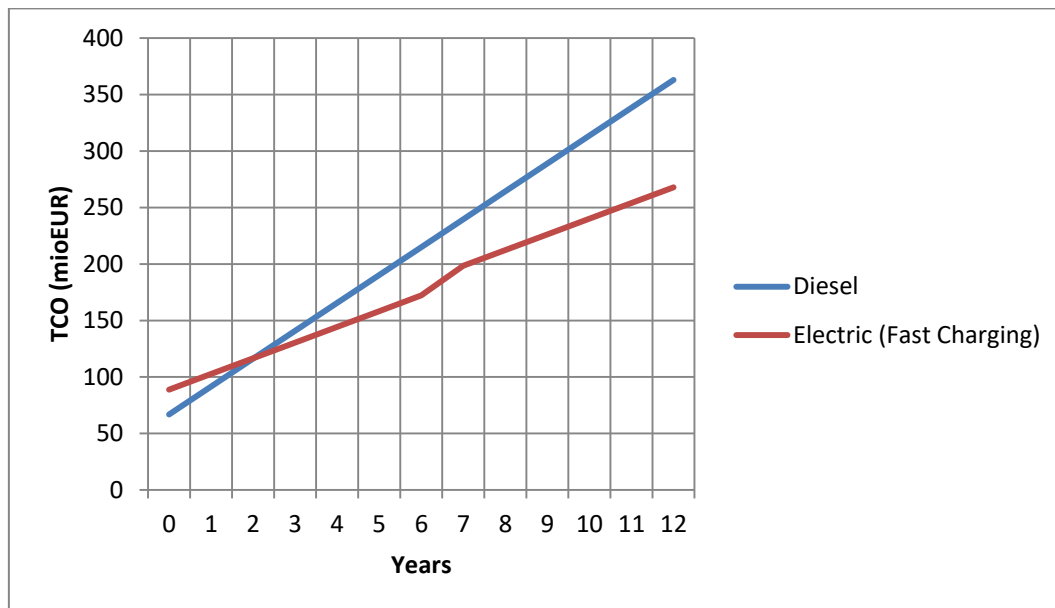
Thanks to the fast charging feature, a small battery is sufficient for the system. This reduces the initial investment cost of the battery. Thus, in less than 3 years fast charging electric bus system becomes economically more feasible. On the other hand, slow charging electric bus becomes economically more feasible in 10years because of it higher initial cost due to its big battery.

6.1.3.4.5 Line 34Z

Total cost of ownership is calculated for a 12-year period. The change of TCO of diesel, fast and slow charging electric bus fleets against time are shown in Figure 6-5.

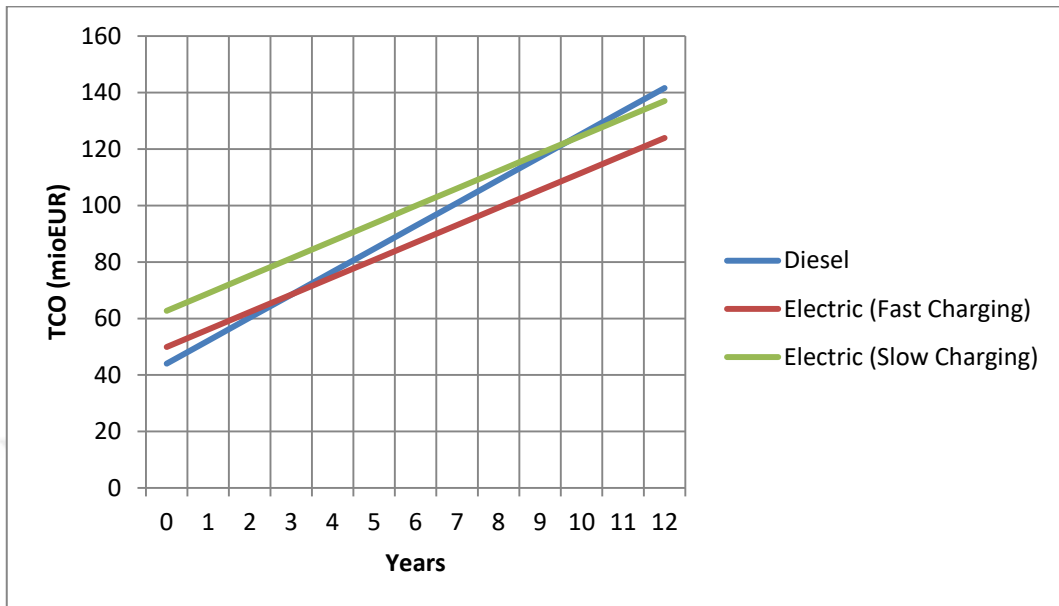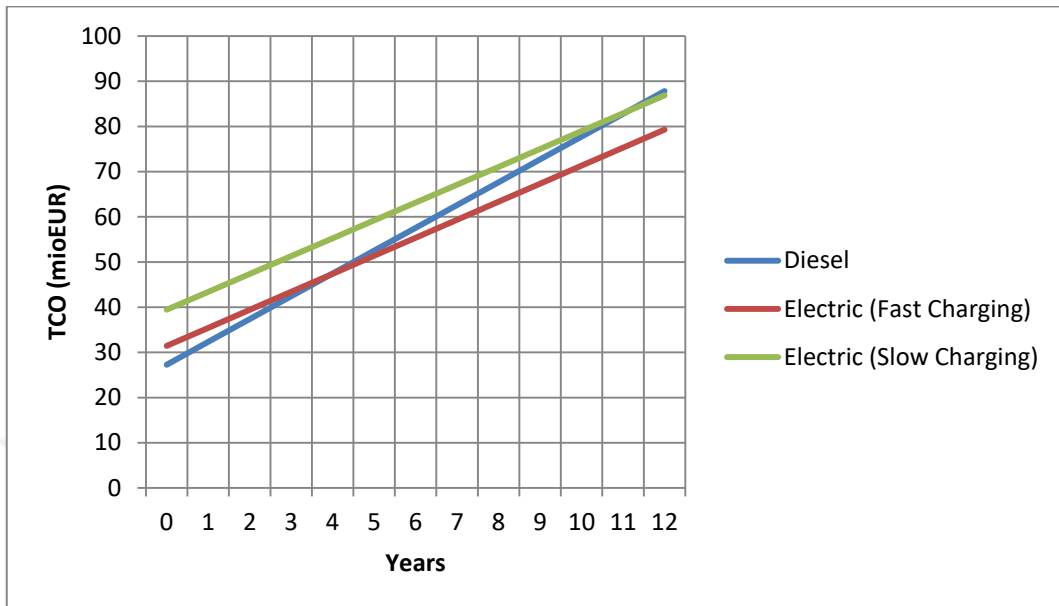**Figure 6-5 Total cost of ownership comparision of Line 34Z**

Thanks to the fast charging feature, a small battery is sufficient for the system. This reduces the initial investment cost of the battery. Thus, in less than 3 years fast charging electric bus system becomes economically more feasible. On the other hand, slow charging electric bus becomes economically more feasible in 10years because of it higher initial cost due to its big battery.

7   CONCLUSIONS AND FUTURE WORKS

For all lines fast charging electric buses are technically feasible, on the other hand slow charging system is only technically feasible for line 34, 34C and 34Z. Length of these three lines, 34,34C and 34Z are smaller. Furthermore, since they are only working at peak hours, they can be charged when they are not in service between these peak hours however, buses of line 34AS and 34BZ are working non-stop from 6h00 to midnight.

According to TCO calculations electric bus systems are more feasible than diesel bus system. When compared to fast and slow charging systems, fast charging system is economically more feasible, because thanks to their smaller batteries, their initial costs are smaller than the slow charging system. However, fast charging systems require more charger and more buses. Additionally, electric buses of line 34AS and 34BZ need battery replacement at the end of the 6th service life, because their daily travelled distance are bigger than other lines. Even though these additional costs, fast charging electric fleets are economically more feasible for all lines and their average return of investment times are 3 years.

In addition to the economic advantage, electric buses are less polluting. PNC and soot levels are 32% and 46% higher in diesel buses compared with electric powered buses [83]. In addition to environmental externalities associated with carbon emissions, a diesel bus also emits conventional pollutants that affect public health. The exhaust gases of diesel buses releases particulate matter, ozone, sulfur dioxide, nitrous oxide, and other pollutants. These increase the risk of heart disease, respiratory issues, and risk of cancer [84]. Electric powered bus have less rotating unbalanced parts than diesel buses, so this reduced the level of vibration, thereby it reduces the noise of the vehicle. This results in a much more comfortable transportation system for passenger and livable cities [85].

It is expected that the battery prices will decrease and the initial cost of the electric buses will be lower than the diesel buses [86]. On the contrary, it is predicted that fuel prices will increase [87]. Thereby electric buses will much more feasible solution for public transportation in future.

The total number of bus of the fast charging electric bus fleet is 772 and the total number of charger is 132. Chargers are located in five different stations these are Beylikdüzü, Avcilar, Cevizlibağ, Zincirlikuyu and Söğütlüçeşme. Even if chargers are distributed in different locations, during peak hours all chargers have to work at the same time so the total power requirement reach up to 93.28MW and the largest power requirement arises at the Beylikdüzü station with 24.03MW. Design of electric distribution network for high power demand of chargers could be an interesting topic for future work.

HVAC consumption is a major part of total energy consumption of the vehicle. If HVAC consumption can be reduced, the consumption and size of the battery will be reduced thus the initial cost of the vehicle reduced. Namely, the vehicle will be more feasible. Design of more efficient HVAC systems for electric buses is an issue for future research to explore.

Furthermore, future research should consider the potential reuse of batteries more carefully, for example usage of these batteries for energy storage in renewable energy industry. Additionally, further studies should investigate the second hand market of used electric vehicle batteries.

8 REFERENCES

[1]   H. Levinson, S. Zimmerman, J. Clinger, S. Rutherford, R. Smith, J. Cracknell and R. Soberman, "Bus Rapid Transit, Volume 2: Implementation Guidelines," The National Academies Press, Washington, 2003.

[2]   "Wikipedia," [Online]. Available: https://upload.wikimedia.org/wikipedia/commons/f/f3/Map_of_the_Istanbul_Metro b%C3%BCs.png. [Accessed 1 May 2019].

[3]   "omnibusarchiv," 22 August 2009. [Online]. Available: http://www.omnibusarchiv.de/include.php?path=content&mode=print&contentid= 531. [Accessed 1 May 2019].

[4]   T. Nordhaus and M. Shellenberger, "The death of environmentalism," 2004.

[5]   A. A. Juan, C. A. Mendez, J. Faulin, J. De Armas and S. E. Grasman, "Electric vehicles in logistics and transportation: A survey on emerging environmental, strategic, and operational challenges," *Energies,* no. 9, pp. 1-21, 2016.

[6]   M. Pihlatie, S. Kukkonen, T. Halmeaho, V. Karvonen and N. O. Nylund, "Fully electric city buses - The viable option," in *2014 IEEE International Electric Vehicle Conference*, 2015.

[7]   I. Graurs, A. Laizans, P. Rajeckis and A. Rubenis, "Public bus energy consumption investigation for transition to electric power and semi-dynamic charging," *Engineering for Rural Development,* no. 14, pp. 366-371, 2015.

[8]   W. Gis, S. Kruczyński, S. Taubert and A. Wierzejski, "Studies of energy use by electric buses in SORT tests," in *VII International Congress on Combustion Engines*, 2017.

[9]   Aselsan,   "Electric   Traction   System,"   [Online].   Available: https://www.aselsan.com.tr/en-us/capabilities/transportation-systems/electrical-vehicle-systems/electric-traction-system. [Accessed 20 January 2019].

[10]   P. Sinhuber, . W. Rohlfs and D. U. Sauer, "Study on Power and Energy Demand for Sizing the Energy Storage Systems for Electrified Local Public Transport Buses," in *2012 IEEE Vehicle Power and Propulsion Conference*, Seoul, Korea, 2012.

[11]   M. Rogge, S. Wollny and D. U. Sauer, "Fast Charging Battery Buses for the Electrification of Urban Public Transport—A Feasibility Study Focusing on Charging Infrastructure and Energy Storage Requirements," *Energies,* pp. 4587-4606, 2015.

[12]   A. Kunith, R. Mendelevitch and D. Goehlich, "Electrification of a city bus network—An optimization model for cost-effective placing of charging infrastructure and battery sizing of fast-charging electric bus systems," *Internationa Journal of Sustainable Transportation,* no. 10, pp. 707-720, 2017.

[13]   D. Göhlich, A. Kunith and T.-A. Ly, "Technology assessment of an electric urban bus system for Berlin," in *Urban Transport 2014*, Alvor, 2014.

[14]   D. Göhlich, T.-A. Fay, D. Jefferies, E. Lauth, A. Kunith and X. Zhang, "Design of urban electric bus systems," *Design Science,* no. 4, 2018.

[15]   O. Vilppo and J. Markkula, "Feasibility of electric buses in public transport," in *KINTEX*, Korea, 2015.

[16]   M. Potkány, M. Hlatká, M. Debnár and J. Hanzl, "Comparison of the Lifecycle Cost Structure of Electric and Diesel Buses," *Nase More,* pp. 270-275, 2018.

[17]   A. Lajunen and T. Lipman, "Lifecycle cost assessment and carbon dioxide emissions of diesel, natural gas, hybrid electric, fuel cell hybrid and electric transit buses," *Energy,* pp. 329-342, 2016.

[18]   E. C. McKenzie and P. L. Durango-Cohen, "Environmental life-cycle assessment of transit buses with alternative fuel technology," *Transportation Research Part D Transport and Environment,* 2012.

[19]   A. Millner, "Modeling Lithium Ion battery degradation in electric vehicles," in *Innovative Technologies for an Efficient and Reliable Electricity Supply (CITRES)*, 2010.

[20]   E. Tosun, M. Bilgili, G. Tuccar, A. Yasar and K. Aydin, "Exergy analysis of an inter-city bus air-conditioning system," *International Journal of Exergy,* vol. 20, no. 4, 2016.

[21]   D. Ružić and F. Časnji, "Thermal Interaction Between a Human Body and a Vehicle Cabin," in *Heat Transfer Phenomena and Applications*, 2012, pp. 295-318.

[22]   F. Stancato, H. Onusic, R. Anton and P. Avila , "Experimental and Numerical Analysis of Cooling Loads in a Road Bus," *SAE Technical Paper Series,* 1992.

[23]   M. A. Fayazbakhsh and M. Bahrami, "Comprehensive Modeling of Vehicle Air Conditioning Loads Using Heat Balance Method," in *SAE 2013 World Congress & Exhibition*, 2013.

[24]   F. Sangtarash, V. Esfahanian, H. Nehzati, S. Haddadi, M. A. Bavanpour and B. Haghpanah, "Effect of Different Regenerative Braking Strategies on Braking Performance and Fuel Economy in a Hybrid Electric Bus Employing CRUISE Vehicle Simulation," *SAE International Journal of Fuels and Lubricants,* pp. 828-837, 2009.

[25]   J. Zhang, X. Lu, J. Xue and B. Li, "Regenerative Braking System for Series Hybrid Electric City Bus," *World Electric Vehicle Journal,* 2008.

[26]   Mercedes-Benz, *Technical Information catalogue of Mercedes CapaCity,* Stuttgart: Mercedes-Benz.

[27]   G. Ulsoy, H. Peng and M. Cakmakci, Automotive Control Systems, Cambridge University Press, 2012.

[28]   I. Preda, D. Covaciu and G. Ciolan, "Coast Down Test – Theoretical and Experimental Approach," in *CONAT 2010 - International Automotive Congress*, Brasov, 2010.

[29]   *Technical Data OM457 LA,* Mercedes-Benz, 2009.

[30]   Dewesoft, *DEWESoft Product Catalogue,* 2018.

[31]   M. A. Aktacir, O. Büyükalaca, H. Bulut and T. Yılmaz, "Influence of different outdoor design conditions on design cooling load and design capacities of air conditioning equipments," *Energy Conversion and Management,* no. 49, pp. 1766-1773, 2008.

[32]   K. Eda, R. Kanaga, W. H. Yang, T. Hirota, Y. Kamiya and Y. Daisho, "Development and Performance Evaluation of Advanced Electric Bus Transportation System," in *28th International Electric Vehicle Symposium and Exhibition 2015*, Goyang, 2015.

[33]   American Society of Heating, Refrigeration and Air Conditioning, ASHRAE Handbook of Fundamental, Atlanta, 2001.

[34]   J. W. Lee, E. Y. Jang, S. H. Lee, H. S. Ryou, S. Choi and Y. Kim, "Influence of the spectral solar radiation on the air flow and temperature distributions in a passenger compartment," *International Journal of Thermal Sciences,* pp. 36-44, 2014.

[35]   L. JY, C. JW and K. H, "Determination of Body Surface Area and Formulas to Estimate Body Surface Area Using the Alginate Method," *Journal of Physiological Anthropology,* pp. 71-82, 2008.

[36]   D. Y. Goswami, "Solar Energy Resources," *2015.*

[37] S. Becker, "Calculation of Direct Solar and Diffuse Radiation in Isreal," *International Journal of Climatology,* vol. 12, no. 21, pp. 1561-1576, 2001.

[38] W. Li and J. Sun, "Numerical simulation and analysis of transport air conditioning system integrated with passenger compartment," *Applied Thermal Engineering,* pp. 37-45, 2013.

[39] American Society of Heating, Refrigerating and Air-Conditioning Engineers, ASHRAE Standard 62, "Ventilation for Acceptable Indoor Air Quality", 1999.

[40] Turkish Statistical Institute, "Health Survey Health Survey," 2010.

[41] N. Tran, R. L. Powell, H. Marks, R. West and A. Kvasnak, "Strategies for Design and Construction of High-Reflectance Asphalt Pavements," *Journal of the Transportation Research Board,* no. 2098, pp. 124-130, 2009.

[42] . L. H. S. Bernard, A. Tay and W. Zhang, "Thermal Management of Lithium-ion Battery Pack with Liquid Cooling," in *Thermal Measurement, Modeling & Management Symposium (SEMI-THERM)*, San Jose, 2015.

[43] A. Pesaran, "Battery Thermal Management in EVs and HEVs: Issues and Solutions," in *Advanced Automotive Battery Conference*, Las Vegas, 2001.

[44] I. L. Krüger, D. Limperich and G. Schmitz, "Energy Consumption Of Battery Cooling In Hybrid Electric Vehicles," in *International Refrigeration and Air Conditioning Conference*, 2012.

[45] J. Kim, J. Oh and H. Lee, "Review on battery thermal management system for electric vehicles," *Applied Thermal Engineering,* pp. 192-212, 2019.

[46] D. A. P.Artuso, P. Artuso, L. Rambaldi, D. A. Sbordone and A. Santiangeli, "Energetic evaluation on auxiliary systems of an hydrogen hybrid minibus," in *Dubrovnik conference on sustainable development of energy water and environment systems*, Dubrovnik, 2011.

[47]   C. Andersson, *On auxiliary systems in commercial vehicles,* Lund: Media-Tryck, 2004.

[48]   "homerenergy," [Online]. Available: https://www.homerenergy.com/products/pro/docs/3.11/nominal_battery_capacity.html. [Accessed 2 February 2019].

[49]   D. H. Lee, N. W. Kim, J. R. Jeong, Y. I. Park and S. W. Cha, "Component sizing and engine optimal operation line analysis for a plug-in hybrid electric transit bus," *International Journal of Automotive Technology,* pp. 459-469, 2013.

[50]   S. Ito, N. Miura and K. Wang, "Performance of a Heat Pump Using Direct Expansion Solar," *Dolar Energy,* vol. 3, no. 65, pp. 189-196, 1999.

[51]   Karayolları Standartlar Kurulu, "Karayolları Geometrik Standartları," Karayolları Genel Müdürlüğü, 1993.

[52]   S. Koetniyom and S. Mongkonlerdmanee, "Investigation of Brake Force Distribution for Three axle Double Deck Bus in Thailand," in *The 20th Conference of Mechanical Engineering Network of Thailand*, Nakhon Ratchasima, 2006.

[53]   M. Elwell and S. Kimbrough, "An Advanced Braking and Stability Controller for Tow-Vehicle and Trailer Combinations," *Journal of Commercial Vehicles,* vol. 102, pp. 107-119, 1993.

[54]   M.-W. Suh, Y.-K. Park, S.-J. Kwon, S.-H. Yang and B.-C. Park, "A Simulation Program for the Braking Characteristics of Tractor-Semitrailer Vehicle," *Journal of Commercial Vehicles,* vol. 109, pp. 540-550, 2000.

[55]   S. A. Milani, *Modeling, Simulation, and Active Control of Tractor-Semitrailer Combinations,* Ankara, 2015.

[56]   A. Goodarzi, M. Behmadi and E. Esmailzadeh, "An optimised braking force distribution strategy for articulated vehicles," *Vehicle System Dynamics,* p. 849–856, 2008.

[57] M. Ehsani, Y. Gao, S. Gay and A. Emadi, Modern Electric, Hybrid Electric, and Fuel Cell Vehicles, CRC Press, 2005.

[58] J. F. Peters, M. Baumann, B. Zimmermann, J. Braun and M. Weil, "The environmental impact of Li-Ion batteries and the role of keyparameters–A review," *Renewable and Sustainable Energy Reviews,* vol. 67, pp. 491-506, 2017.

[59] E. Wikner and T. Thiringer, "Extending Battery Lifetime by Avoiding High SOC," *applied science,* 2018.

[60] European Batteries , "EB 45 Ah," www.europeanbatteries.com, 2019.

[61] KOKAM, "KOKAM Li-ion/Polymer Cell," http://kokam.com, 2019.

[62] Toshiba, "Toshiba Rechargeable Battery SCIB," www.scib.jp, 2019.

[63] E. Waffenschmidt and T. Staring , "Limitation of inductive power transfer for consumer applications," in *2009 13th European Conference on Power Electronics and Applications*, Barcelona, 2009.

[64] heliox, "Opportunity Charger 600kW," https://www.heliox.nl, 2019.

[65] ABB, "ABB E-mobility Electric Vehicle Infrastructure Global product portfolio," www.abb.com, 2019.

[66] M. Luthfi, "State Estimation of Lithium Ion Battery Using Non-Invasive Method," 2018.

[67] efacec, "Buses Quick Charge Station," http://electricmobility.efacec.com, 2019.

[68] heliox, "Fast DC 150 kW," https://www.heliox.nl, 2019.

[69] C. Zhou, K. Qian and M. Al, "Modeling of the Cost of EV Battery Wear Due to V2G Application in Power Systems," *IEEE TRANSACTIONS ON ENERGY CONVERSION,* no. 4, 2011.

[70]   O. Olsson, A. Grauers and S. Pettersson, "Method to analyze cost effectiveness of different electric bus systems," in *EVS29 Symposium*, Montréal, 2016.

[71]   D. Göhlich, A. Kunith and F. Spangenberg, "Stochastic Total Cost of Ownership Forecasting for innovative Urban Transport Systems," in *IEEE International Conference on Industrial Engineering and Engineering Management*, Bangkok, 2013.

[72]   H. Bängtsson and M. Alaküla, "Cost Analysis of Electric Land Transport," ProjectT2.11, 2015.

[73]   Transport & Environment, "Electric buses arrive on time," Transport & Environment, 2018.

[74]   A. Kunith, R. Mendelevitch and D. Göhlich, "Electrification of a city bus network - An optimization model for cost-effective placing of charging infrastructure and battery sizing of fast charging electric bus systems," *International Journal of Sustainable Transportation,* pp. 707-720, 2017.

[75]   L. Nurhadi, S. Borén and H. Ny, "A Sensitivity Analysis of Total Cost of Ownership for Electric Public Bus Transport Systems in Swedish Medium Sized Cities," in *17th Meeting of the EURO Working Group on Transportation*, Sevilla, 2014.

[76]   IETT İşletmeleri Genel Müdürlüğü, "2009 yılı idare faaliyet raporu," İstanbul Büyükşehir Belediyesi, İstanbul, 2009.

[77]   J. A. González and X. Wang, "Assessing Feasibility of Electric Buses in Small and Medium-Sized Communities," *International Journal of Sustainable Transportation,* pp. 431-448, 2013.

[78]   J. Aber, "Electric Bus Analysis for New York City Transit," 2016.

[79] J. Neubauer and A. Pesaran, "The ability of battery second use strategies to impact plug-in electric vehicle prices and serve utility energy storage applications," *Journal of Power Sources,* no. 196, p. 10351– 10358, 2011.

[80] C. Heymans, S. B. Walker, S. B. Young and M. Fowler, "Economic analysis of second use electric vehicle batteries for residential energy storage and load-levelling," *Energy Policy,* no. 71, pp. 22-30, 2014.

[81] H. Mohring, "Optimization and Scale Economies in Urban Bus Transportation," *The American Economic Review,* vol. 62, no. 4, pp. 591-604, 1972.

[82] A. Avenali, A. Boitani, G. Catalano, T. D'Alfonso and G. Matteucci, "Assessing standard costs in local public bus transport: Evidence from Italy," *Transport Policy,* no. 52, pp. 164-174, 2016.

[83] M. Zuurbier, G. Hoek, M. Oldenwening, V. Lenters, K. Meliefste, P. van den Hazel and B. Brunekreef, "Commuters' Exposure to Particulate Matter Air Pollution Is Affected by Mode of Transport, Fuel Type, and Route," *Environmental Health Perspectives,* no. 6, pp. 783-789, 2010.

[84] L. Noel and R. McCormack, "A cost benefit analysis of a V2G-capable electric school bus compared to a traditional diesel school bus," *Applied Energy,* no. 126, pp. 246-255, 2014.

[85] "Air-pollution and economics: diesel bus versus electric bus," *CURRENT SCIENCE,* no. 5, pp. 858-862, 2016.

[86] Bloomberg, "Electric Buses in Cities Driving Towards Cleaner," Bloomberg, 2018.

[87] S. Shafiee and E. Topal, "An econometrics view of worldwide fossil fuel consumption and the role of US," *Energy Policy,* vol. 36, no. 2, pp. 775-786, 2008.

HACETTEPE UNIVERSITY
GRADUATE SCHOOL OF SCIENCE AND ENGINEERING
THESIS/~~DISSERTATION~~ ORIGINALITY REPORT

HACETTEPE UNIVERSITY
GRADUATE SCHOOL OF SCIENCE AND ENGINEERING
TO THE DEPARTMENT OF MECHANICAL ENGINEERING

Date: 03/07/2019

Thesis Title / Topic: AN ELECTRIFICATION SOLUTION FOR ISTANBUL METROBUS LINE

According to the originality report obtained by ~~myself~~/my thesis advisor by using the *Turnitin* plagiarism detection software and by applying the filtering options stated below on 03/07/2019 for the total of 150 pages including the a) Title Page, b) Introduction, c) Main Chapters, d) Conclusion sections of my thesis entitled as above, the similarity index of my thesis is 10 %.

Filtering options applied:
1. Bibliography/Works Cited excluded
2. Quotes ~~excluded~~ / included
3. Match size up to 5 words excluded

I declare that I have carefully read Hacettepe University Graduate School of Sciene and Engineering Guidelines for Obtaining and Using Thesis Originality Reports; that according to the maximum similarity index values specified in the Guidelines, my thesis does not include any form of plagiarism; that in any future detection of possible infringement of the regulations I accept all legal responsibility; and that all the information I have provided is correct to the best of my knowledge.

I respectfully submit this for approval.

		Date and Signature
Name Surname:	Mustafa Nicem Tanyeri	03/07/2019
Student No:	N16125396	
Department:	Mechanical Engineering	
Program:	Mechanical Engineering-Master of Science	
Status:	☒ Masters ☐ Ph.D. ☐ Integrated Ph.D.	

ADVISOR APPROVAL

APPROVED.

Doç. Dr. Selahattin Çağlar Bağlamışlı

(Title, Name Surname, Signature)

CURRICULUM VITAE

Credentials

Name, Surname   : Mustafa Nicem TANYERİ

Place of Birth   : Ankara, TURKEY

Material Status   : Married

E-mail   : nicemtanyeri@gmail.com

Address   : Ankara, TURKEY

Education

BSc.   : Middle East Technical University

MSc.   : -

PhD.   : -

Foreign Language

English, French

Work Experience

Engineer, ASELSAN INC (2015 -)

Areas of Experiences

-**Project and Budgets**

-**Publications**

- M. N. Tanyeri and H. M. Gültekin, "Railway Vehicle Model Developed by ASELSAN", *IFToMM*, 2017

- B. Ince, S. Ç. Başlamişli, D. Yildirim, B. Çetinkaya, S. F. Kara and M. N. Tanyeri, "Testing of Railway Traction Control Algorithm with Dynamometer System", *OTEKON*, 2018

- B. Ince, S. Ç. Başlamişli, B. Çetinkaya and M. N. Tanyeri, "Slip Slide Protection Algorithm Design and Development for Railway Traction Systems", *TOK*, 2017

Oral and Poster Presentation

-